Traction Processes of Wheels in Loose, Granular Soil

Submitted in partial fulfillment of the requirements for

the degree of

Doctor of Philosophy

in

Mechanical Engineering

Scott Jared Moreland

B.A.Sc., Mechanical Engineering, University of Toronto
M.S., Mechanical Engineering, Carnegie Mellon University

Carnegie Mellon University
Pittsburgh, PA

August, 2013

Acknowledgments

This research was supported by NASA, Glenn Research Center (Grant NNX07AE30G) and by the Jet Propulsion Laboratory, Caltech (Grant 1220-DRDF-104425).

I would like to thank the members of the thesis committee for their dedication to providing their time and for support of the research. Thank you William Messner of Tufts University; Brian Wilcox of the Jet Propulsion Laboratory; (committee chair) David Wettergreen of Carnegie Mellon University; and William “Red” Whittaker of Carnegie Mellon University.

This thesis could not have been completed without the contributions of many individuals. Vivake Asnani and Colin Creager of Glenn Research Center, and Krzysztof Skonieczny of Carnegie Mellon University are to be recognized for their major contributions to the research presented in this document.

Abstract

This dissertation presents analyses of subsurface motions of soil beneath different traction devices and develops new explanations of traction processes of wheels operating in loose granular soil based on these observations. This dissertation shows how these findings are useful for the development of planetary rover mobility systems.

Shear Interface Imaging Analysis (SIIA), is a new technique, developed as part of this thesis research. SIIA is employed for visualizing the effects of wheel operation on the soil beneath a rim, in richer detail than before possible. SIIA relies on high-speed imaging of sub-surface soil and on computer vision software to produce soil displacement fields, of high fidelity. The resulting data provides new insight and can reveal misconceptions about how wheels generate traction.

Two comprehensive studies relying on SIIA are undertaken: the investigation of wheel grouser mechanics and the investigation of push-roll locomotion. Soil forward motion, at a wheel leading edge, is identified as a key behavior for the grousered wheels. As a result, an equation for grouser height/spacing relationship to achieve a higher performance grouser configuration is developed and validated. This expression relates grouser configuration to wheel parameters (wheel radius) and operational parameters (sinkage and slip).

The soil mechanics behind Push-roll locomotion for high net traction and soft ground applications are presented. SIIA reveals that high thrust generated by push-roll locomotion is due to ground failure of the soil. Confirmation of the type of soil failure and of the application of operation in soft ground (where most vehicles would be embedded), brings forward the mobility gains of this non-typical locomotion mode and as a possible use for future planetary missions.

Additionally, insight into fundamental traction processes such as thrust, sinkage and motion resistance, are discussed with experimental evidence from soil displacement fields. This research proves that accounting for soil motion is of the utmost importance for the understanding of traction in loose, granular soils.

As a result of the specific technique utilized for directly studying soil motion, this research enables improved analysis and new design relevant to planetary rover mobility.

Table of Contents

List of Tables

List of Figures

1 Introduction

1.1 Introduction and Motivation

Limitations on mobility imposed by the terrain of planetary surfaces indicate a need for improved traction devices, such as wheels, for robotic vehicles. Specific scientific targets and larger areas of interest occur in terrain that is beyond the capability of state-of-art mobility platforms (Figure 1). This results in the loss of scientific data and potential scientific discovery. Particularly challenging are flat ground of low-strength materials and slopes of loose soil. Excessive sinkage can lead to entrapment on level ground and slip on slopes or any incline poses multiple potential failure modes. Either has the potential to end a mission (Figure 2). These obstacles block traverse or are avoided due to risk, leaving scientifically interesting locations inaccessible. This motivates the development of mobility systems with traction capabilities well beyond those currently available.

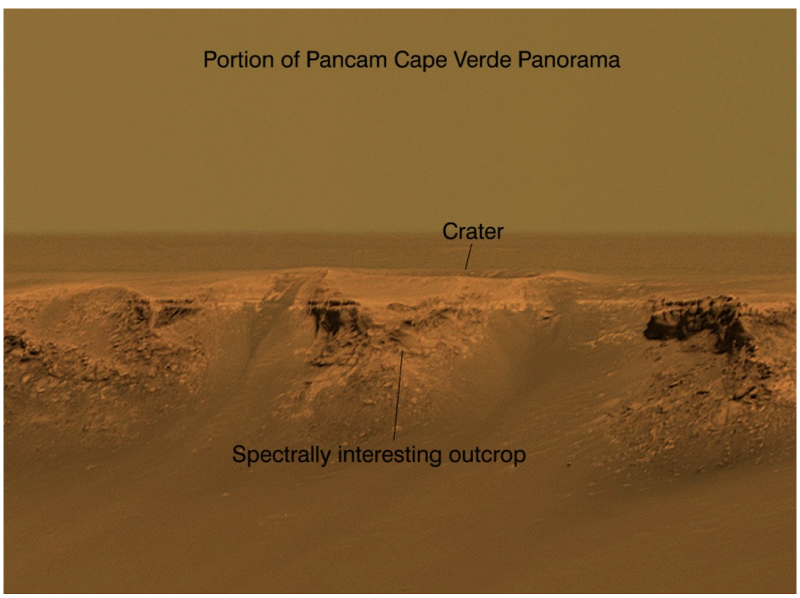

Figure 1: Example of scientific target, of interest, that is outside the mobility capability of currently available systems. Steep slopes, of loose material, prevent rovers from reaching destinations, such as an outcropping on a slope during the NASA Mars Exploration Rover missions shown in the figure. Image credit [1].

In addition to needing direct capability to overcome obstacles, and a high margin of safety against vehicle entrapment on low-strength ground, operation of a vehicle remains a challenging task. Vehicle capability, safety and operation all require an understanding of how the system interacts with terrain and more specifically, a detailed knowledge of the wheel-soil mechanics governing traction. The processes involved in traction related to vehicles in loose, granular soils, such as planetary rovers, are not well understood. Both empirical data and existing models have yet to describe the soil processes under a wheel in detail.

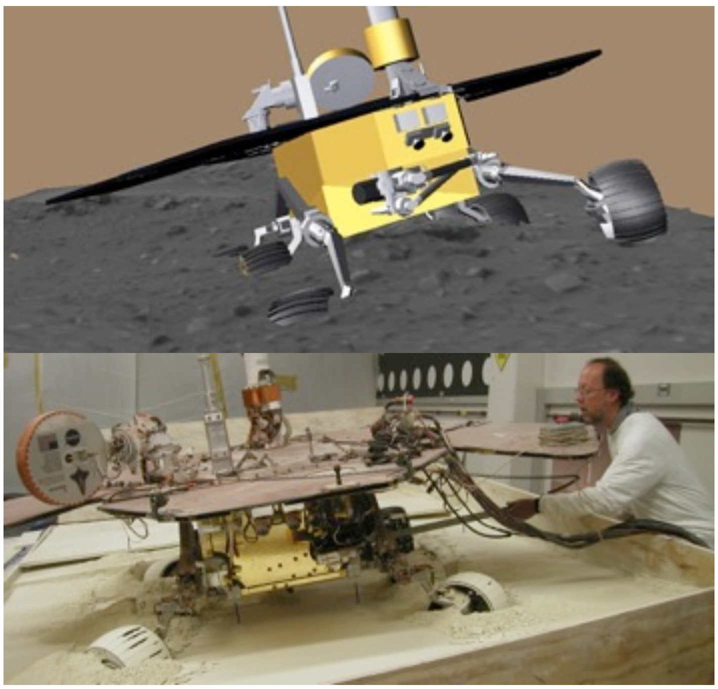

Figure 2: Mars Exploration Rover (MER), "Spirit" entrapped, in weak soil, as a result of excessive slip and sinkage. This image is an example of a scenario that systems might encounter on the Moon or on Mars. The top image is visual representation of MER Spirit rover stuck in weak soil on Mars. Bottom image is Earth testing of MER rover testbed in stuck scenario. Image credit [2].

With the continued exploration of the Moon, Mars and of other planetary bodies, the study of wheel-soil behavior in loose, granular material remains imperative for developing systems to enable future scientific discoveries.

1.2 Problem and Technical Approach

Terramechanics is the field of engineering that investigates off-road vehicle locomotion. This field combines soil mechanics theory and vehicle engineering originally for the purpose of agricultural vehicle research. There exists a well-developed theory for vehicles in this application, however as the models are highly empirical, generalization to other applications becomes difficult [3]. The vehicles and terrain materials related to planetary rovers and agricultural systems are substantially different, thus many fundamental assumptions are not applicable for both applications. A separate theory, with alternative assumptions is not available for planetary rovers, leading to the reliance on the original models intended for large terrestrial vehicles operating in organic soils. This results in a fundamental problem. Many assumptions required for conventional terramechanics theory are not applicable to the traction scenario involving small diameter rigid wheels operating loose, granular soil, as is the case for planetary rovers. As such, there is a lack of adequate traction mechanics theory for planetary rover applications, and the design and analysis process of these vehicles are in part limited by this deficiency.

Commonly used models, for designing wheels and vehicles, are empirically derived and the theory frequently relied upon lacks support in terms of actual soil response. M.G. Bekker, widely considered the founder of terramechanics, states that the models, *"are based on more or less arbitrary assumptions. The variable properties of soil have been expressed by certain empirical coefficients whose meaning and significance were not quite based on any physical facts. Although some of the results obtained have a definite practical value, their theoretical generalization is impossible because of the lack of systematic studies of the stress-strain pattern of soils under the action of a wheel…"(pp. 187)* [4]. The inability of the theory to generalize and possibly to misrepresent soil traction processes below a of wheel operating in loose, granular material leads to limitations in the design of high performance systems and has also led to mature systems of which the traction processes might not be fully understood. Two points, in which existing models do not adequately address physical realities, are the assumption of overly idealized wheels and the inability to account for mechanics related to loose, granular materials where significant particle motion occurs.

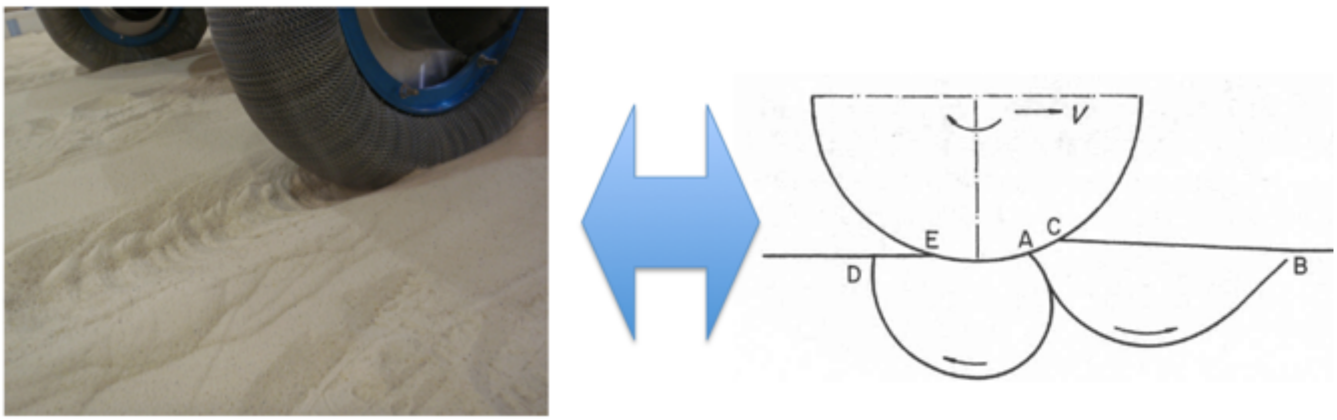

Figure 3: All wheels in loose granular materials create complex soil displacement fields that govern traction. Details of sub-surface soil failure patterns and soil flow processes is limited. Right image credit [5].

Examples of wheel non-idealities leading to complex soil stress-strain patterns are finite width, small radius, tread features, and non-flat profiles. Particles of loose soils undergo large transport due to a rotating rim that is sunken into the ground. As such, a pumping like action creates primary soil failure planes that can occur well below a wheel (Figure 3). Current terramechanic models, originally developed for organic soils/clays, do not account for these subsurface failure planes that govern traction in loose, granular soil. Additionally, there is no accounting for soil transport, which may render aspects of analytical models for loose, granular soil unsound.

It is the objective of this thesis to provide new insight into wheel-soil mechanics related to the design and operation of wheeled planetary vehicles in loose, granular soil. Current theory is quite limited for this application and development of high fidelity analytical models remains to be too complex a problem to be a viable research path. As such, an alternative approach of empirical analysis was followed, rather than to attempt advancement of analytical models.

This research chose to follow an empirical approach, as it was expected to be a more direct route to research findings capable of informing design via new insight into traction processes. The specific experimentation method employed is a technique for visualizing the effects of wheel operation on the soil beneath a rim. This technique, called Shear Interface Imaging Analysis (SIIA), is a new method for analysis developed as part of this research. SIIA measures soil particle motion within a large vertical cross-section of soil as is influenced by a wheel or other traction device [6]. The SIIA technique relies on high-speed imaging of sub-surface soil and on computer vision software to produce soil displacement fields of high fidelity that are used for wheel traction analysis. This method enables visualization of wheel-soil interactions in richer detail than possible before. The resulting data provides new insights and can reveal misconceptions about how wheels generate traction. For example, a commonly accepted theory is that wheels with grousers increase net traction by engaging deeper soil or provide a high friction rim-soil interface by directly engaging the soil. However, sub-surface soil motion analysis, utilizing SIIA, shows that traction gains are produced by reduction of motion resistance from the soil transport effect of the grousers, thus resulting in greater net traction [7]. The observation of the sub-surface soil behaviors led to this alternative explanation of grouser traction mechanics. Findings such as this would not be possible without the empirical analysis method enabled by SIIA. The grouser mechanics example demonstrates the need to conduct studies of wheel interaction effects on sub-surface soil behaviors, due to geometrically complex rim features, usually ignored in analysis.

The tractions processes are not well understood for lightweight, wheeled vehicles operating in loose, granular materials (i.e. planetary rovers) as current theory and models for this situation lack sufficient complexity to describe many of the processes present underneath a rover wheel. To improve design through research of vehicles in this application, the empirical approach of observing sub-surface soil behaviors is undertaken using SIIA, as this method provides a significant increase in the value of soil motion data compared to the past. New insight into the soil mechanisms below a wheel could enable the development of new theory and improved design.

1.3 Thesis Statement and Objective

1.3.1 Thesis Statement

This research reveals the nature of wheel-induced soil behaviors and their significant influence on traction. An empirical method of observing sub-surface soil particle motion *can be employed in analysis to explain traction processes. This method can be used to improve wheel design and control strategy.*

1.3.2 Thesis Objective and Intended Contributions

The two main objectives, of the thesis research, rely on the method of directly investigating sub-surface soil motion. The first objective of this research is to produce principles of wheel traction for planetary vehicles that explain the wheel-soil mechanics of some common wheel types, in an effort to aid in design and operation. Many aspects of wheels utilized in planetary mobility create complex interactions with the ground that are not described by current theory. The second objective is the development of experimentation tools and methodologies, based on sub-surface soil motion analysis, that can be used for evaluation and validation of wheel designs. These tools and methodologies are intended to be of use to both designers and the terramechanics research community. The maturation of the SIIA technique and demonstration of its value was an important step in this objective.

The overarching goal of this thesis is to enhance the limited knowledge of traction processes that occur within soil underneath a wheel by analyzing sub-surface soil motion and soil failure patterns. The unique method of analyzing sub-surface soil behaviors generates new insight and ultimately leads to new explanations of traction mechanisms that enable improved design.

It is the intention of this thesis to make the following contributions to the planetary rover mobility and terramechanics community.

- Developing the Shear Interface Imaging Analysis (SIIA) technique to enable direct study of traction processes via soil motion analysis. The highly detailed, empirical data SIIA provides can aid in design, can help validate theories in non-standard applications such as planetary mobility and can help validate simulation methods. As such, SIIA might have great impact on terramechanics research and in engineering of terrain-vehicle systems such as planetary rovers.

• Show that distinct wheel types generate traction differently due to subsurface soil responses. Soil motion itself, is shown to be not only a response to loading, but many times also plays a major role in governing traction.

It is not the goal to explain all traction processes or to explain how all wheel types work, but rather to show a few important examples. The hope is that this research will spark renewed interest in fundamental terramechanics research and provide a framework to do so. This impetus will have a positive effect on the terramechanics research community beyond increasing performance due to specific design recommendations as a topic of research is revealed and a methodology is provided.

• Formatting of principles describing wheel-soil mechanics to aid in design when developing a wheel or operating a vehicle. Explanation of traction processes specific to unique design features will allow designers to have knowledge of the soil shearing and mechanics that lead to performance gains. A design process accounting for actual soil response can then be undertaken. This enables an approach of design by soil behavior, rather than relying on models known to have limitations and on solely reaction force measurements. The investigation and resulting design considerations of grousered wheels and push-roll locomotion serve as examples of implementation for high performance utilizing SIIA and soil behavior analysis.

1.4 Approach

To prove or to refute the thesis statement specified in Section 1.3.1 and to achieve the objectives anticipated in Section 1.3.2, an approach relying on experimental results of SIIA was undertaken. This approach has three aspects:

1. Investigate the nature of wheel-induced soil behaviors by directly observing sub-surface soil motions. A variety of common wheel types and operating scenarios are investigated for soil motion behavior variation between wheel types, consistency of findings with literature and if observed soil behaviors have been documented during prior research.

2. Observe sub-surface soil motions directly to determine how soil behavior and traction processes influence wheel traction. The in-depth investigation of a limited set of soil motion behaviors is conducted during the analysis of grousered wheels and push-roll locomotion for the purpose of associating soil behaviors with measured traction gains.

3. Formulate explanations of traction processes and to improve design of traction devices by employing sub-surface soil motion analysis. The investigation of grousered wheels and push-roll locomotion is continued to demonstrate how soil motion analysis can be utilized discover traction processes specific to each device and how to use this information to inform design.

To summarize the approach, a survey into the soil motion response of common wheel types is conducted to show differences that are likely to influence traction through a variety of processes. This survey is followed by in-depth investigation of soil motion behavior of a sub-set of traction devices from the survey. The grousered type wheel and push-roll locomotion are investigated, in detail, through a rigorous SIIA test campaign to determine the mechanisms that govern numerous soil behaviors and how these soil behaviors in turn affect traction. The investigation into the wheel traction mechanics, based on observed sub-surface soil motion behaviors, leads to explanation of mechanisms behind specific traction processes occurring and how traction capability might be affected. These new explanations of specific traction mechanisms are then shown to be directly applicable to design of traction devices and to lead to increased performance. Performance gains are demonstrated for grousered wheels and push-roll locomotion. This approach will show that an empirical method of observing sub-surface particle motion can be employed in analysis to explain traction processes and inform design for improved traction.

1.5 Scope and Applicability of Research

This thesis investigates soil displacement fields (i.e. soil motion), underneath wheels operating in loose, granular soil. The purpose is to discover how observable processes within the soil govern traction and ultimately lead to exploiting these processes for gains in mobility through design. The limitations of the thesis research define the scope in two ways. First, the experimental approach, relying on Shear Interface Imagine Analysis, is restricted by the type of information that it provides: measured soil motion. Secondly, scope is limited by the traction scenarios studied, such as the wheel types, the loadings and the soil types investigated.

The SIIA method produces high fidelity soil displacement field measurements of a cross-section below a wheel. Although this allows for quantitative measurements, the studies conducted in this body of research are mostly qualitative. Comparative studies, observing phenomena of soil as acted on by a wheel, are utilized to discover new processes or to explain complexities of traction that are not well described. The high level of resolution, the ability to see time varying soil displacement and the experimentation of many wheel types/scenarios make for a unique set of experimental results that provide numerous first time insights into many traction processes. As such, simply observing soil displacement fields allowed for conclusions to be drawn, forming new explanation of mechanisms governing traction for multiple devices. This qualitative approach forms the basis of this research but also is a limitation that must be recognized. As many important aspects of the soil are not measured, it must be recognized that conclusions formed from this research were not confirmed via stress measurements or load measurement within the soil volume. Additionally, local soil strength is not measurable via the technologies used in this research. Findings are based off soil motion analysis, including failure planes, and reaction force measurements. This does not imply a lack of empirical evidence for support of the major conclusions as comprehensive experimentation campaigns were conducted to provide compelling evidence for each explanation of traction processes. The limitation, however, indicates a possible avenue for additional verification.

The wheel types, sizes, loading and soils investigated are typical of those encountered during planetary surface missions (i.e. planetary exploration rover scenario). Key aspects that define this scenario are lightweight vehicles (<1kN payload per wheel), relatively small diameter wheels (<50cm), operation in loose granular soil (low cohesion, highly frictional), and at low speeds (<10cm/s). Most, if not all terrestrial vehicles (including off-road vehicles) do not have all of these characteristics and therefore this research generally does not apply. Although, some aspects of this work can be extended to other applications, specific results, describing traction processes, focus on the exploration-class rover scenario. There are systems, from both past missions and from recent prototypes, that exist which operate at high speeds, high wheel loadings or different surface materials where results from this thesis might not apply. However, the scenario encountered most often, and to be expected in the near future, is that of the scenario within the scope of this work; exploration-class rover for environments such as the Moon and Mars. To summarize, the findings generally apply only to the planetary rover scenario, where the vehicle and soil of interest have characteristics as described above.

In addition to the general traction scenario that planetary rovers form, the research presented in this document focuses specifically on loose, granular soil. The soils that were utilized in experimentation were prepared to a homogeneous state, consisted solely of a pure regolith simulant and were leveled to form flat terrain. No gravel or small rocks were added to the material and the maximum particle size was 1.5mm in diameter. This narrow scope of terrain type does not faithfully represent real terrain, such as intermittent rocks, inclines and bedrock under-layers, however, it approximates many worst-case conditions and enables research of fundamental traction elements; thrust and motion resistance. The focus on pure loose, granular soils allows for generalization of many of the findings to more complex terrain scenarios.

1.6 Thesis Organization

This thesis is organized as follows. The chapters should be read in order as concepts build from previous chapters and because the document follows the chronology of the research.

Chapter 2 describes primarily the deficiencies of current terramechanics theory and models. This chapter offers the technical motivation for the research conducted in subsequent chapters and provides background on the general approach to using terramechanic models and underlying assumptions.

Chapter 3 gives a detailed explanation of the novel analysis method and apparatus (hardware and software) developed as part of the thesis research. Interpretation, of example results, is provided for demonstration of use as a terramechanics analysis tool. The SIIA method is relied upon for all experimentation in the thesis research and is the source of the experimental data used in support of proving the thesis statement and in fulfilling the thesis objectives.

Chapter 4 provides an overview of experimental results (using SIIA) from a survey of soil response due to the operation of common wheel types, vehicle parameters (such as payload) and a non-typical locomotion mode called push-roll. By simultaneously taking a broad look at the soil behaviors due to many wheel types, this chapter, early on, reveals that the soil below the wheel undergoes complex processes of which there exists little knowledge with respect to different wheel types. The variation observed and characteristic differences of soil shearing planes, flows and resistive processes, are readily evident and SIIA visualizations make for compelling support that an in depth study is warranted to further explain traction processes.

Chapter 5 details two significant experimental campaigns conducted to investigate specific observed soil behaviors or specific wheel parameters that might govern traction. This chapter sets out to prove that the empirical method of observing soil behaviors due to a wheel in operation, can lead to new explanation of mechanisms affecting traction. The explanation of traction mechanisms formed from this research are then extended to design in order to show that this new understanding can lead directly to performance gains. Two traction device types are thoroughly studied to show, by example, that soil behaviors can be researched to learn new terramechanics processes and to achieve improved performance of designs.

Chapter 6 provides concluding remarks and discusses of the principle results of this research. The results are shown to directly support the thesis statement (from Section 1.3.1). In addition to these results, experimental highlights are discussed to capture major findings of potentially significant impact on the terramechanics research community and on the rover development field. A summary of the major contributions of the research is provided and significance is discussed in the context of terramechanics as it exists today. Future research is discussed in terms continuation of the SIIA experimental program that has sprung from the research initiated as a part of this thesis.

2 Prior Work and Background on Terramechanics Modeling

2.1 Terramechanics Models and Theory Basic Assumptions

Terramechanic theory, that is routinely relied upon to explain physical phenomena for planetary rover applications, has been shown to be insufficient as soil shearing planes and soil displacement other than compaction has not been taken into account. Additionally, soil behavior implied often does not act as observed in reality for loose, granular material. Of the established theories, Wong states, *"the basic assumption underlying existing wheel theories is inadequate in that soil does not flow akin to that beneath a plate."* Continuing he states, *"There is a close relationship between the characteristics of the flow patterns beneath a wheel and its performance. Therefore, a sound theoretical basis for the prediction of wheel performance should be established on the knowledge of actual soil flow beneath wheels*."(pp. 268) [5] Theories must be developed that take the above into account. It is arguable that Wong's statement has not yet been fulfilled, as rigorous investigation into actual soil response to wheel operation has not been conducted. Ad hoc methods of accounting for wheel slip and soil displacement have been established, however these methods are not related to actual mechanics, but rather employed to fit to trends in measured reaction loads such as increasing net traction with wheel slippage. Additionally, existing terramechanic theory and models have limitations when employed to aid design, as they have been developed primarily for prediction of performance and do not account for effects of commonly implemented traction improving features such as grousers or wheel compliance due to complexity of modeling the wheel-soil interaction.

Current terramechanics methods are based off the works summarized by Bekker over half a century ago [4]. The foundation of the theories used today has remained essentially unchanged from those original works. Many assumptions that are employed to describe wheel-soil interaction for loose, granular materials, have been criticized for discrepancies when compared to real systems and for being mostly empirical rather than mechanics-based [8]. A brief explanation of the underlying principles of terramechanics, applied to wheel traction, will help show the current state of this field and how it has motivated the this thesis research.

2.2 Basic Terramechanics Analytical Models

2.2.1 Soil Properties as Related to Terramechanics Models

Two principles are used to determine soil response to loading and the ability to predict soil failure under wheels. These principles are the Pressure-Sinkage relationship, Equation 1, and the Mohr-Coulomb failure criterion, Equation 3.

$$p = kz^n \qquad \text{Equation 1}$$

Equation 1 simply states that the average *pressure,* p, under a plate, pushed into homogeneous, terrain is dependent on an exponential function of *sinkage,* z. Where the *sinkage exponent,* n, is a soil property dependent on wheel size and k is the *proportionality constant*.

$$p = \left(\frac{k_1}{b} + k_2\right) z^n \qquad \text{Equation 2}$$

Equation 2 is a more widely relied upon expression describing the Pressure-Sinkage Relationship of wheels. The *proportionality constant* has been modified to account for the contact area dimensions. Where b is the smaller dimension of contact (typically wheel width). k_1 and k_2 are again soil *sinkage parameters* that are not sensitive to contact area dimension for large plates and large aspect ratios [9]. The Pressure-Sinkage relationship, although semi-empirical, is the most important expression in terramechanics as shear strength is largely related to normal load (pressure) and motion resistance is proportional to sinkage (i.e. pressure and sinkage). It should be noted that this expression could take on many forms depending on the traction device (track, small/large wheel, pneumatic tire, etc.), on the accuracy required versus the number of empirical terms and on the users ability to experimentally determine the various constants that might be dependent on their system.

$$\tau_{max} = c + \sigma tan\varphi \qquad \text{Equation 3}$$

The maximum shear stress that a soil can support before a limit is reached in ability to support increasing shear load is considered failure by the commonly relied upon Mohr-Coulomb criteria shown in Equation 3 [9] [10]. This equation describes the relationship of shear strength to normal pressure, where τ_{max} is the *shear strength* of the material, c is the *apparent cohesion* and φ is the *angle of internal shearing resistance (friction angle)*. This equation shows the dependence of shear strength on normal loading.

There are three methods that are commonly used to determine the two soil strength values (c,φ), each yielding different results with respect to wheel mechanics due to different boundary conditions imposed. The *triaxial shear test* is a method commonly utilized by geotechnical engineers for a wide range of granular materials. It allows loads to be applied independent of a constant confining pressure [11]. A key aspect of this method is the ability to produce soil failure that is representative of the bulk material, typical of an engineering property. Strength properties are measured by applying an external load, to a soil sample in an extensible membrane, while hydrostatic pressure is applied. The sample is allowed to dilate (expand/contract volumetrically) naturally as shearing occurs (i.e. constant pressure, free volume change). This method is designed to evaluate the principle stresses, at failure, by use of stress-strain information inferred from external loading and bulk displacement measurements. These stress measurements are used to calculate the soil *apparent cohesion*, and *angle of internal shearing resistance* values (c, φ). Another method commonly used to find soil property values (k, n, c, φ) is the bevameter test, that was developed by Bekker [3]. This method relies upon an apparatus representative of a wheel since steps are taken to have similar interaction between the test plate and the soil, to that of a wheel rim with the ground. As such, more accurate results can be obtained when using the Pressure-Sinkage and Mohr-Coulomb relationships because many of the complexities in modeling of the soil failure are encapsulated in the bevameter measurements. The bevameter produces soil strength values that are of practical use if these relationships are used to look at trends in changing basic wheel parameters or during trade studies over a limited design space. However, generalization of the soil property values becomes difficult as much of the response is dependent on the test plate itself. The grouser effects on soil failure, on sidewall drag and on sidewall bearing capacity, are examples of test plate parameters that cannot be independently represented by current theory.

The bevameter apparatus (Figure 4) typically consists of a flat plate (sometimes two) and of a ring shaped plate (annulus) with grouser like protrusions that apply shear loads when applying torque. Both the flat plate and ring are of similar size to the contact area of the wheel of interest to model [12]. The flat plate is used for Pressure-Sinkage relationship data, while the ring (annulus) is used for Mohr-Coulomb failure data. The measurement of torque, at soil failure over various normal loads, is used to determine shear strength versus normal load. Applied load, versus penetration depth, determines the $k \; and \; n$ pressure-sinkage parameters.

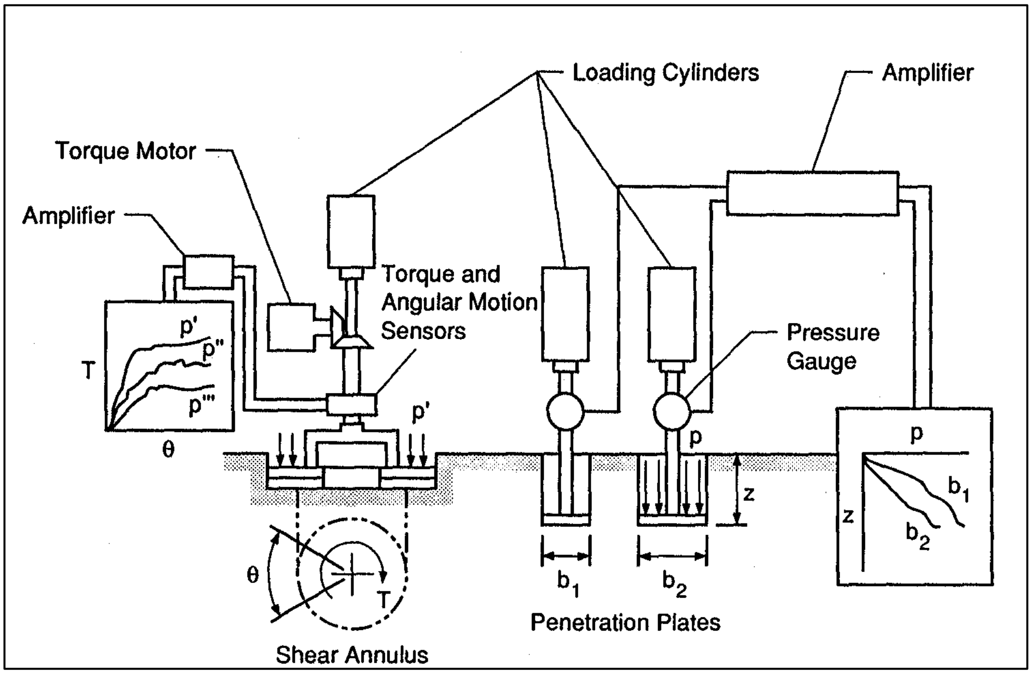

Figure 4: Schematic representation of Bevameter measurement unit [9]

A third alternative, to measure *apparent cohesion* and *angle of internal shearing resistance* values (c, φ), is the direct shear test. This test is similar to the bevameter torque ring. However, a rectangular plate is forced to displace in a linear motion to infer shear strength.

An explanation, of these methods to measure soil properties, is provided as it is important to realize how the soil test implement differs from a wheel it represents. Also, the measured soil properties are strongly dependent on the geometry of the measurement unit plate compared to that of the wheel of interest for modeling. These issues are discussed later in the chapter.

2.2.2 Terramechanics Analytical Models

The Pressure-Sinkage and Mohr-Coulomb failure criteria are the two underlying expressions utilized to model wheel-soil interaction and predict traction performance. There are many assumptions made to apply these equations to the form of a wheel that supports a payload, reacts torque and generates thrust. Generally speaking, the over-arching assumption is that a wheel, in its basic form, will interact with the soil the same way as a flat plate and that the Pressure-Sinkage relationship can be used to account for the non-flat geometry of the rim. More specifically, soil shearing and failure are of the same type as a plate, soil displacement or transport is insignificant and soil properties are homogeneous throughout the affected regions during wheel operation.

The net traction generated by a terrain-vehicle system, termed *Drawbar Pull*, is the *thrust* generated minus any *motion resistance* forces apposing vehicle travel. This is often expressed as in the form of Equation 4, where DP is the *drawbar pull*, H is *thrust* and R is the sum of *motion resistances* [3] [10]. This expression, allows for easy explanation of the basic processes involved in the operation of a traction device.

$$DP = H - R \qquad \text{Equation 4}$$

Drawbar pull normalized by vehicle weight (or wheel payload) is a form often referred-to. This form is called *pull coefficient* [13].

$$Pull\ coefficent = {}^{DP}/_{W} \qquad \text{Equation 5}$$

where W= vehicle weight or weight-on-wheel.

Explaining the derivation of wheel *resistance*, R, will highlight assumptions made and the lack of accounting for many physical considerations, such as soil displacement. These expressions are remarkably simple and, unfortunately, make the assumption that the behavior of soil underneath a wheel, in motion, is similar to that of a flat plat at rest in the ground.

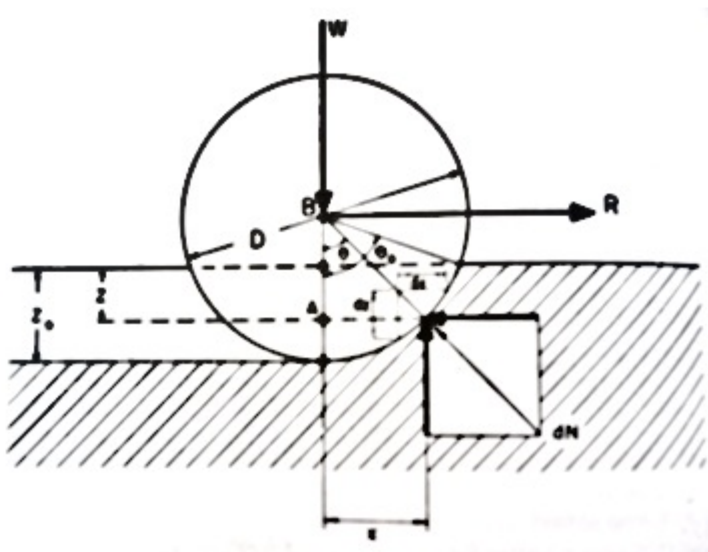

Figure 5: Diagram of rigid wheel, in deformable ground, with loads relevant to motion resistance indicated. Image credit: [9].

The use of the motion resistance relationship, R, and assumptions involved with applying it is described below.

$$R = \int_0^{z_0} pb\ dz \qquad \text{Equation 6}$$

Where R is *motion resistance*, p is rim pressure (described by Pressure-Sinkage relationship, Equation 1), b is wheel width, z is sinkage a point along the rim, and z_0 is total sinkage (see Figure 5 for meaning of variables).

The motion resistance expression (Equation 6) [9] has a physical meaning. It assumes that the net motion resistance is the horizontal component of the normal pressure, on the wheel rim, created as the result of sinkage. The normal pressure, p, is governed by the Pressure-Sinkage relationship (Equation 1). Equation 6 implies that the motion resistance, on a wheel, is equal to the horizontal component of the soil acting on a static rim when pushed vertically into the ground. Applying this concept to estimate the performance of wheels is not valid for the planetary rover application, as small diameter rigid wheels in loose, granular soil do not push on soil in a manner similar to a vertically loaded plate. In this application, sinkage is significant, soil flow is present and the wheel rim pushes soil in a horizontal manner. It should be noted, that this equation was formed for the prediction of motion resistance of a towed wheel, however, it is often assumed to apply to driven wheels [14].

The issue of most concern is the lack of accounting for soil transport and non-vertical soil displacement. Both the calculation of normal pressure along the rim (which is the resisting force) and the quantity of soil interacting with the rim are drastically altered if or when the soil moves horizontally. Of common understanding is that the sinkage of a wheel can be dominated by slip-induced sinkage as a result of soil transport [3]. This is especially the case for planetary rovers where wheels are operating in loose, granular soil, resulting in a non-zero slip rate that is routinely medium to high. Only static sinkage is accounted for in the pressure sinkage relationship. As soil transport is not modeled, calculations relying on sinkage, such as motion resistance and thrust, cannot be estimated with reasonable accuracy. Additionally, much of the soil at the front of a wheel that is assumed to be resisting travel might be pushed to the side for narrow wheels, or transported away from the contact region due to wheel rotation when slippage occurs. These issues lead to difficulty in determining the sinkage value, z, of the pressure-sinkage relation, resulting in large error in motion resistance estimates.

Of predicting sinkage, Bekker states "the sinkage of powered wheels (including slip sinkage) appears to be beyond solution with a workable analytical model. Only static sinkage, such as is expressed by equations… , can be used as a first approximation, and although this is good in wet cohesive soils, it is poor in dry sand." (pp. 452) [3]

2.3 Recent and Past Work to Improve Analytical Models

Research attempting to fix shortcomings in common terramechanics models, have focused on improved pressure distributions over the contact area [15] and on changes in pressure distribution with respect to slip [16] [17]. Recent research to account better for the curved shape of a wheel, has been undertaken to develop a modified pressure-sinkage relationship [18]. However, this does not address the issue of soil movement and adds additional empirically determined terms for curvature and width. Unlike the terramechanics community, current planetary robotics mobility research has been focusing primarily on three themes: wheel prototype performance analysis; vehicle motion prediction via computer modeling and development of novel mobility systems. Performance analysis studies have focused on the net traction produced by a wheel and have endeavored to make discoveries through the study of net traction changes due to parameter variation rather than a parametric study involving experimental investigation of the traction mechanisms of the wheels. This method has resulted in a lot of research that describes the potential performance of many example wheel configurations but lacks well supported explanations as to sources of traction gains and the traction processes occurring.

As an example, parametric studies of grousered wheels are repeatedly encountered [19] [20]. To date, these investigations, of the function of grousers have taken the approach of relying solely on performance measurements. Net traction, sinkage, slippage, wheel torques, power and reaction forces are typically measured during single wheel testing over a wide range of parameter changes, such as grouser spacing or height. Trends in the data are used to determine optimal parameter combination and conclusions are often inferred from these results. This approach is suitable for determining the response and performance of specific designs, but provides limited information on the unique mechanisms within the soil that governs traction for the wheel type of interest. Therefore, an incomplete picture of how grousers function still exist and a lack design guidelines persists.

2.4 Current Planetary Mobility Research Efforts

Investigation of vehicle configuration and suspension types has also been a topic of interest to the planetary mobility research community. Vehicles, with a great number of different configurations, have been prototyped and studied over the last decade. These systems vary in number of wheels, suspension kinematics and articulation types, passive and active control, and even walking or hopping locomotion. These vehicles are designed to traverse more extreme terrain and perform more complex tasks, but are still governed by poorly understood processes occurring in soil during locomotion. Many prototype systems such as the ExoMars rover mobility system [21], designed for a European Space agency Mars exploration mission, have undergone extensive analysis utilizing tools to assess the effects of vehicle configurations. These analysis tools include the Rover Chassis Evaluation Tool (RCET) [22], LocSync framework [23] and other efforts to standardize performance evaluation [24]. These methods provide great insight into the potential changes that basic vehicle configuration can have on performance. However many of the complexities, such as the effects of wheel type and even locomotion mode, cannot be accurately represented. More importantly, these tools may have limited use for development of novel systems with complex wheel-soil interactions, such as the recent JPL ATHLETE platform [25] and the NASA Chariot mobility system [26], both with active suspensions and possible secondary mobility modes.

In recent years, the incorporation of analytical terramechanics models into multi-body simulators has received the most effort from the robotics-terramechanics research community. Full mobility system simulation modeling vehicle kinematics and wheel-soil interaction allow for prediction of vehicle path or response to three-dimensional terrain [27] [28]. This research is valuable in providing a framework for simulation and rover control development [29]. However, as advancement of the underlying terramechanic models is not undertaken, little is provided in terms of aid in detailed design or insight into developing novel full vehicle systems.

2.5 Past Subsurface Imaging Work

2.5.1 Soil Particle Motion Analysis for Terramechanics Research

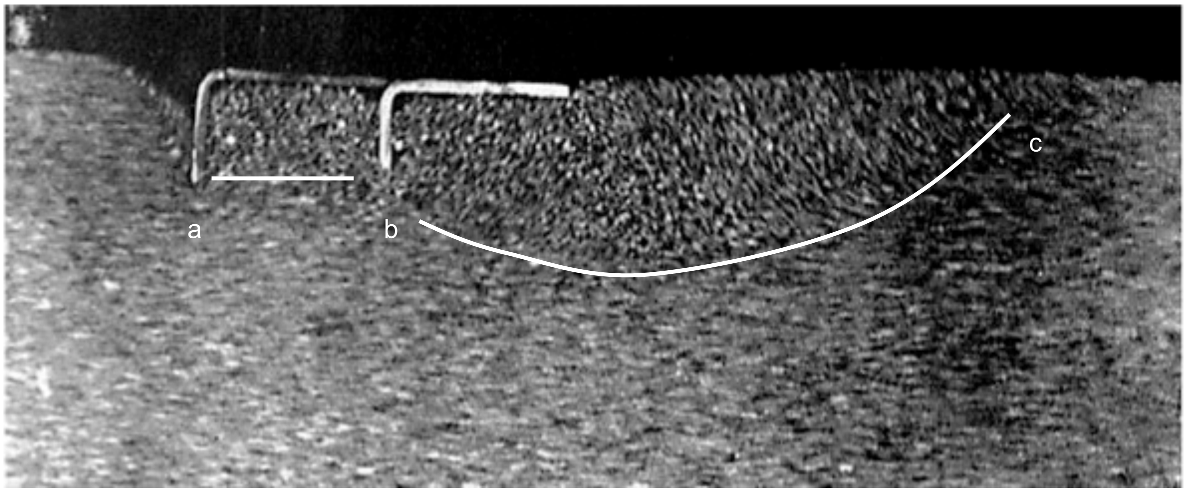

Figure 6: Example of previous sub-surface soil imaging methods, conducted by M.G. Bekker, that rely on long exposure film to infer moving and stationary soil, as affected by a traction device [14]. Planes, a-b and b-c, are interpreted to be primary soil failure planes as transition between blurred (moving) and non-blurred (stationary) soil particles.

The Shear Interface Imaging Analysis, method developed during this thesis research, builds off of earlier analysis methods utilized by Bekker (Figure 6), Wong (Figure 7), Harrison [30] and others. There have been prior efforts made to image soil effects due to wheel travel [5] and to image the operation of other devices such as excavation implements or footings [30] [31] [32]. For terramechanics research, the technique of observing soil motion utilizing long-exposure film photography has been the most extensively used. The film exposure time is sufficiently long in duration to intentionally create image blur and particle streaking. Soil engaged by the wheel is maintained in the camera frame and thus does not blur. The interface between blurred and non-blurred regions is interpreted as primary soil failure planes (Figure 6, lines a-b and b-c). Streaking of visually identifiable particles enable inference of soil motion direction.

The 'shear interface' is a term describing the primary failure planes and outer extent of soil shearing that develop in the soil below a wheel. It is sometimes also called "slip planes." Figure 6 shows an example of this concept. The lines drawn on the figure, a-b and b-c, denote the shear interface.

The imaging work conducted by these researchers produced extensive results in their respective fields, but a limited amount of the work can provide direct insight into the application of design for planetary mobility systems. Previous research focused on the validation of existing terramechanic theory, however the analytical models of interest are limited to simplified wheels. As such, the experimentation space was also limited to simple/idealized wheels (rigid, wide, no grousers, low slip ratios), without an investigation of soil behaviors due to a range of common design parameters and common operating scenarios. Also, these film photographic techniques, of soil imaging, produced lower fidelity results, were not quantitative and could not assess time varying responses present in soil during wheel operation. Results of this thesis research show the inability to assess time varying response is a limiting aspect of previous research and hid many important soil motion processes.

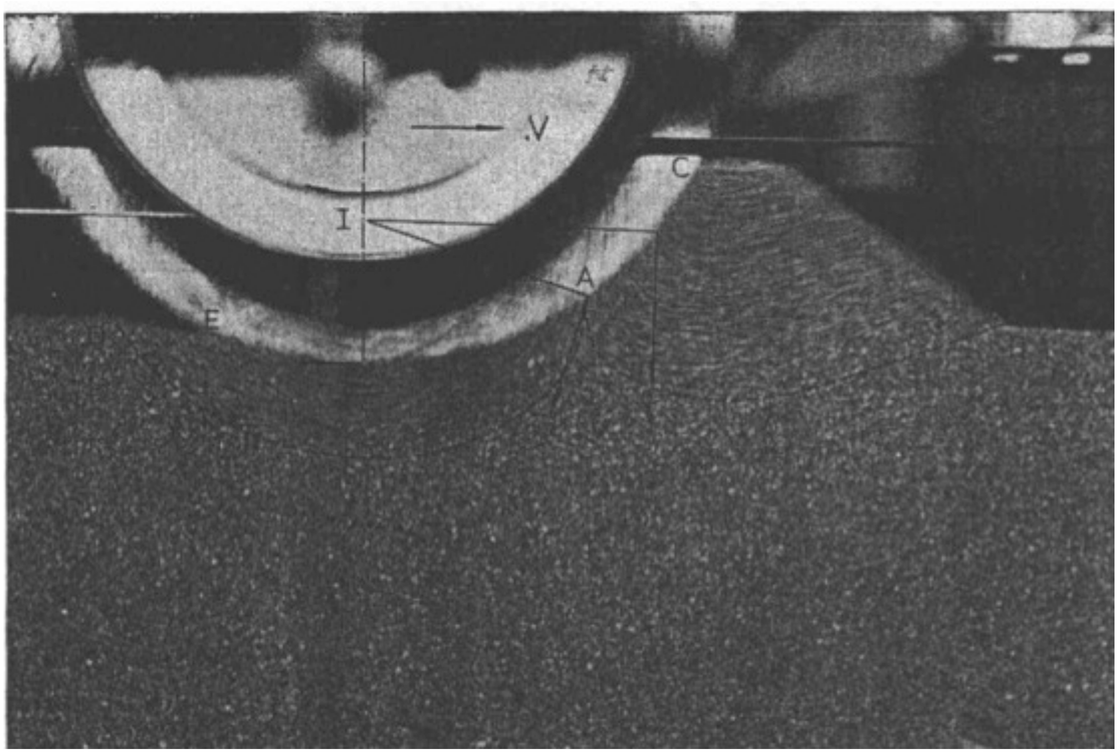

Figure 7: Photographic long exposure film method to infer primary soil shearing planes underneath a wheel. A wheel, at 37% slip, is shown as operating in loose, granular soil (dry sand). Wong noted many important conclusions from these results shown [5].

Many of the early terramechanics imaging researchers, relying on long exposure imaging, concluded that terramechanic theory does not represent the large motions soil undergoes and that similar experimentation methods should be utilized for model development and validation of design [5]. These findings further motivate the research being conducted that utilizes the new Shear Interface Imaging Analysis method for higher fidelity soil motion measurement.

2.5.2 Modern Techniques of Particle Velocity Measurement

Modern techniques for particle image velocimetry (PIV), the method relying on image cross-correlation, originate from the need to measure fluid velocity fields. PIV became a common research tool in the field of fluid dynamics in the 1980's [33]. More recently PIV has been used to measure soil displacement of granular materials. Most of these techniques rely on conventional PIV methods, developed for the measurement of fluid velocity. Adaptations to produce visualization of soil motion have included tracking tracer particles exposed to UV light [34], observing changes to a grid pattern of different-colored particles [35], and applying white light speckle autocorrelation to an arrangement of natural and colored sand grains [36]. These techniques utilize specialized equipment such as high-speed cameras, pulsed lasers, multi-phase LED lamps [37] [36] and/or the alteration of the soil specimen via reference markers or coloring [38] [36].

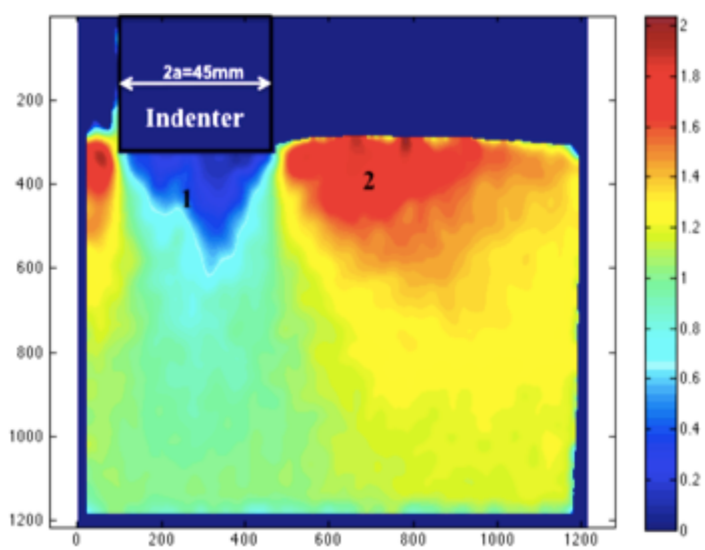

Figure 8: Velocity field of granular material derived from optical flow algorithm. Soil motion is due to the action of an indenter. Image credit [39].

Even more recently, the optical flow computer vision algorithm has been utilized in the measurement of granular soil displacement for the purpose of localizing soil failure planes under the action of simple indentation loading [39] (Figure 8). The use of optical flow in this in this application is limited and usually part of a hybrid system requiring other PIV techniques as well [38]. Optical flow has many benefits as it enables high fidelity measurement of soil motion (both accuracy, resolution and spatial density of information) while requiring only relatively low cost digital cameras and readily available software packages, and no alteration of the soil specimen. Optical flow is the image processing technique utilized by the SIIA method presented in this thesis. SIIA, for the first time, applies the optical flow algorithm for the purpose of studying soil particle motion underneath a wheel. The key innovation of SIIA is the application of optical flow specifically for terramechanics research.

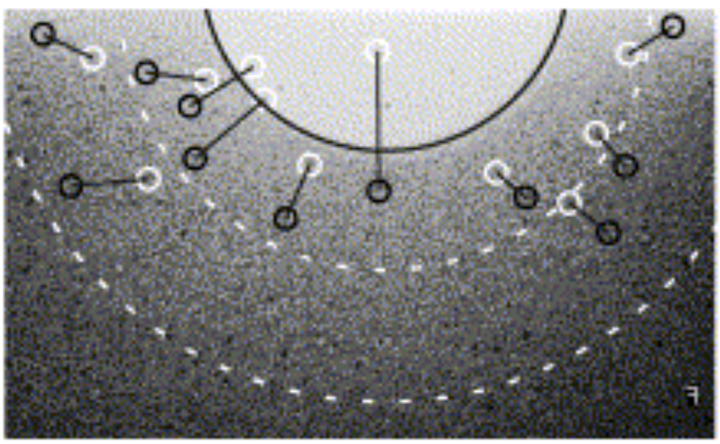

Figure 9: X-ray image of sub-surface soil deformation are used to visually validate pressure-sinkage model. This image enables analysis of the dilation of the soil being acted on by a wheel shaped indenter. Image credit [40].

Another visualization technology utilized for terramechanics and soil mechanics research is x-ray imaging. Both standard x-ray imaging and x-ray computed tomography (CT scan) are widely used for localization of shear bands within soil [41] (similar to failure planes) and detection of void ratio [42] (density) for the purposes of soil mechanics research. Standard 2-dimensional x-ray imaging has been used in static testing of wheel-like specimens for the development of modified terramechanics models. This primarily provides relative density information and shear band information by comparing experiment “before and after” images. Figure 9 illustrates an example of these two aspects of soil during the study of soil response to various wheel curvatures [40].

2.6 Conclusions Drawn From Previous Work

The theory that is currently available to support the design and evaluation of wheeled planetary mobility systems is not of sufficient accuracy to estimate performance and is inherently not useful in guiding design. Current wheel-soil models are not representative of the actual soil shearing processes occurring, thus leading to misunderstandings of traction fundamentals. In addition, this misunderstanding of traction can also lead to poor operation of vehicles during actual missions.

Previous research, as discussed in this chapter, highlights the need to identify complex soil strain fields and failure planes as influenced by a wheel in operation. Methods of modeling wheel performance would benefit from accounting for these soil processes. However, simply understanding how the soil strain fields affect traction can allow for new terramechanics understanding to be generated thus aiding in traction device design.

3 Development of Shear Interface Imaging Analysis

3.1 Motivation for Sub-surface Soil Analysis

In an effort to directly investigate the soil shearing patterns and traction processes occurring due to wheel operation, the approach of empirically investigating soil particle motion was taken for this thesis. The design of traction devices, such as wheels for planetary rovers, rarely involves the analysis of the soil motion, of failure patterns and of soil transport processes. As the performance of a traction device in loose, granular soil is ultimately governed by both the bulk soil properties and the complex conditions induced a wheel, it is important to account for varied and intricate soil failure patterns and transport processes. Minute details of the wheel rim geometry or mechanics of the wheel carcass have a profound effect on the shearing processes. The study of wheel induced soil motion provides insight into these poorly understood aspects of traction that often occur in the case of planetary rovers on loose, granular soils.

3.2 Description of Shear Interface Imaging Analysis Technique

Development of a technique, called "Shear Interface Imaging Analysis (SIIA)," for detailed measurement and observation of the shear failure planes and soil transport processes, was undertaken as part of this research. This method relies on photographing soil, through a glass-walled bin, as a traction device operates. These images are then used to produce full-field motion plots at soil particle level detail via computer vision algorithms. The soil particle motion data is subsequently used for terramechanics analysis. The SIIA technique has proven to produce accurate results enabling in-depth investigation of unconventional locomotion modes such as push-roll [43] [44] and of various wheel types for planetary surface vehicles [6] [7]. This technique is also useful for investigation of more generalized wheel parameters and fundamental traction processes in various traction scenarios such as on the Moon and Mars.

This chapter introduces the method of Shear Interface Imaging Analysis and, by use of examples, shows the value of using the SIIA technique for sub-surface soil investigation.

3.3 Description of Apparatus

The experimental apparatus, constructed to analyze the soil motions below a wheel, consists of a glass-walled soil bin (Figure 11) filled with granular material, of a traction device (such as wheel), of an actuated horizontal axis of motion (Figure 10) and of an imaging system. The wheel module (Figure 13) of the SIIA test bed is controlled, in coordination with the horizontal axis, to create a commanded, constant slip as the wheel travels forward. A linear rail allows the wheel to translate freely, in the vertical direction, allowing for natural sinkage to occur. The free vertical axis also allows for the transmission of payload to be applied to the wheel in the form of dead weights. A 6-axis force/torque sensor is incorporated to measure reaction loads, specifically in the horizontal (travel) direction, as a result of traction generated. Sinkage is measured via an optical encoder affixed to the vertical free linear axis. All telemetry: wheel angular velocity; travel velocity; slip, sinkage; load and power, are logged simultaneously, at 20Hz or higher, to a central desktop computer that also controls the experiment configuration and imaging system.

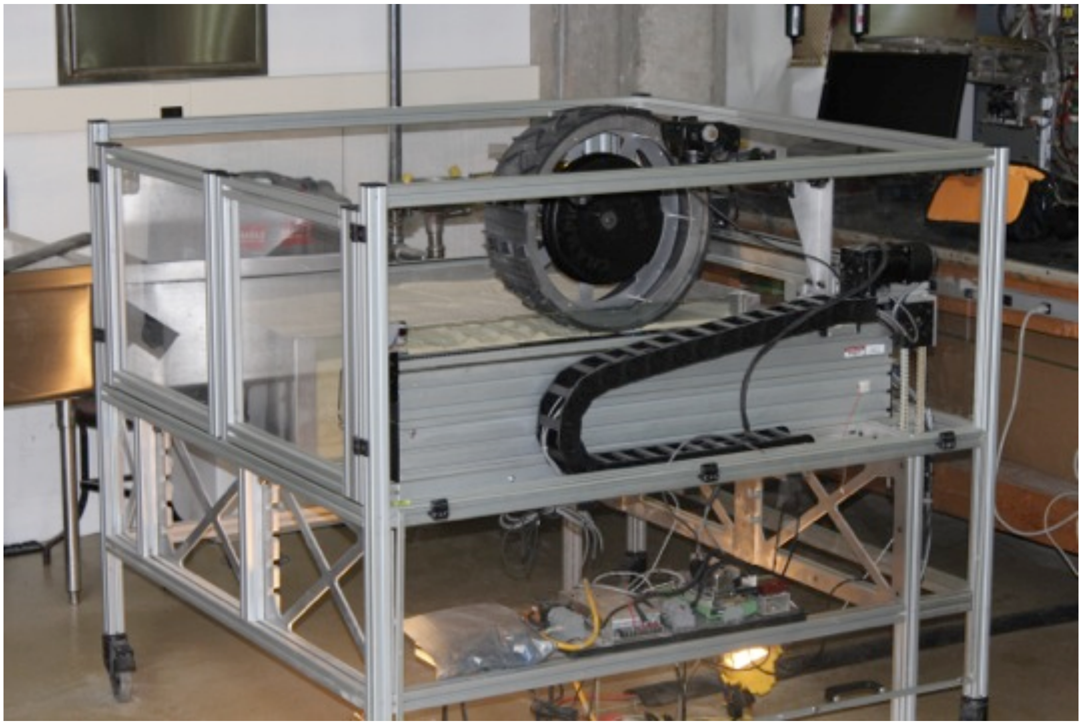

Figure 10: Single Wheel Soil Imaging Testbed. Wheel travels, from left to right, with controlled slip along a belt-driven linear axis or travels, in a self-propelled condition, with no external horizontal load or restriction applied. Note, a 50cm diameter half-wheel against the glass is shown.

Figure 11: Alternate view to show glass wall of soil bin and depth of sand.

The wheel for SIIA experiments is pressed against a sheet of tempered glass that extends the depth of the soil bin. The wheel utilized in experimentation, is of half the width of the actual specimen of interest (example shown in Figure 12). That is, for a symmetrical wheel, it is equivalent to cutting the wheel in half, perpendicular to the axis of rotation. It should be noted that most wheels are symmetrical in their tread and rim profile, so no special consideration due to utilizing a half-wheel is needed.

Figure 12: Example of a half-width specimen shown (left) and the full-width wheel of actual interest that it represents (right).

The payload applied must also be half of what the full wheel normally carries. The half-width wheel and half payload method results in reaction loads such as drawbar pull, normal load and torque to be half of that of the actual wheel specimen of interest. This method remains a valid technique since the soil response is the same to that of the full-width wheel. As such, reaction loading can be assumed to be twice what is measured for the half-width wheel. The use of a half-wheel and glass wall, has been relied upon for over 50 years [31] and has been experimentally validated for loose granular soils and clays. The most important consideration is that the shear stress, at the glass-soil interface, should be the same as that of the soil-soil plane at the center of a full-wheel. If the shear stress (created by soil-glass friction) is negligible [45], then the glass surface acts as a plane of symmetry, allowing for the soil to behave as it would directly below a wheel, twice as wide, due to symmetrical soil flows [5]. This boundary condition, of sufficiently low (ideally zero) shear stress along the plane of symmetry, is achieved by the use of tempered glass with a high hardness surface and by the low pressure of the soil particles against the glass wall. It should be noted, that for a symmetric wheel, there is symmetric soil flow and, therefore, no transverse soil motion occurs at the center plane of symmetry. Therefore, the boundary condition imposed by the glass restricting transverse flow is valid.

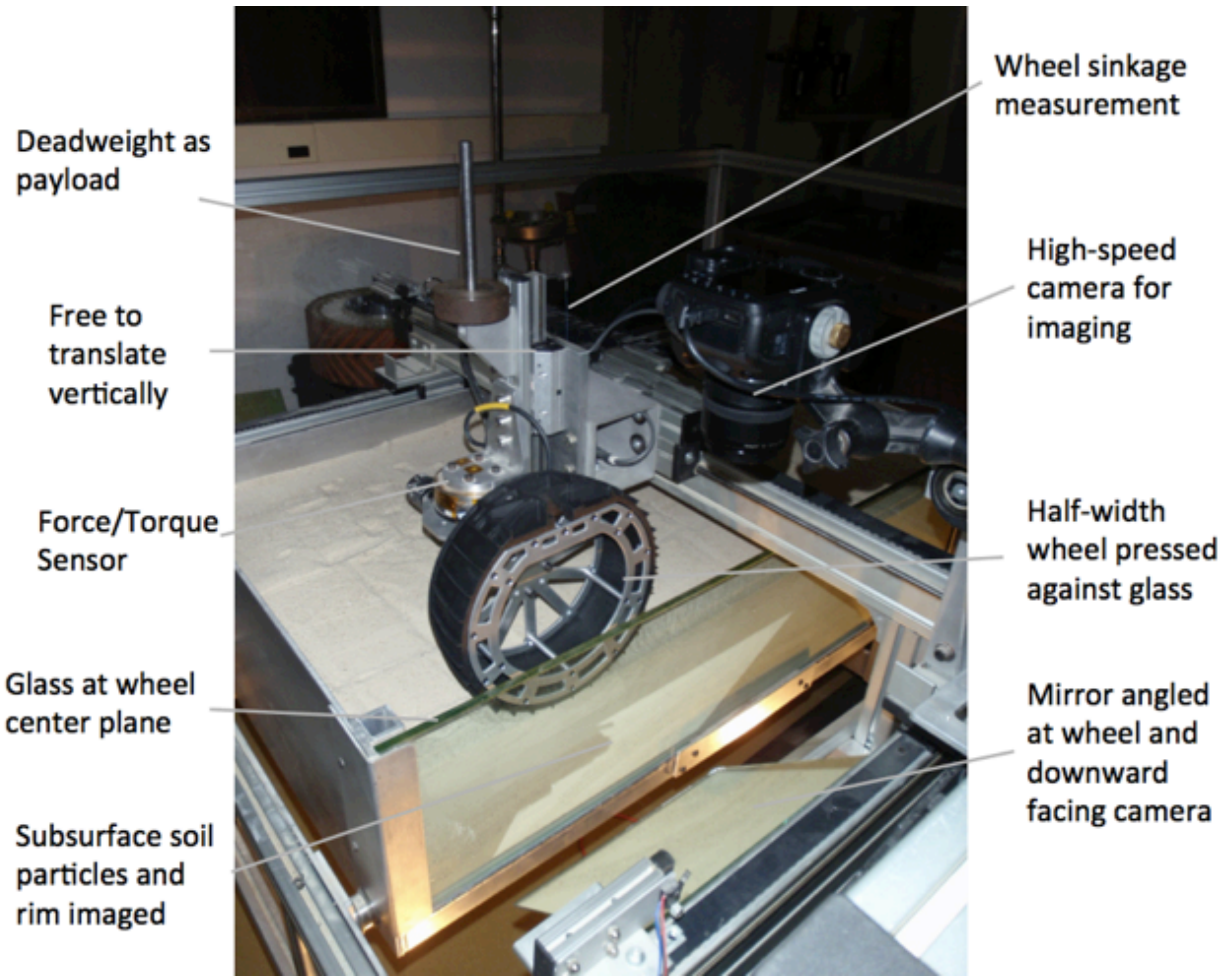

Figure 13: Wheel module, carriage (travel axis) and glass-walled soil bin. A 31cm wide by 22cm high cross-section of soil, below the wheel, is imaged with a still camera.

Figure 14: Example image from wheel testbed camera. This image acts as the raw data to be processed by computer vision techniques that produces a full velocity field of the soil motion. Note that the camera moves with the wheel travel (right).

Imaging, a cross-section of soil below the wheel, allows for the observation of soil processes at that plane only and of two-dimensional motion only. There are two assumptions made, when only observing the center plane, for conducting terramechanics analysis. First, the processes that can be seen, such as shearing planes or forward flow, are representative of most of the wheel width. For wheels that are not narrow, which most planetary rover wheels are not, this assumption is fair as the gradient of soil responses, such as shearing magnitude, from wheel center to edge would be expected to be quite low. The gradient in soil response is low because the confining pressure, due to the rim normal load, is much higher than that at the sidewall (rim edge) where there is little surcharge (i.e. sidewall effects not significant). The dominance of the rim normal load is especially true for loose, granular soils where cohesion is not present or when there is not extremely high sinkage (in which soil mass acts as significant surcharge). The second assumption is that the soil processes, observed at the wheel center, are the most important and dominant in governing traction. One would expect resistive processes, such as bulldozing and compaction resistance, to be highest at the wheel center where no lateral flow is present and where greatest soil mass is accumulated. Soil motion, produced by thrust generating areas, are also expected to be at peak magnitude at the center plane due to symmetrical flow underneath a wheel. These assumptions are reasonable. However, there exists little experimental data to prove that these assumptions hold true. When narrow wheels are studied, special consideration must be made to acknowledge the limitations of these assumptions.

The shearing analysis requires the ability to track soil motion. A digital SLR camera, model Canon D7, with a Canon EF 50mm Compact Macro lens (Figure 13), is used to image the wheel-soil interface and a cross-section of the soil below the wheel (Figure 14). Frames are logged simultaneously to a central desktop computer with the rest of the telemetry previously discussed. A frame rate of 8 frames-per-second is used and is sufficiently fast for the low speeds of wheel travel applied (1cm/sec). The frame rate utilized and the wheel travel speed result in a maximum soil displacement between frames of 1.6mm, however, the maximum displacement during most test conditions is 0.25mm. Extreme scenarios with high sinkage and lower slip rate result in the higher soil displacement condition.

The digital camera is mounted perpendicular to the soil bin glass wall and travels with the wheel in the horizontal direction as the carriage moves. For most wheel specimens (23cm to 50cm diameter), a 31cm wide by 22cm high patch of soil is framed and captures the complete shear interface and secondary flows produced by the wheel in the soil types within the scope of this research. Halogen floodlights are utilized to illuminate the soil particles and are placed at a high angle normal to the glass to prevent direct reflection of light in the imaging system.

3.4 Description of Algorithms

A novel aspect of this work, is the use of a computer vision technique not previously implement for terramechanics purposes, to measure soil motion below a wheel. The image processing comprises of an optical flow algorithm and clustering techniques. An overview of the complete process, from imaging to analysis plots, is presented in Figure 15. Clustering is used to initially separate each image into "soil" and "not soil" regions. The region classified as “soil,” then, undergoes further processing.

An optical flow algorithm [46] is implemented to track displacement of soil regions relative to a prior frame and to calculate a motion vector for each pixel. This step provides a high-density displacement field of size and resolution up to that of the raw camera images. The majority of SIIA plots, generated in this work, were processed from down sampled images to reduce processing times. Most results have frame dimensions, of 700 x 1300 pixels, which result in an effective pixel size of 0.19mm in terms of actual distance on the soil plane. The pixel size is smaller than the mean particle size (by weight) of the soil simulant, GRC-1, [47] that is used for most experiments in this research. Therefore, it is assumed that pixel displacement is representative of individual soil particle movement. The minimum resolution of measured displacement is not determined only by the effective pixel size (0.19mm) because the optical flow algorithm is capable of sub-pixel resolution [46]. As such, validation of the whole SIIA imaging system, with optical flow software, was undertaken to assess minimum resolution and absolute error. See Appendix 8.1 for validation and error analysis of the soil tracking implementation developed for SIIA.

Following calculation of the displacement field, soil motion is clustered into "significant" and "insignificant" magnitudes. No explicit threshold is used to demarcate these clusters, rather automatically adaptive clustering is used. The shear interface can then be derived from the boundary between significant and insignificant motions. Soil motion direction is calculated from the optical flow displacement vector fields, for regions exhibiting significant motions. Soil motion, in any direction, is plotted and an additional boundary is identified at points where the soil transitions between forward and rear flow.

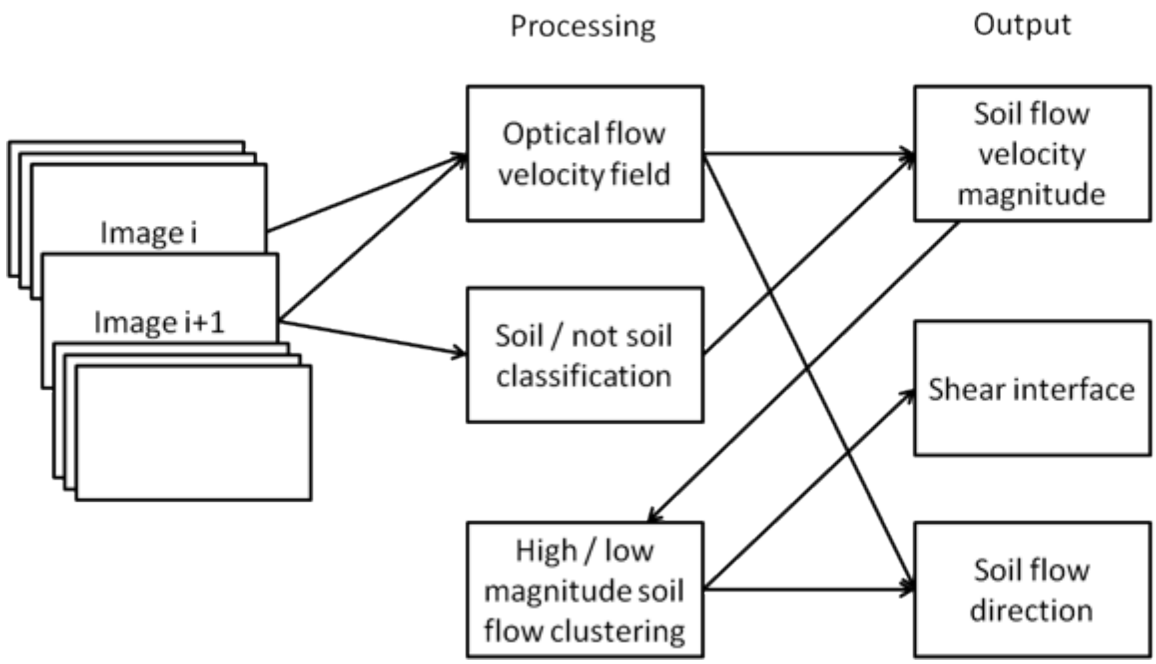

Figure 15: Processing steps, for image analysis, to produce soil motion and shear interface output plots.

Figure 16 is a sample output of the process. Shown is soil velocity magnitude, shear interface between moving and non-moving soil, soil motion direction (within region of significant motion) and boundary between forward and rear flow.

3.5 Use of Soil Displacement Plots in Terramechanics Analysis

The soil displacement field generated during single wheel experimentation can be used to identify the affect wheel parameters and design features have on performance by inferring traction mechanisms from the measured soil motion. Performance metrics such as net thrust produced, referred to as drawbar pull [4], are critical for evaluation. However, when relying solely on measured reaction forces, there is little information provided that aids in investigation of the underlying traction mechanisms governing the measured performance.

Observing soil failure planes and soil motion enables the qualitative analysis of how soil structure develops and reacts to thrust loads, causes of sinkage and travel resistance mechanisms. The shear interface is indicative of soil failure processes and soil failure type. In the SIIA plots, the shear interface is the boundary between moving and non-moving soil as determined by the clustering technique. When clustering is not employed, the shear interface is often determined by visual inspection.

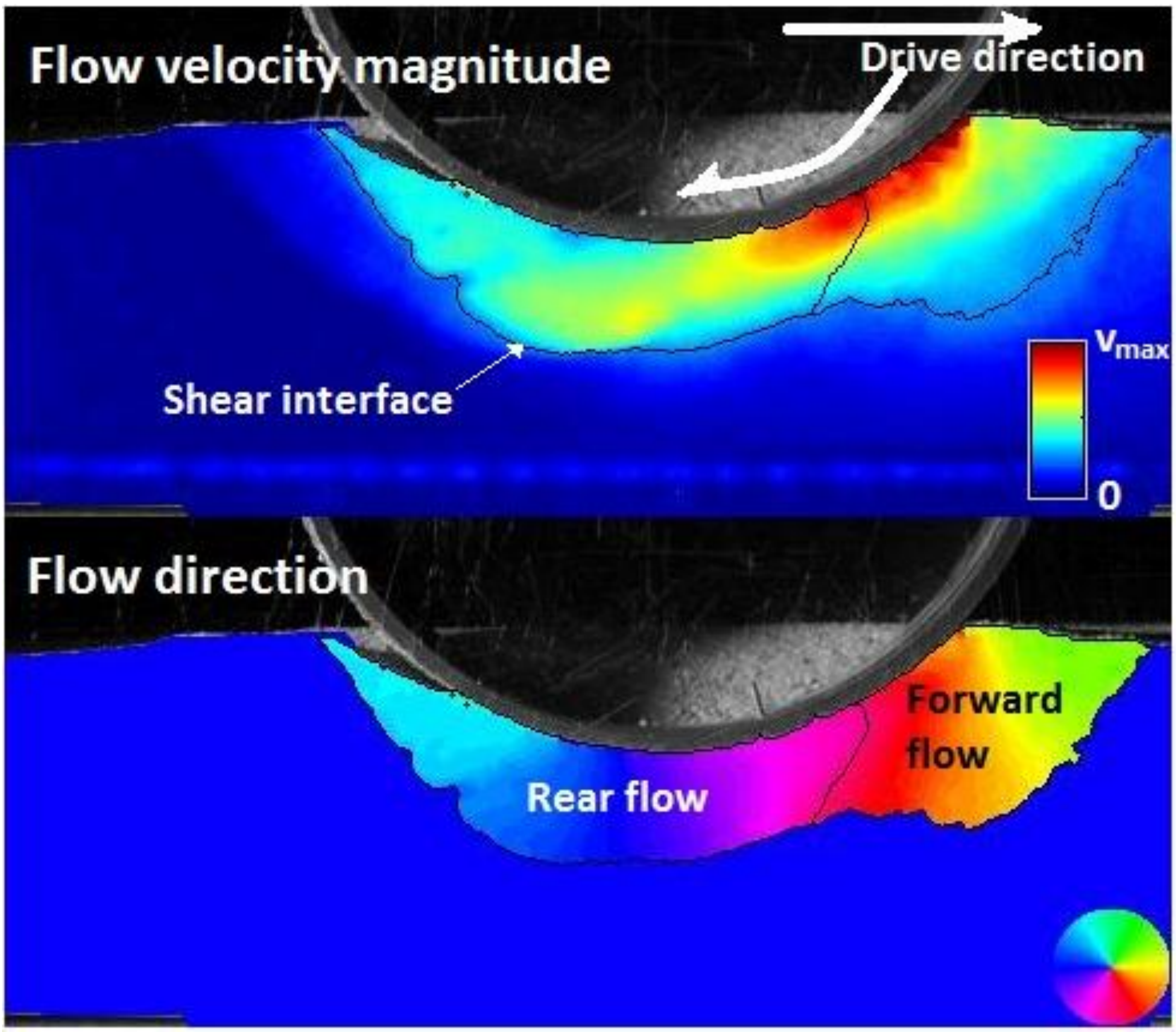

Figure 16: Shear Interface Imaging Analysis plot showing soil velocity magnitude (top) and direction (bottom). Magnitude is plotted from dark blue (stationary soil) to red (representing the soil moving at highest speed). Direction (within the shear interface) is as shown in the circular color legend (ex. yellow forward). Note, conventions of all plots are wheel travel left to right and at 20% slip unless otherwise noted.

Figure 16 shows two types of soil displacement plots (velocity magnitude and direction) of a single wheel shear interface imaging analysis experiment. These plots show processes typically present within the soil under a wheel operating in loose, granular soil.

The velocity magnitude plot is a visualization generated from the optical flow velocity field measured between image pairs. These plots (Figure 16, top) scale from dark blue (stationary soil) to red (representing the soil moving at maximum speed, V_{max}). This type of plot allows for the evaluation of the soil motion due to a specific wheel design. The shear interface is a key indicator of the means by which the wheel produces traction since it is representative of the soil failure planes.

The soil motion direction plot (Figure 16, bottom) displays the direction of soil particle motion as measured by the velocity field. The multi-colored wheel is the legend that maps color to direction with respect to ground coordinate frame. 'Dark blue' indicates soil particles moving completely horizontal in the left hand direction (e.g. at wheel bottom), opposite to the direction of wheel travel, while 'yellow' soil is being pushed forward (e.g. at wheel front). The direction of soil motion aids in determining what type of soil failure process occurs, what design features that might contribute to the failure and in the identification of multiple flows, such as resistive types at the wheel front. The separation of two flows (Figure 16, bottom), as detected by the developed analysis software, allows for the identification of regions of forward soil motion and for the measurement of the location of point of the theoretical maximum shear stress along the rim [9]. This point occurs at the intersection of the wheel rim and the flow separation line.

3.6 Example Analysis

SIIA magnitude and direction plots can be used in wheel design analysis and in terramechanics research in many ways. Two types of examples are given as to how the plots might be used. The first example, Figure 16, shows how a specific wheel specimen can be analyzed, possibly for validation purposes. The second example, Figure 17, illustrates, how for fundamental terramechanics research, SIIA plots can be used to study the influence of a specific vehicle-wheel parameter.

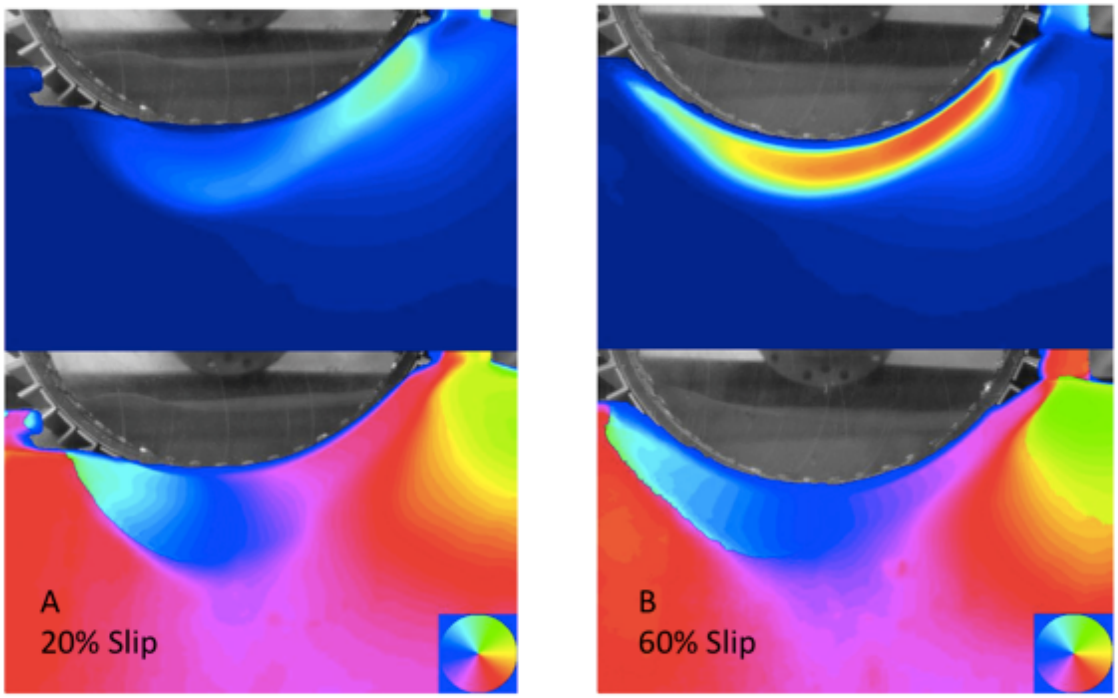

Figure 17: Example analysis investigating the effects of varying wheel slip on soil behavior. Wheel motion is to the right (as convention in this document). In this example, demarcation of forward and rearward flow is not done. Both velocity plots share the same color scale. Additionally, clustering of "insignificant motion" is not conducted. These two features are sometimes not applied in image processing in order to hide as little information as possible. The wheel velocity magnitude plots are normalized by ground speed and are at equal scale, allowing for direct comparison.

In the first example, Figure 16, if the small diameter wheel shown were to be assessed in the operating scenario as tested (slip, sinkage, soil type), one can draw conclusions regarding important traction processes occurring specific to the wheel. Looking at the SIIA results, in Figure 16, forward motion of soil in front of the wheel is evident from the direction plot (bottom). The "yellow" and "green" soil, at the wheel leading edge, indicates soil that is pushed forward by the rim that might result in resistance to vehicle travel. The velocity magnitude plot suggests that the soil forward motion is significant compared to other soil motion underneath the wheel and is likely an indicator of considerable motion resistance. This result might motivate design changes to reduce motion resistance. It should be noted that these conclusions could not be made by observing soil from the surface as only minor bulldozing occurs (accumulation of soil).

The second example, Figure 17, investigates changing a single wheel parameter in order to analyze potential affects on traction processes. Figure 17 shows two experiments with all controlled parameters held constant other than a change in slip rate. The wheel velocity magnitude plots are normalized by ground speed and are at equal scale, allowing for direct comparison. The soil magnitude velocity distribution, in front of the wheels, varies with slip rate. The wheel at 20% slip (Figure 17A) shows a larger extent of soil forward motion (forward flow) at the wheel leading edge than the wheel operating at 60% slip (Figure 17B). The soil forward motion is similar evidence of motion resistance as in the previous example. Soil pushed forward in front of a wheel leading is an indicator of motion resistance. A conclusion that can be made, from this observation, is that increasing slip might result in lower motion resistance. This comparison is an example of how the SIIA method can be used to study a basic terramechanics parameter such as slip. The next step in a test campaign would be to use this method to explain why the region of soil forward motion is reduced with increasing slip. Although only the forward motion of the soil in front of the wheel leading edge was discussed, there are many other soil motion behaviors observable in Figure 17 that are informative of the wheel traction processes. For example, soil transport below the rim leading to slip induced sinkage can be compared.

The above two examples, Figure 16 and Figure 17, are provided to illustrate the application of the SIIA technique.

3.7 General Experiment Procedure and Single Wheel Test Considerations

As an example of the experimental procedure, the testbed configuration for the SIIA data collection of the wheel that is shown in Figure 14 and in Figure 16 is described. The single wheel imaging testbed is prepared with GRC-1 lunar soil simulant [47] [48] before each test run (See Table 1 for properties and description of soil simulants used in the research presented in this thesis). First, the soil is loosened to a state of lowest relative density by using a trowel to lift the sand, allowing it to expand. Then, the soil is lightly compacted, by use of a drop tamper method, to increase compaction and to flatten the soil surface. The wheel specimen, shown in Figure 14, is rigid, 23cm diameter by 5.72cm wide (11.5cm effective width), with the rim covered by course grain sandpaper. A 10kg payload is applied in the vertical direction via deadweight. The experiments are typically evaluated at steady-state response of the soil and reaction loads. The test run begins at static sinkage and then travels under a controlled slip rate for approximately five wheel diameters in distance. All rigid wheels (rough rim or grousers) quickly enter steady-state sinkage, reaction loading and soil shearing behavior within the first wheel revolution for a nominal soil simulant such as GRC-1.

Table 1: Soil simulant properties and description.

	GRC-1 Lunar Simulant	**Fillite (fly ash)**	**JSC-1A Lunar Soil Simulant**
Mean Particle Size by weight (micron)	280	150 (approx.)	90
Density, ρ (g/cm^3)	1.60-1.89	0.60-0.85	1.43-1.91
Particle shape	Sub-angular	Spherical (hollow particles)	Angular
Internal Angle of Friction, φ (degree)	29.8-44.4°	Unknown	41.9-56.7°
Cohesion, c (kPa)	<1	Assumed zero	<1
Modulus of Shear Deformation, K (cm)	1.81-2.58	Unknown	2.9
Use	General purpose planetary vehicle mobility testing. Low cost for high volume needed for full vehicle experimentation. Lunar simulant.	Construction concrete additive. Material is collected coal fly ash.	Lunar mare simulant with mechanical properties designed to match returned Apollo regolith samples.

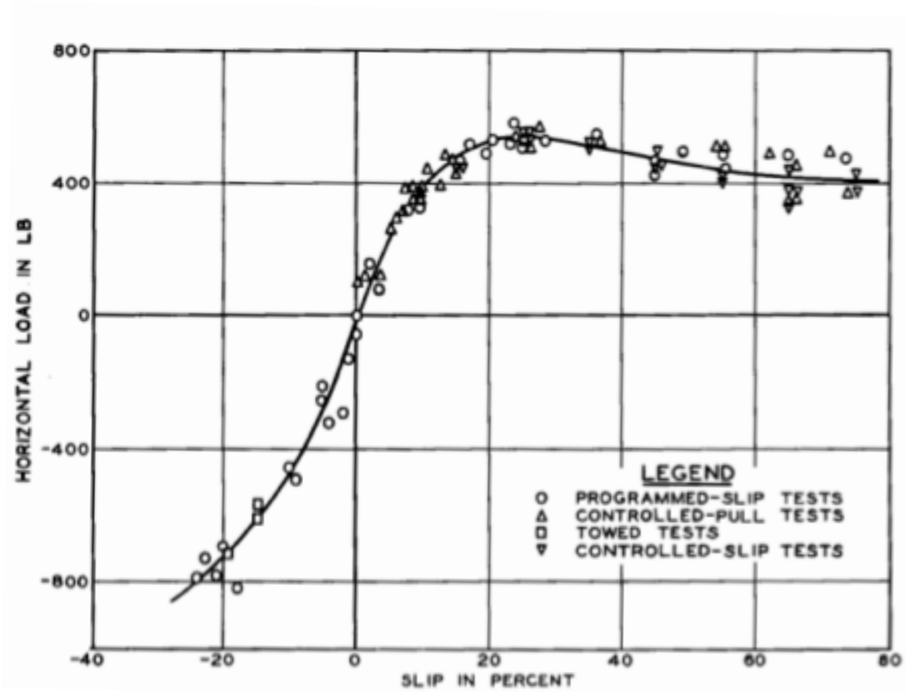

Figure 18: Drawbar pull controlled experiments and slip controlled experiment [13] shown on same plot to demonstrate valid use of slip control utilized in single wheel testbed (data is from large diameter wheels in dry sand). It should be noted that this only shows the uniqueness of the drawbar-slip curve; it does not verify the soil response is unique. Drawbar pull and horizontal load, as referred to in the figure, can be used interchangeably.

The testbed controls wheel slip by maintaining a tangential rim speed of 1cm/sec and by varying horizontal travel (carriage) speed. This coordinated motion produces a slip controlled type experiment. Consideration for the validity of this experiment type must be made since a vehicle does not interact with real terrain in a slip-controlled fashion. The slip-controlled method has been validated experimentally, except for very small slip values near zero and is seen as an acceptable method for performance evaluation [13] [49]. See Figure 18 for an example of this work. The SIIA single wheel testbed can also be configured for wheel self-propelled experiments (included in this research) where no external resistance is applied, resulting in free wheel slippage. Self-propelled mode is useful for testing flat ground (no inclination) wheel performance, specifically sand-trap scenarios, where vehicle entrapment might occur.

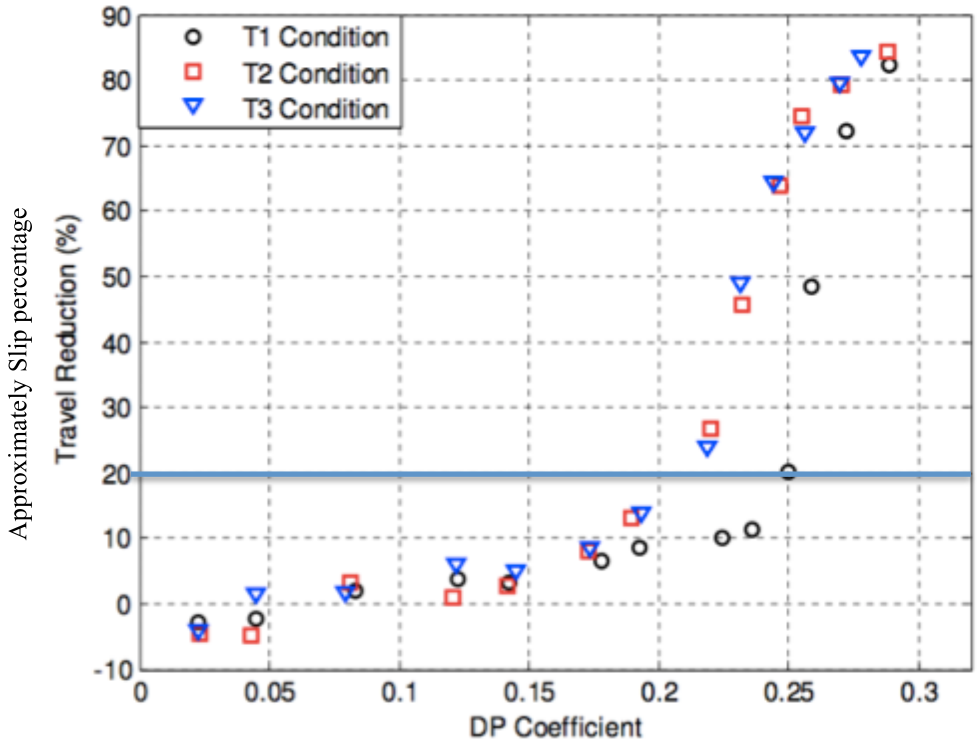

Figure 19: Most wheeled systems see sharp drop in drawbar pull ("DP coefficient") increase with slip near the 20% slip point. The example, in this figure, is from a four-wheel rover operating in GRC-1 lunar soil simulant with various soil compaction levels [50]. Evaluating a traction device, such as a wheel or a full vehicle at 20% slip, is a good metric for drawbar pull performance before the system enters high slip and therefore in a potentially unsafe operating state.

Generally, wheel peak performance in loose, granular material occurs between 15-30% slip. The drawbar pull, at 20% slip, is a common point of evaluating planetary mobility systems [10]. Even though this is the most common traction performance measurement point, it might not be the most informative from a sub-surface soil analysis stand point. However, as there is no established method for soil motion analysis, the 20% slip operating point was chosen for nominal evaluation in this thesis research. Shear displacement theory [51] and the stress-displacement response of dry sand [9] suggests that the soil reaches peak stress at 20% slip for wheels with contact length and with soil shear deformation modulus relevant to planetary vehicles. See work by Rula, et. al, for explanation of relationship of contact length, slip and shear deformation modulus [52]. Therefore, a physical explanation for soil response that might be visible within the soil structure exists at this point. Even though 20% was the nominal evaluation point for this research, many wheel configurations did undergo a full range of slip values (5-65% slip, with 5% slip intervals) to observe if behaviors changed with respect to slip. For each experiment, at least three repeats were conducted.

3.8 Other Applications and Visualizations

The soil displacement data collected, by means of soil imaging, can be utilized for many purposes. As the displacement data is digitized and corresponds to many small time steps, it can be manipulated for different visualizations. When coupled to soil models, forming a hybrid experimental-modeling technique, this data can also be used to infer other information that might be desired such as soil stresses. Soil displacement data might be valuable in the validation of new, state of the art, wheel-soil modeling methods currently being developed.

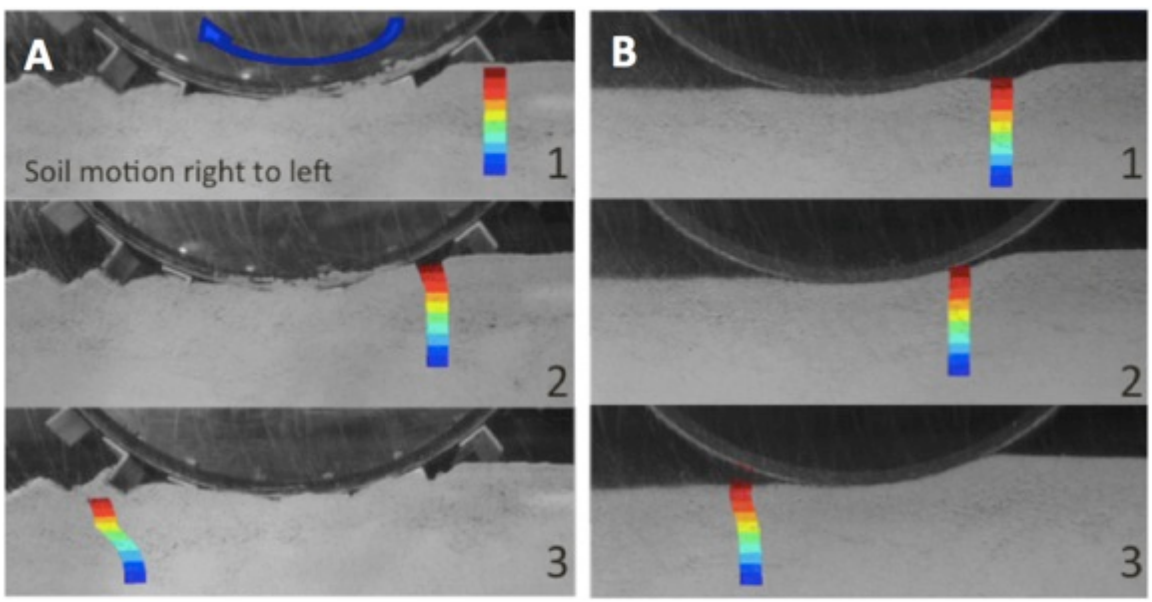

Figure 20: Virtual coloring of sand particles allows for a visualization of soil shearing and displacement as it interacts with the wheel. This visualization allows for easy comparison of shearing magnitude and of soil forward motion absolute soil displacement. Note that the soil is pushed forward in step 1 for wheel 'B' (flat rim) wheel, while wheel 'B' (grousered) is unaffected.

The visualization shown in Figure 20 is one example of the many ways of visualizing soil motion due to interaction with a wheel. This figure illustrates an intuitive way to observe both total and relative displacement of soil. It is useful to look at each time step throughout the duration in which the soil cells are being affected by a wheel. In this example, there is a higher total shear displacement of the soil due to the wheel on the left. Also, looking closely, wheel 'B' shows evidence of soil pushed forward, in step 1 and 2, before it contacts the rim (colored soil cells appear to "lean" to the right), while wheel 'A' does not exhibit this lean, but actually "pulls" in the soil. There is much value in visualizing the displacement data in multiple ways and many more visualizations are possible than are shown in this research. For example, sparsely distributed vector fields allow for an alternative view of the same data provided in the SIIA plots of this thesis. Sparsely distributed lines representing particle motion over many frame pairs enable tracking of soil particles over time. This visualization of absolute soil motion can be used for analysis of shear displacement of the thrust and motion resistance portions of soil interaction with the wheel.

Novel hybrid experiment-model methods might be achieved utilizing the SIIA data. This type of approach is motivated by the difficulty in predicting soil motion over long distances and ground interaction with complex wheel geometries. The research by Vlahinic, et al, introduces a method that relies on high-fidelity soil displacement fields from SIIA experimentation, coupled with a physics-based computational framework to infer soil stress at high spatial density [53]. The method relies on Finite Element Modeling (FEM) and a Drucker-Prager (type of material failure criterion) material description for the soil model. Measured wheel reaction forces (applied loads) and local soil dilatancy (inferred from SIIA) are married with FEM enabling deviatoric stress and deviatoric strain to be inferred. The SIIA data enabled for this novel hybrid experimental-model method to be initiated. See Figure 21 for preliminary results.

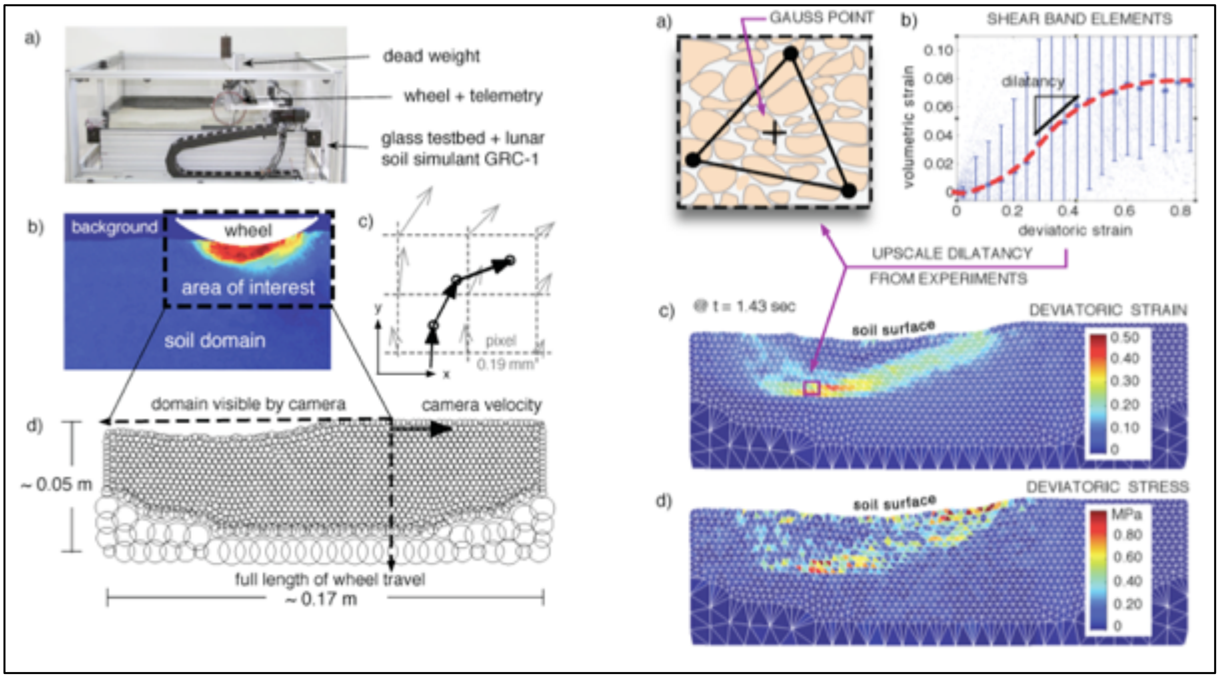

Figure 21: High resolution displacement fields, of actual experiments, can allow for hybrid experiment-modeling methods to infer additional information such as soil stress due to wheel operation [53].

The low accuracy of traditional terramechanics analytical models, for the purpose of planetary rover mobility, stems from assumptions that might not be valid for the specific application. Physics based methods, such as Discrete Element Modeling (DEM), do not rely on the same type of macro-system level assumptions, but rather on soil particle level interactions. This type of modeling calculates forces and displacements due to the contact mechanics of individual soil particles representative of actual soil grains. Now these simulations can be conducted for particle counts on the order of millions and higher.

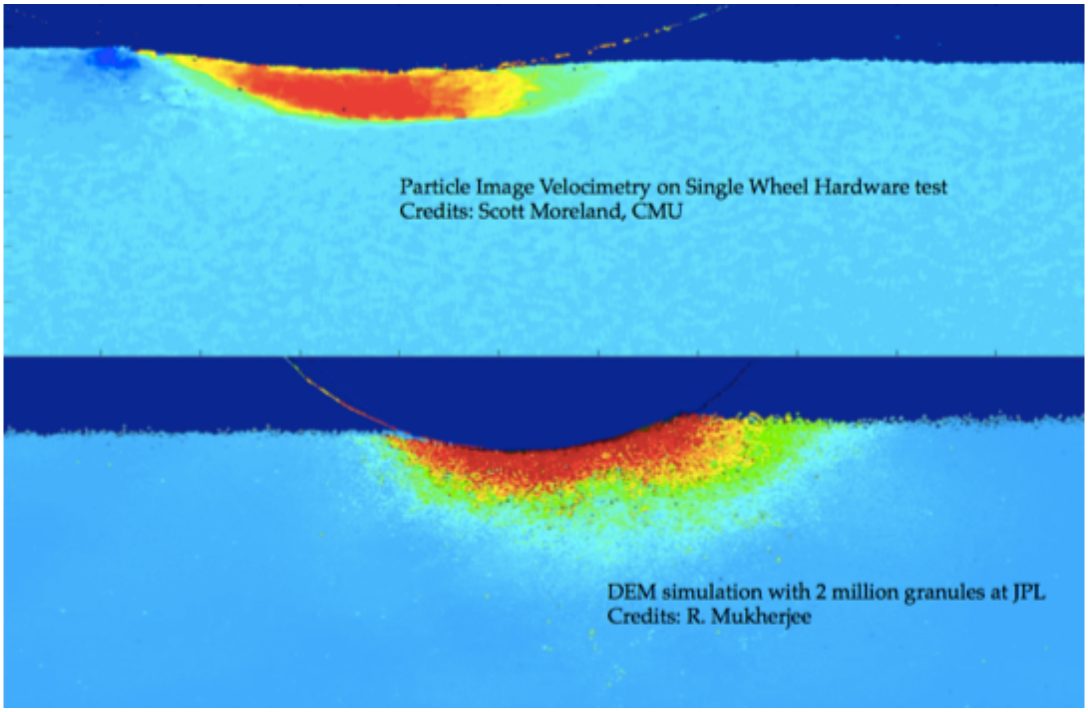

Figure 22: High fidelity soil displacement plots can be used to validate promising, new soil simulation methods, such as Discrete Element Modeling (DEM), that model individual soil particles. Image courtesy of R. Mukherjee, JPL.

The SIIA soil displacement data provide a unique method of validating these emerging simulation methods beyond traditional reaction force comparison (as a common single-wheel dynamometer provides). In addition to providing a second method of validation for DEM simulation software, SIIA provides data to directly compare/validate soil failure patterns and strain fields that might be desired as an output of the DEM simulations (see Figure 22 for example comparison used for possible validation of DEM). That is, the DEM models can provide the same data that SIIA offers, therefore allowing for terramechanics studies similar to those as conducted in the results chapters of this thesis document. This example demonstrates another application of the SIIA method and the inherent value of providing a novel data type, that up until recently did not exist.

The various visualization types, possible novel hybrid modeling methods and aid in development of new wheel-soil software illustrate the potential significance of using high-fidelity soil displacement plots.

3.9 Summary and Conclusion

Though much research has been conducted regarding traction of wheels in loose, granular terrain, little empirical data exist on the motion of soil particles beneath the wheel. The Shear Interface Imaging Analysis experimental method directly addresses this poorly understood aspect of terramechanics: what happens to the soil below a wheel in operation (see Figure 23 for overview of the technique). This chapter provides details on the development of the novel experimentation and analysis technique relying on sub-surface soil displacement fields to investigate terramechanics fundamentals in great detail. Shear Interface Imaging Analysis (SIIA) provides visualization and analysis capability of soil motion at and below the wheel-soil interface. This method places a wheel (or other traction device), in granular soil, up against a transparent sidewall. While driving or towing the wheel, images are taken of the sub-surface soil at a constant frame rate and are processed with optical flow software. The resulting soil displacement field is of high fidelity and is useful for analysis of specific wheel mechanics and terramechanics fundamentals. Identification, of clusters of soil motion, of primary soil shearing planes and soil motion direction/magnitude enables analysis of mechanisms governing traction. The Shear Interface Imaging Analysis tool visualizes soil motion in richer detail than possible before and allows for deeper investigation of the mechanics involved in wheel-terrain interaction.

The SIIA technique forms the experimental method that this research follows to produce the results in the coming chapters of this thesis. Both example results given in this chapter and the detailed results in the following chapters, show the SIIA method is a valuable tool for both design of traction systems and for research of terramechanics fundamentals.

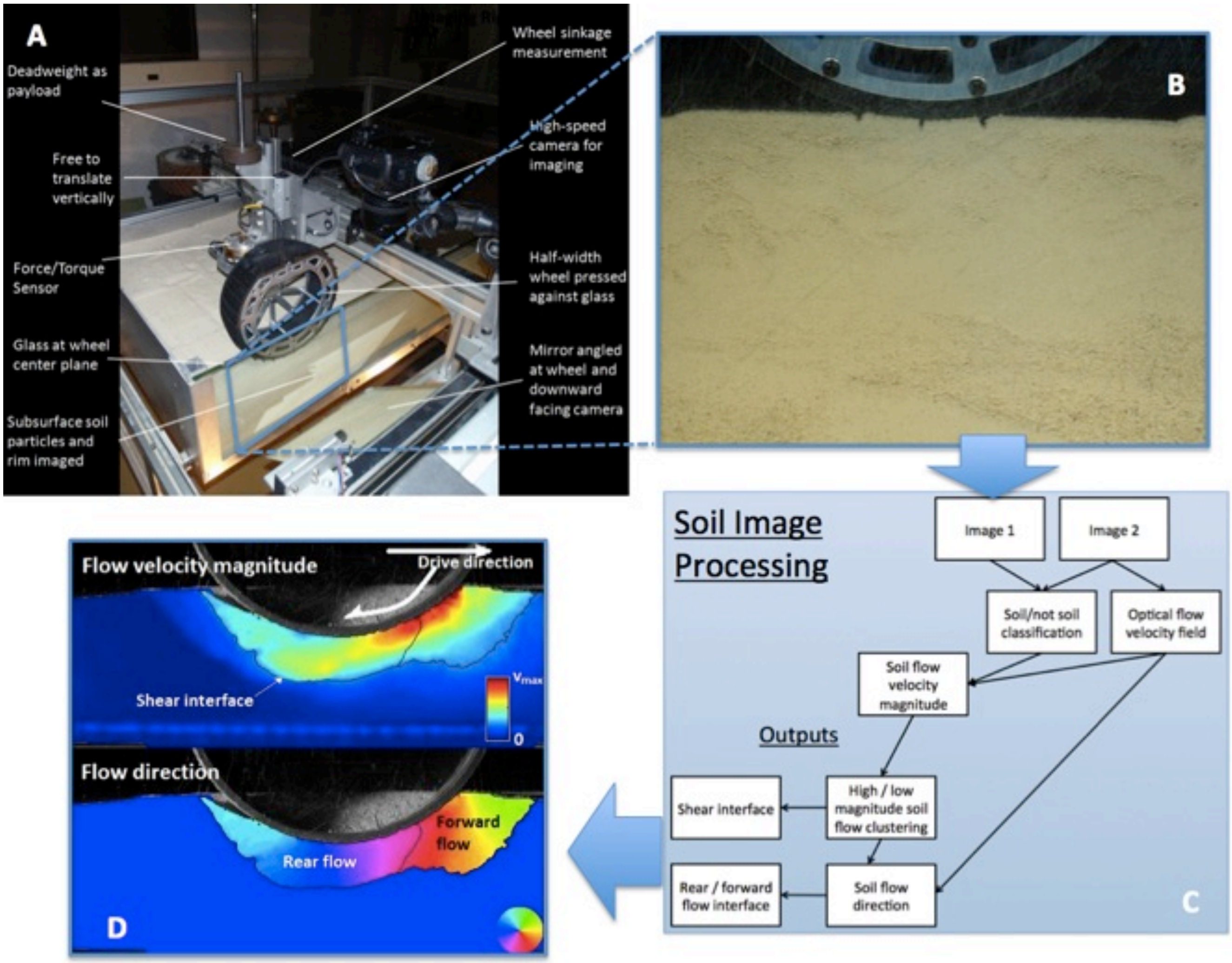

Figure 23: Recap of SIIA technique. Flow chart of critical steps of the Shear Interface Imaging Analysis (SIIA) technique. (A) Wheel module, carriage and glass-walled soil bin. A cross-section of soil below the wheel is imaged via high-speed camera. (B) Image from high-speed camera taken of soil seen through glass wall. Subsequent image pairs are fed into image processing software to produce useful output. (C) Image processing steps produce soil velocity and shear interface output plots. (D) Example Shear Interface Imaging Analysis plots generated.

4 Examples of Direct Observation of Soil Motion Behaviors

4.1 Approach

The SIIA technique is used to gather data to form a survey of wheel induced soil motion behaviors over a range of common wheel types and vehicle parameters. This approach is undertaken to reveal the nature of these soil behaviors, such as the general state of knowledge, variation between wheel types and possible influence on traction. Experimentation is the preferred method for this study as analytical terramechanics models do not recognize or predict distinct soil behavior between many wheel forms and operating points, such as grousered wheels or changes in slip rate.

To show that the soil behaviors differ between wheel types, numerous specimens and operating points were investigated. These wheels are selected to represent a reasonable range of commonly implemented wheel types considered in the design space of planetary vehicles and in vehicle states that are encountered. Figure 24 shows example wheels and systems that represent the range that the study covers. This survey is not intended to be comprehensive, but to reveal some differences in soil processes between wheel types, and to have a sufficient breadth of soil behaviors as to reveal general characteristics that might occur during planetary rover wheeled mobility. The wheel types studied, due to their prolific use in planetary robotics, are rigid, compliant, small/large diameter, and grousered. The effects of unique locomotion modes such as push-roll are also studied in an effort to show key soil motion behavior differences that have large effects on traction; not due to common use.

Each wheel specimen underwent testing in soil simulant, at loads (payload), and at operating conditions (slip rate) relevant to planetary rover applications. All reaction forces (including net traction) are measured as well as sub-surface soil particle motion, to produce a snapshot of wheel state and soil motion behaviors that might influence the measured traction. Refer to Table 3 for experiment type and corresponding test configurations for which results are shown in the next sections.

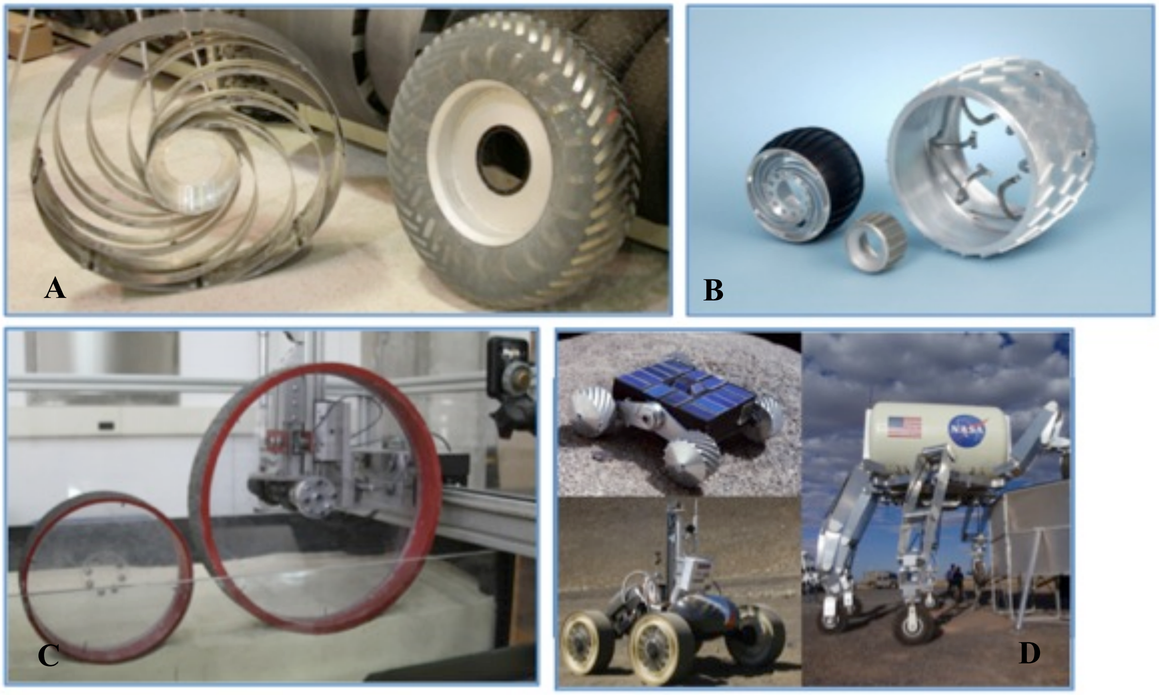

Figure 24: Common wheel types and alternative locomotion modes within the soil behavior survey conducted. Note, these are not the specimens tested. (A) Compliant wheels, such as Lunar Roving Vehicle (LRV) are shown. (B) Rigid wheels shown; Mars rovers Sojourner, MER and MSL wheels pictured. Image credit [54].(C) Wheel diameter study specimens. (D) Example locomotion mode that might affect soil behaviors. Vehicles capable of "Push-roll" locomotion shown (top-left image credit [55]).

To summarize, the approach followed at the stage of the research of this chapter investigates the nature of wheel-induced soil behaviors by directly observing sub-surface soil motions of a variety of common wheel types and operating scenarios. The analysis focuses on soil motion behavior variation between wheel types, consistency of findings with literature and if observed soil behaviors have been documented during prior research. These metrics provide a categorization to show the general status sub-surface soil behaviors have in current terramechanics research and the potential influence on traction.

Table 2 summarizes the survey portion of this thesis and of all subsequent research in this thesis (remaining results chapters). Also, this table can be looked at as an overview of the research conducted to satisfy results needed to prove or refute the thesis statement made in Section 1.3.1.

Table 2: Wheel Aspects Studied at Each Step of Approach of Thesis Research

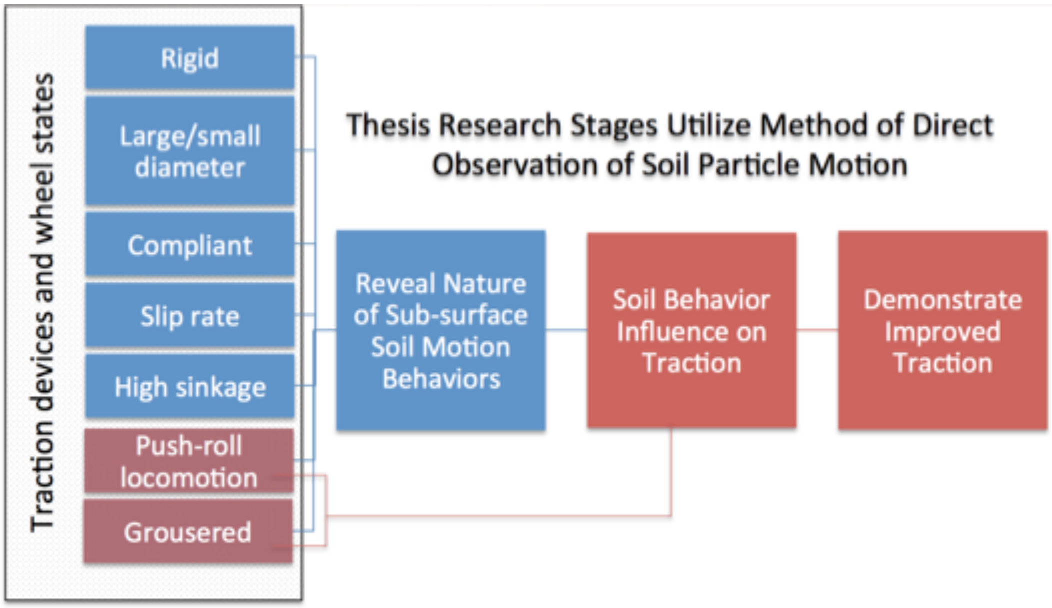

Table 3: Soil Behavior Survey Test Configurations

Related Figure	Parameter of interest	Wheel Details	Soil	Slip Rate	Payload
Figure 25	**Rigid**	Ø23cm x W5.7cm, flat profile, sandpaper rim	GRC-1	0.20, slip controlled	5.0kg
Figure 32-34	**Grousered**	Ø23cm x W5.7cm rim with 24 grousers of 1.3cm length	GRC-1	0.20, slip controlled	5.0kg
Figure 30-31	**Compliant**	Ø23cm x W5.7cm, flat profile, flat contact, sandpaper rim	GRC-1	0.05, drawbar pull controlled	5.0kg
Figure 26-29	**Diameter large/small**	Ø41cm x W5.7cm Ø23cm x W5.7cm	GRC-1	0.20, slip controlled	5.0kg
Figure 35-36	**Push-roll**	Ø23cm x W5.7cm, flat profile, sandpaper rim	GRC-1	Roll at 0.20 controlled slip then push 5mm (both fig.)	5.0kg
Figure 37-38	**Slip Rate**	Ø23cm x W5.7cm, flat profile, sandpaper rim	GRC-1	Range: 0.05-0.60 at 0.05 steps, controlled	5.0kg
Figure 39-40	**High Sinkage**	Ø23cm x W5.7cm, w/ 48 grousers of 12.7mm length Ø23cm x W5.7cm, sandpaper rim	Fillite (fly ash)	0.30 and 0.60 respectively, self-propelled condition	5.0kg

4.2 Experimental Results – Survey Over Range of Common Wheel Types

Most of the soil response behaviors observed in this chapter are either unaccounted for by terramechanics analytical models, might be documented for the first time as a result of this work or are inconsistent with literature. These behaviors are listed to illustrate the wide range of processes occurring underneath a wheel and to point out that most are unexplained to date. The goal is, that by bringing attention to these behaviors, it will be apparent that further understanding is needed and that an explanation of how the behaviors are related to traction might lead to improved design or models.

Table 4 provides examples of SIIA results from the wheel survey and they show that the sub-surface soil motion behaviors vary widely over wheel type and are inadequately understood. The lack of understanding is evident due to inconsistency with literature, lack of previous direct observations and lack of accounting for in models. After Table 4, sections 4.2.1-4.2.6 elaborate on the survey and provide specific support for concluding that the observed soil behaviors are not adequately understood and warrant further research.

Table 4: Example SIIA plots displaying sub-surface soil motions of numerous wheel types and a locked/pushed wheel.

<table>
<tr><th>Wheel Type Examples</th><th>Observed Soil Behavior</th><th>First direct observation</th><th>Not consistent with literature</th><th>Not accounted for in models</th></tr>
<tr><td rowspan="3">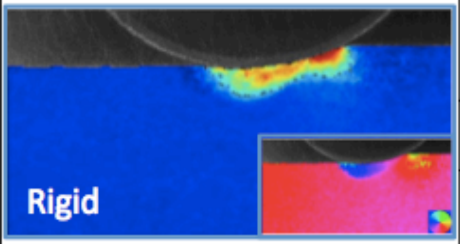
</td><td>soil flow direction steep with drastic change, does not follow rim tangent</td><td>✔</td><td>✔</td><td>✔</td></tr>
<tr><td>non-grip soil failure</td><td></td><td></td><td>✔</td></tr>
<tr><td>shear interface confined to contact area</td><td>✔</td><td>✔</td><td></td></tr>
<tr><td rowspan="3">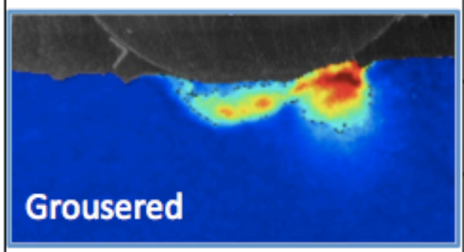
</td><td>periodic soil response</td><td>✔</td><td></td><td></td></tr>
<tr><td>grousers interacts individually</td><td>✔</td><td></td><td></td></tr>
<tr><td>non-grip failure</td><td>✔</td><td>✔</td><td></td></tr>
<tr><td rowspan="4">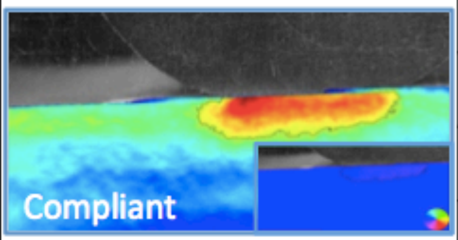
</td><td>thick shear interface</td><td>✔</td><td>✔</td><td>✔</td></tr>
<tr><td>horizontal soil motion</td><td>✔</td><td></td><td></td></tr>
<tr><td>small soil displacement</td><td>✔</td><td>✔</td><td>✔</td></tr>
<tr><td>non-grip soil failure</td><td>✔</td><td>✔</td><td></td></tr>
<tr><td rowspan="3">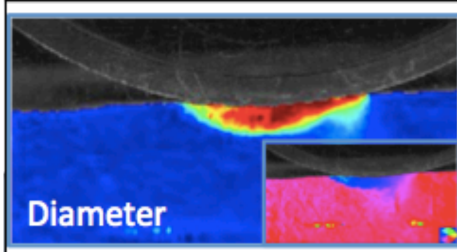
</td><td>thinner shear interface</td><td>✔</td><td></td><td>✔</td></tr>
<tr><td>lower magnitude of shearing</td><td>✔</td><td>✔</td><td></td></tr>
<tr><td>Soil direction horizontal for most of contact</td><td>✔</td><td></td><td></td></tr>
<tr><td rowspan="4">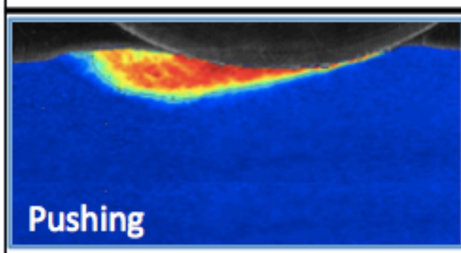
</td><td>unified soil motion</td><td></td><td></td><td>✔</td></tr>
<tr><td>small soil displacement</td><td></td><td></td><td>✔</td></tr>
<tr><td>not confined to contact area</td><td></td><td></td><td>✔</td></tr>
<tr><td>ground failure</td><td></td><td></td><td>✔</td></tr>
</table>

4.2.1 Rigid Wheel

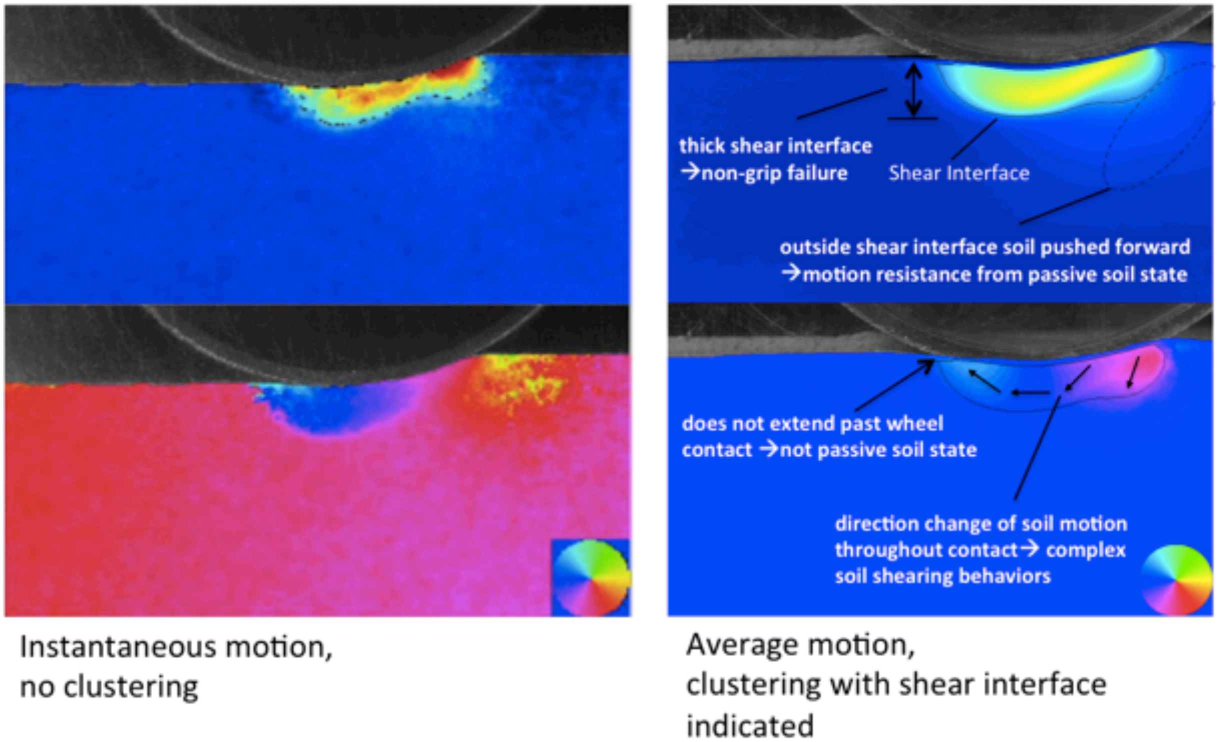

Figure 25: Rigid wheel with simple geometry rim; flat profile with sandpaper surface. Both instantaneous and average soil motions are shown to allow for easier visualization of soil processes such as forward flow.

It is evident from the soil displacement plots of, Figure 25, that the soil fails sharply at the shear interface and that large soil motion occurs within this region; however, there is forward motion of the soil in front of the wheel. The soil failure is not of "grip" type (i.e. slip plane at rim-soil interface) and the shear interface does not terminate beyond the rear contact region, but rather at the wheel back contact point. Both of these observations are inconsistent with terramechanics literature, but are observed for all wheel types throughout this research. Bekker assumes grip failure for rolling wheels [14] while, when non-grip failure has been applied to wheel theory, a passive Rankine zone is assumed to exist and to provide thrust [56]. A passive Rankine zone, which typically has a logarithmic spiral shape extending behind the wheel, is only observed for the pushing wheel in Figure 35 and Figure 36. The confinement of the shear interface to wheel contact might not have been previously observed. Research by Wong, relied on long exposure film, which was not accurate at measuring direction of motion [45]. The inability to accurately determine where the shear interface is located might have occurred due to small soil motions outside the primary shearing planes.

The shape of the shear interface, the point at which it originates at the rim, the point at which it terminates at the wheel rear and the complex path soil motion follows, all indicate failure type not described by existing theory. It should be noted that although there is a distinct shear interface, the soil shearing distance at the shear interface is well below the shear modulus of the soil (GRC-1; shear modulus = 1.8-2.5cm). The above observations and measured soil displacement suggest that the soil, at the shear interface, might not undergo a simple failure determined by shearing distance and by shear modulus.

Wheel models that account for slip and use soil displacement to predict thrust, do so as a result of research introduced by Onafeko and Reece. The assumption is that soil develops thrust are based on this derivation of shear distance, even though soil is not guaranteed to follow the rim motion. The SIIA results, for the small diameter rigid wheel, show that the soil motion along the shear interface, takes a path quite different from that of the rim. This observation and the examples of inconsistencies with literature given above, show that the sub-surface soil failure planes and soil motion processes present might be inadequately understood and that direct analysis of these behaviors could lead to new explanation of traction processes.

4.2.2 Large/Small Diameter Wheel

Figure 26: 41cm and 23cm diameter rigid wheels shown. Both are 5.72cm wide and have a flat profile rim with a sandpaper surface. All results shown for controlled slip tests, at 20% slip and 5kg total payload.

A comparison of the two wheels of different diameters shown in Figure 26 was conducted. The tractive performance, using the drawbar pull metric, measured a 33% increase in net traction for the larger diameter wheel over the smaller. The behavior of the soil motion between the two wheels also is observably different.

Figure 27 shows that the larger diameter wheel has a shear interface, with lower magnitude of soil motion and motion direction that is more horizontal compared to the smaller diameter wheel. Benefits of soil shearing induced by rim rotation that is produced opposite the direction of travel (horizontal) might exist and therefore contribute to the increased drawbar pull of the larger wheel. The soil particles need not shear as much when only acted on horizontally, opposite the direction of travel. A lower shearing magnitude creates a larger portion of the shear interface that can operate at the peak stress of the stress-strain curve of the soil (loose, granular soil shear strength peaks at low shear strain). To note, contact length and average contact pressure are similar and are not any lower for the larger wheel (Figure 28).

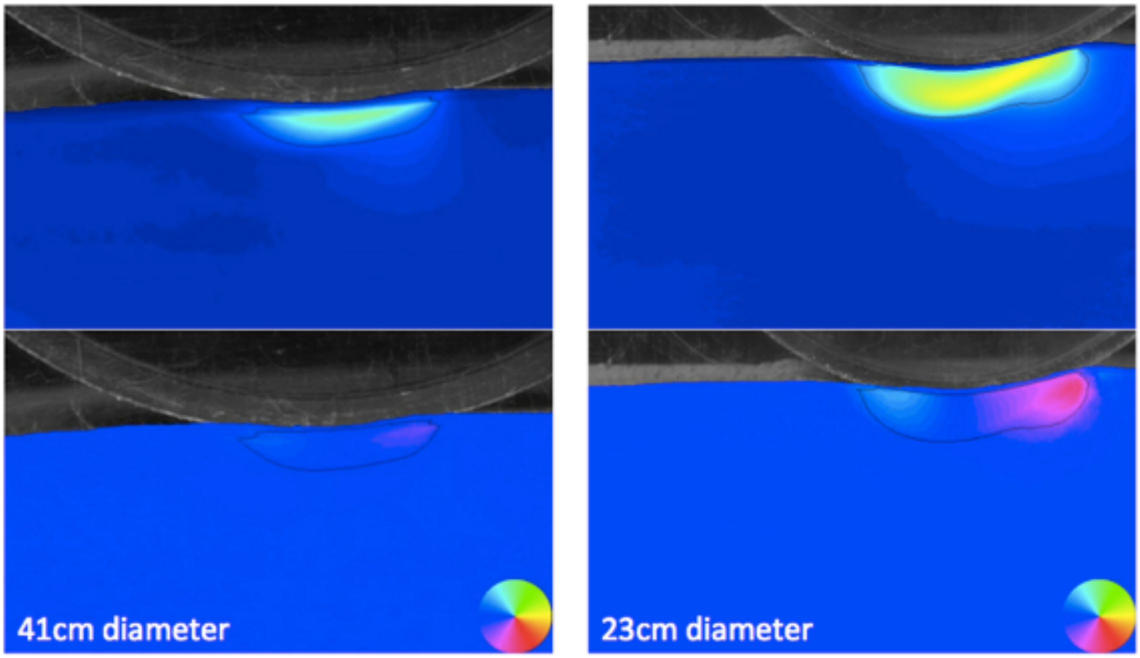

Figure 27: Variation of shear interface with change in wheel diameter for 20% slip tests (both wheels commanded identical rim tangential speed and ground speed). Soil velocity magnitude for both diameter wheels are equally scaled. The large wheel shows nearly horizontal soil motion compared to large changes in direction (down then up) under the small wheel. Note the contact length, of both wheels, are similar, however the drawbar pull is quite different.

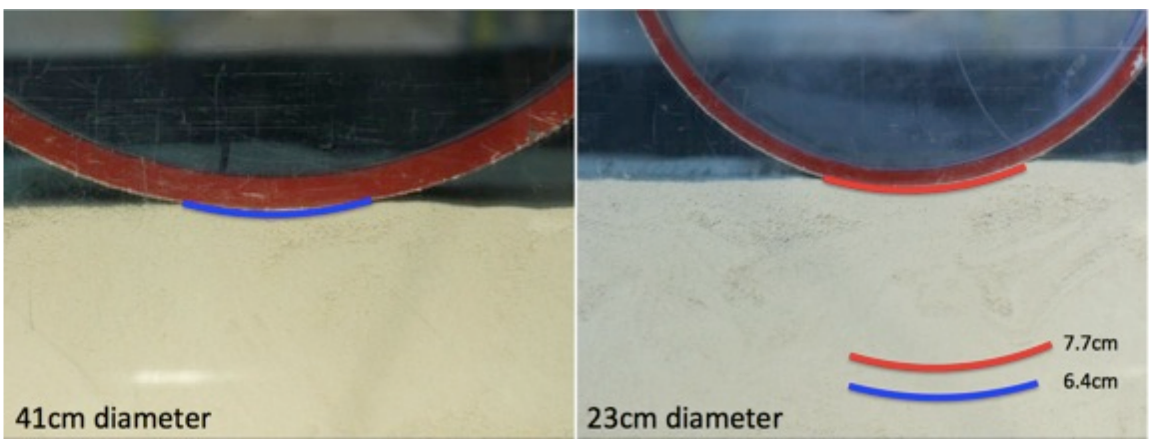

Figure 28: The contact length of the two wheels are similar. The larger diameter wheel has a 6.4cm contact length, while the smaller wheel has a 7.7cm contact length.

Increased sinkage of the smaller diameter wheel is most likely due to a thicker shear interface that is removing soil from underneath the wheel at a higher rate. Unless the smaller wheel replaces soil at a higher rate than the larger wheel, then greater sinkage develops. It is likely that the smaller wheel actually replaces soil at a lower rate than the larger diameter wheel, as it can be seen that more soil is pushed forward instead of being directed underneath the wheel. Other researchers have noted that the excavating mechanism underneath a wheel is the most likely cause of slip induced sinkage. Wong made these comments with respect to sub-soil imaging results [45], while Reece drew these conclusions from conventional performance testing [57]. Differences in soil velocity magnitude, direction and accurate measurement of shear interface thickness, are obtained for the first time from research conducted in this thesis. The SIIA results show that the smaller shear interface, lower magnitude and horizontal soil motion might be responsible for the smaller sinkage of a larger diameter wheel.

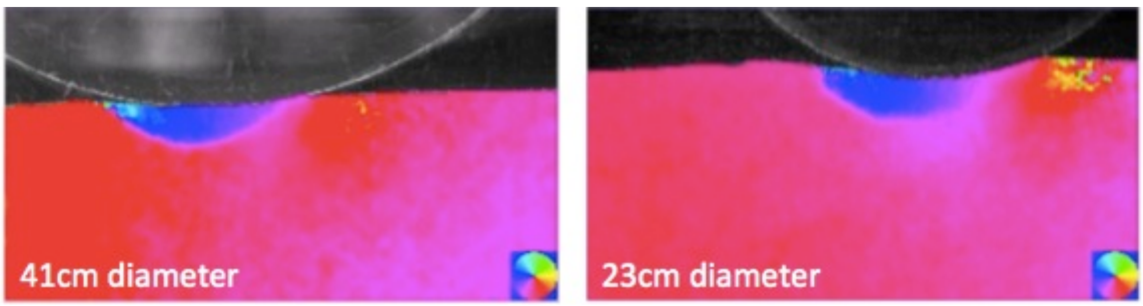

Figure 29: Forward motion at wheel front is evidence of motion resistance (see "yellow" patch). The smaller diameter wheel has a larger area of forward flow, which is expected.

The lower sinkage of the large diameter contributes to the lack of observable forward flow (Figure 29). Lower resistive flows likely contribute to the increase in measured drawbar pull as well as a possible increase in thrust due to a different shear interface.

4.2.3 Compliant Wheel

Experiments were conducted using a 23cm diameter compliant wheel with sandpaper-like tread (unloaded diameter). The compressible foam material, used in construction of the wheel did not produce uniform contact pressure as a pneumatic tire would, however, a flat contact length was achieved.

Many observable differences, between the rigid wheel and compliant wheel, are present in Figure 30. The direction, of the soil displacement, is near horizontal for all soil underneath the wheel (Figure 31). The horizontal soil motion might occur due to the extraordinary low sinkage and the flat shape of the contact along the length of the deformed rim.

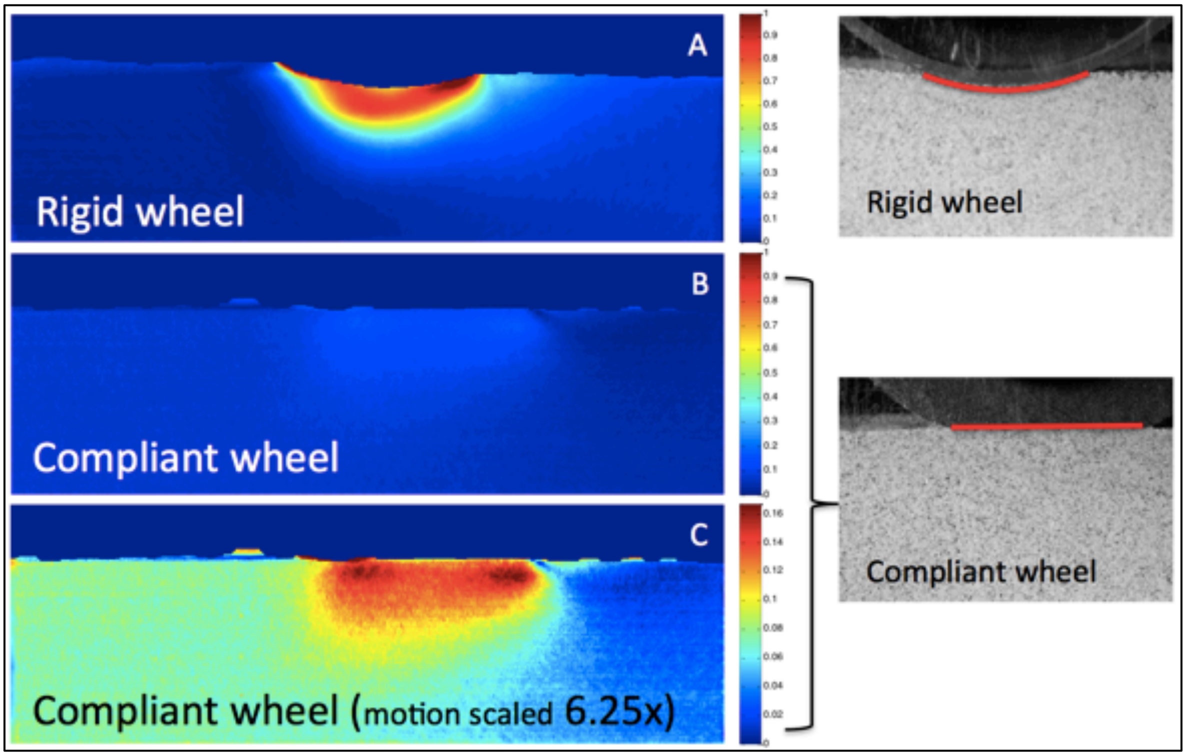

Figure 30: Plots A and B are at the same scale, while plot C is approximately 1/6th full scale. Drawbar pull controlled experiment results shown for a compliant and a rigid wheel of equal non-deflected diameter and width. Both wheels (rigid and compliant) have the same constant external horizontal load applied (0.15 pull coefficient). Different slip rates and soil response are observed between the two wheels. 6-8 times magnitude of motion velocity is seen along the shear interface for the rigid wheel. The slip rates are 5% and 26% respectively for the compliant and rigid wheel. The angular velocities of the two wheels are equal.

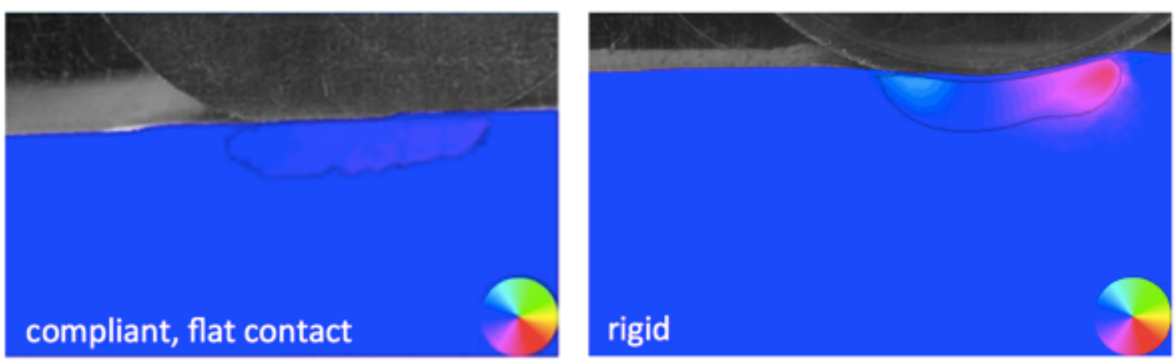

Figure 31: Nearly horizontal motion of soil displacement seen under the compliant wheel while the rigid wheel interaction causes a wide variation in direction with steep up and down motion. However, both wheels are generating similar drawbar pull loads (slightly lower for rigid wheel in these test cases). The slip rates are 5% and 20% respectively for the compliant and rigid wheels.

The soil velocity magnitude of the compliant wheel is less than 1/6th that of the rigid wheel (Figure 30) and the ground speed of the compliant wheel is 1.28x that of the rigid wheel. Therefore, the approximate maximum shear displacement of the soil underneath the rigid wheel was 8x that of the compliant wheel. According to shear displacement theory utilized in terramechanics modeling, the thrust produced by the rigid wheel should be 8x that of the compliant wheel due to the higher shear displacement [51] and because the average ground pressures are similar. However, the drawbar pull of both the wheels is similar (identical for tests of Figure 30). The rigid wheel likely has higher motion resistance than the compliant wheel. However, this cannot account for the significant differences in the theoretical drawbar pull of the two wheels based off soil displacement measurement. These differences in shear interface characteristics between the two wheel types and the inconstancies with theory, raise the question of the role the different soil motion patterns and sol failure patterns might play in governing traction.

4.2.4 Grousers

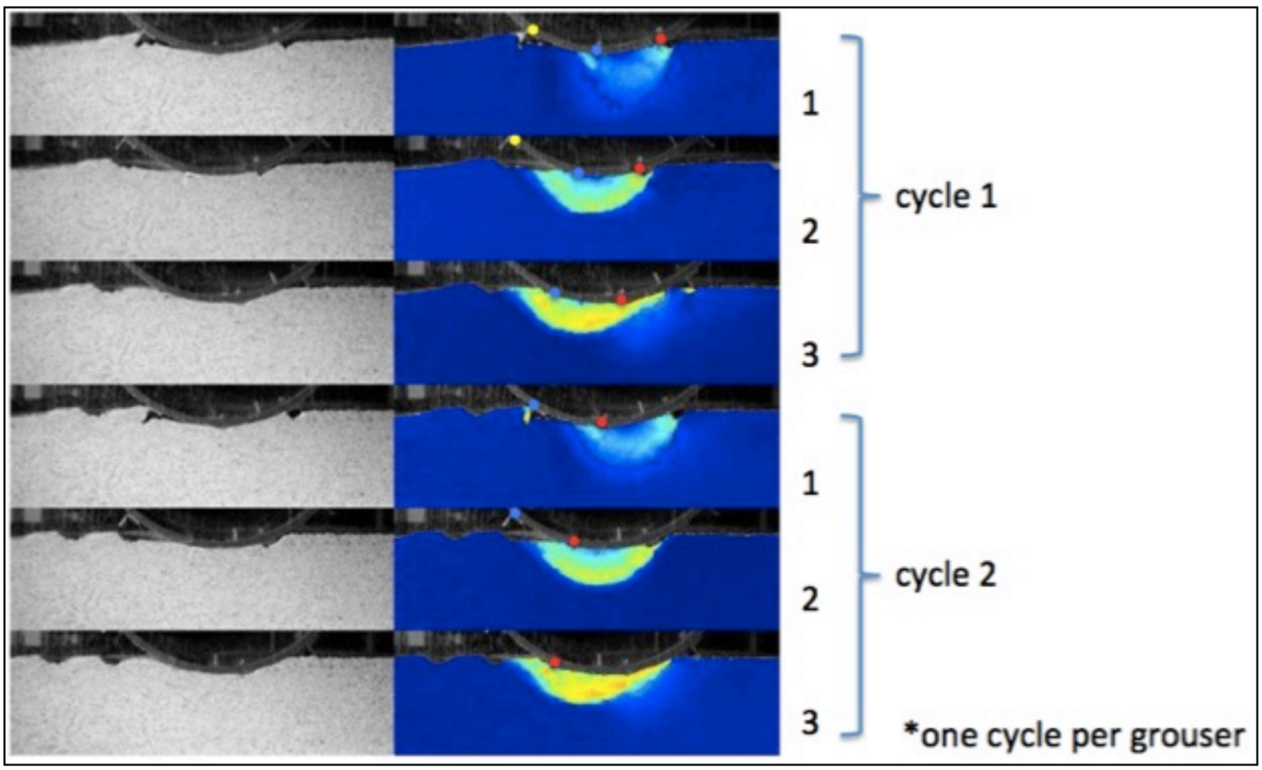

Figure 32: Time-lapse images (top to bottom) of soil shearing by a wheel with grousers over two cycles; two grouser plunges (velocity magnitude plot shown). Distinct, periodic soil motion are present as each new grouser rotates into the soil . Wheel travel is to the right. The three grousers in contact with the ground in the first image are denoted by a red, yellow and blue dot to aid in visualizing motion.

Grousers are often employed in wheel designs for planetary rovers. Grousers are paddle like protrusions from a rim designed to engage the soil. The effect of soil shearing can be studied when analyzing these features. Figure 32 shows the periodic nature of soil shearing due to individual grouser affects. It appears that the grouser at the front of the wheel entering the soil has the greatest effect. Also, experiments with very close spaced grousers showed similar results and exhibited periodicity proportional to spacing. As the optical flow algorithm utilizes overlapping image pairs, high fidelity movies of the grouser shearing effects, can be utilized to observe individual grousers interacting with soil as the rim rotates. This capability records the time varying soil shearing processes for the first time. Periodic forward flow was also observed for grousered wheels (Figure 33) and corresponded to periodic loss of drawbar pull measured

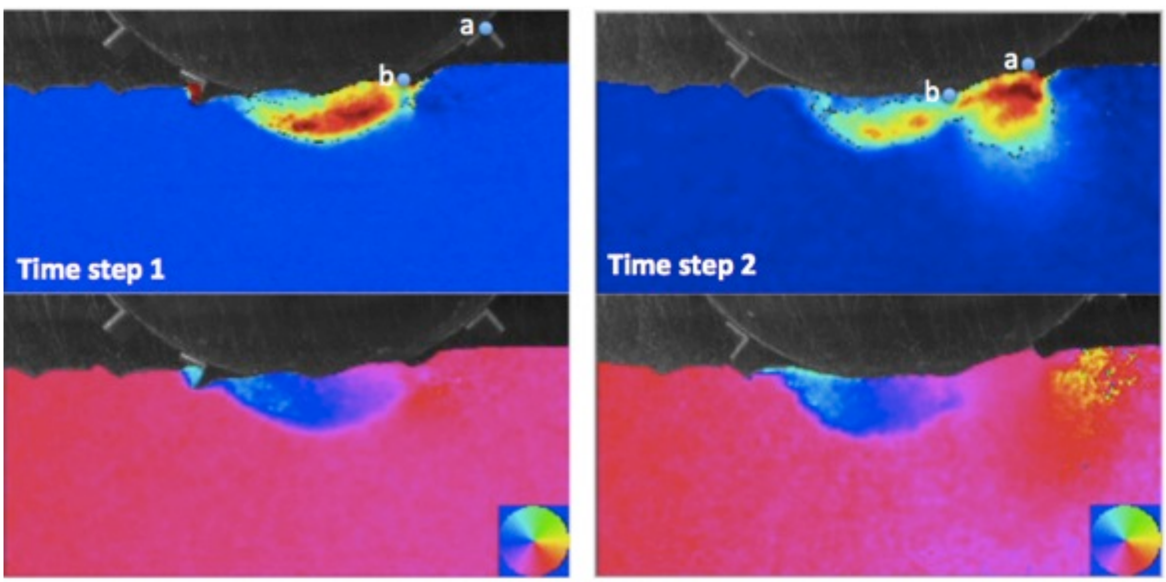

Figure 33: Periodic forward soil motion at the wheel leading edge was observable for most grousered wheels evaluated in the survey. Soil forward motion and periodic drawbar pull behavior might be associated with a loss of traction. In general, the shear interface rearward of the front region, is remarkably similar to the same wheel without grousers (Figure 25). Two grousers are indicated by blue dots to aid in visualization of motion.

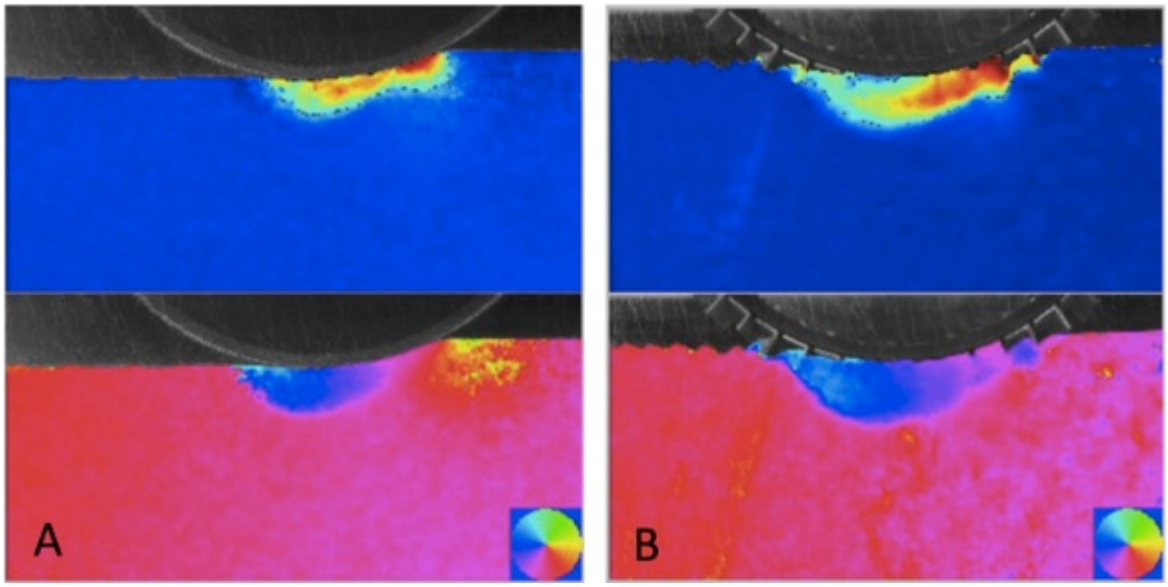

Figure 34: Forward motion of soil is not observed (or significantly smaller) for grousered wheels (B) of higher drawbar pull. The grousered wheel shown is of a configuration that significantly reduces forward motion of soil in front of the wheel leading edge and generates high drawbar pull. Pull coefficient are 0.21 and 0.32 for the grouserless (A) and grousered (B) wheel respective (as shown in figure).

The traction performance of the wheel without grousers (Figure 34A) and of the same wheel with 48 grousers at 13mm height (Figure 34B), act as extremes of the grousered wheel configurations and of the drawbar pull performance of grousered wheels tested. The studying of these two cases leads to an important realization; the soil displacement behavior, of the grouserless wheel Figure 25 and the 48 grouser wheel (Figure 34), are very different at the leading edge of each wheel. The Figure 34A direction plot, no grousers, shows a yellow patch of soil in front of the wheel that moves in a horizontal direction forward. This soil motion is evidence of possible motion resistance that would be reacted against the rim. Motion resistance would reduce the drawbar pull of the wheel. However, a wheel with high drawbar pull utilizing high performance grouser parameters (Figure 34B), does not show evidence of forward soil motion at the wheel leading edge.

The rear and bottom shear interface (regions except for front), of grousered and non-grousered wheels, are quite similar. In fact, they are offset by the height of the grouser. If it is assumed that in the region rearward soil motion, the grousers are full of compacted soil, it will act like a wheel of larger diameter (only for the rearward region, not front entrance area). Differences in shear interfaces, can cause significant changes in thrust.

However the failure modes are of the same type for both shear interfaces observed. As such, the gain in drawbar pull due to implementation of grousers might be dependent on the reduction of motion resistance, indicated by a lack of forward soil motion observed for high performance wheels.

Chapter 5 presents an in-depth analysis of this topic conducted during the thesis research, and therefore limited observations and explanations are provided in this section.

4.2.5 Push-Roll

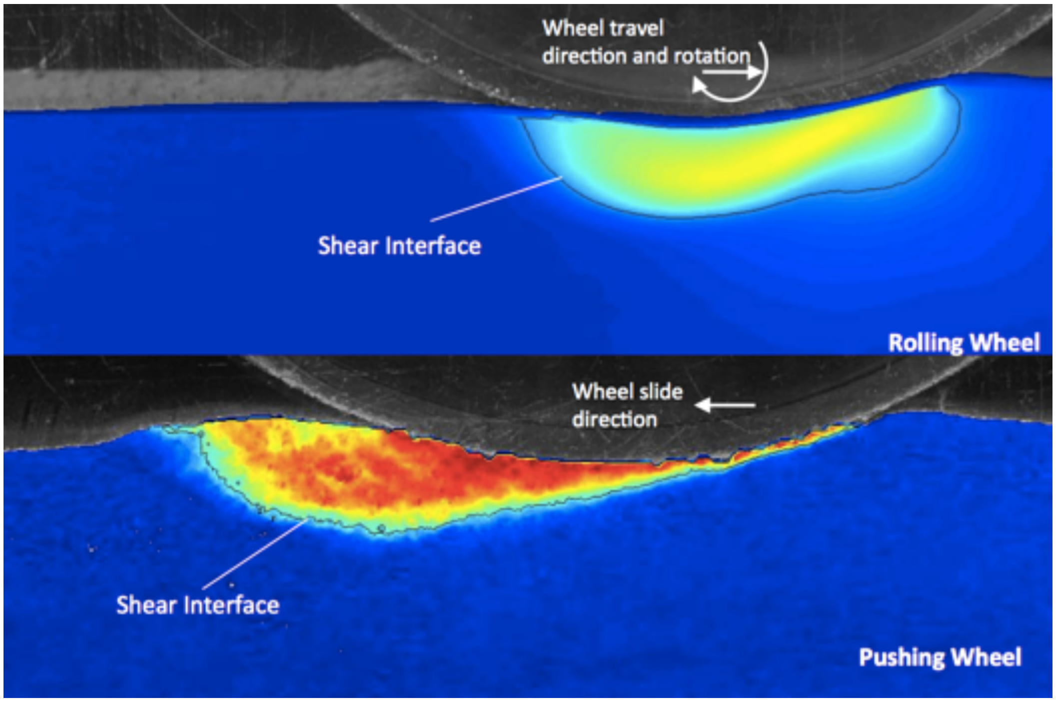

Figure 35: Shear interface analysis comparing rolling wheel to a pushing (non-rotating) wheel utilized in push-roll locomotion. The rolling wheel travels to the right at 20% slip. A “ground failure” type response of the soil is observed for the pushing wheel, identifying a source of tractive gains. Force measurements show that the pushing wheel can generate multiple times the trust, of a rolling wheel, for the same resulting affect on sinkage (see Chapter 5.3). Soil velocity magnitude plots are scaled differently between pushed and rolling wheel.

To investigate the effect of the rotating rim on the generation of thrust, a study comparing pushing locomotion to rolling locomotion was conducted (Figure 35). Push-roll locomotion (use of non-rolling and rolling wheels) has been demonstrated to produce high drawbar pull for increased mobility [43] [44].

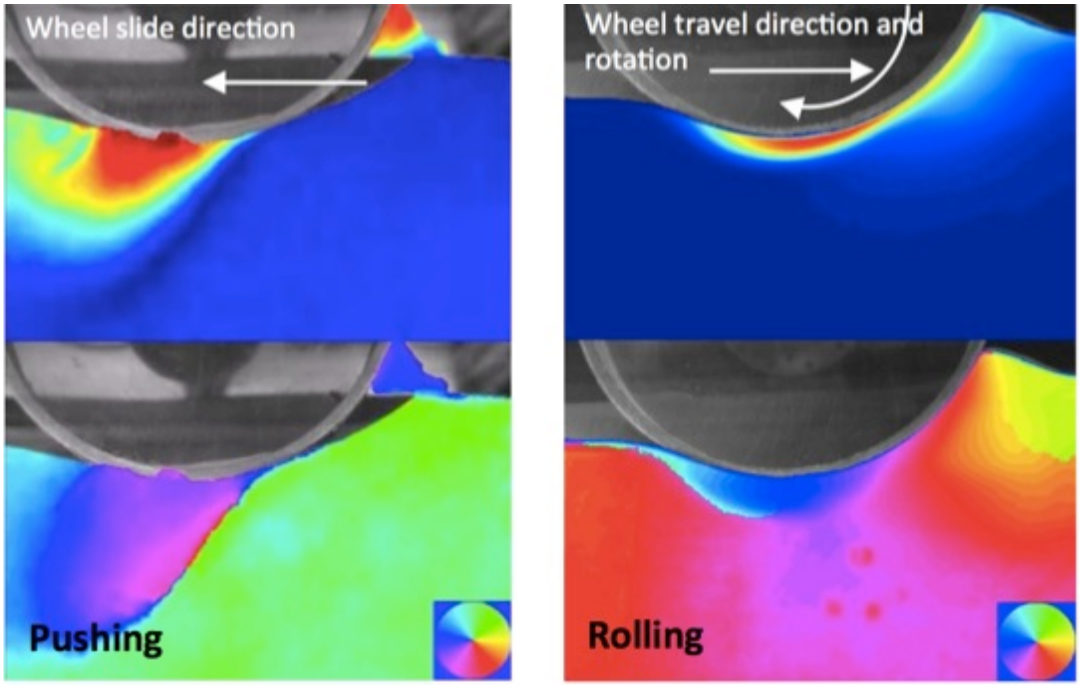

Figure 36: The pushing wheel has a horizontal displacement 6mm and 0.8mm sinkage, generating a pull coefficient of 0.32. The rolling wheel is generating zero drawbar pull (0 pull coefficient) and is operating at high slip in a self-propelled state. This wheel is at 60% slip and 40mm slip sinkage, therefore it might be close to entrapment. It should be noted that the sinkage visible in the pushing wheel plot, is almost solely due to the wheel rolling before the pushing is initiated. Rolling prior to pushing mimics the push-roll type locomotion motions of a suspension. Soil velocity magnitude plots are scaled differently between pushed and rolling wheel.

Utilizing SIIA, it was shown that the soil failure mode, of the pushing wheel, was different from that of a rigid rolling wheel. These key differences can be observed in Figure 35 and Figure 36. Large differences in the direction and shape of the shear interface are evident. The soil beneath the rolling wheel appears to follow the shape of the wheel in a direction somewhat tangential to the wheel rotation. The failure occurs close to the wheel-terrain contact and is confined to the wheel contact area. However, the pushing wheel produces a much different response in the soil and a much larger thrust (see Section 5.3.3. for measured thrust). The soil displacement occurs as a unified mass moving together in the same direction and magnitude. The shear interface extends well beyond the contact region and looks like the shape of a logarithmic spiral failure (slip) plane that is common in soil mechanics theory [58]. Bekker describes this soil response as “ground failure” [14].

Terramechanics theory does not discriminate between soil failure modes and therefore cannot account for this. It is likely that the thrust mode being generated by a bevameter or direct shear test apparatus actually creates a soil failure mode that is similar to that of the pushing wheel, not to that of the rolling wheel which it is used to represent. These types of apparatus that measure the effective internal angle of friction, ϕ, for a wheel are flat plates that move more similar to the pushed wheel. This issue is of concern as these values are widely used for terramechanics models to predict rolling wheel traction in loose, granular soil.

Push-roll locomotion and the pushing wheel are studied in depth in Chapter 5.3 therefore limited observations and explanations are provided in this section.

4.2.6 Slip Rate

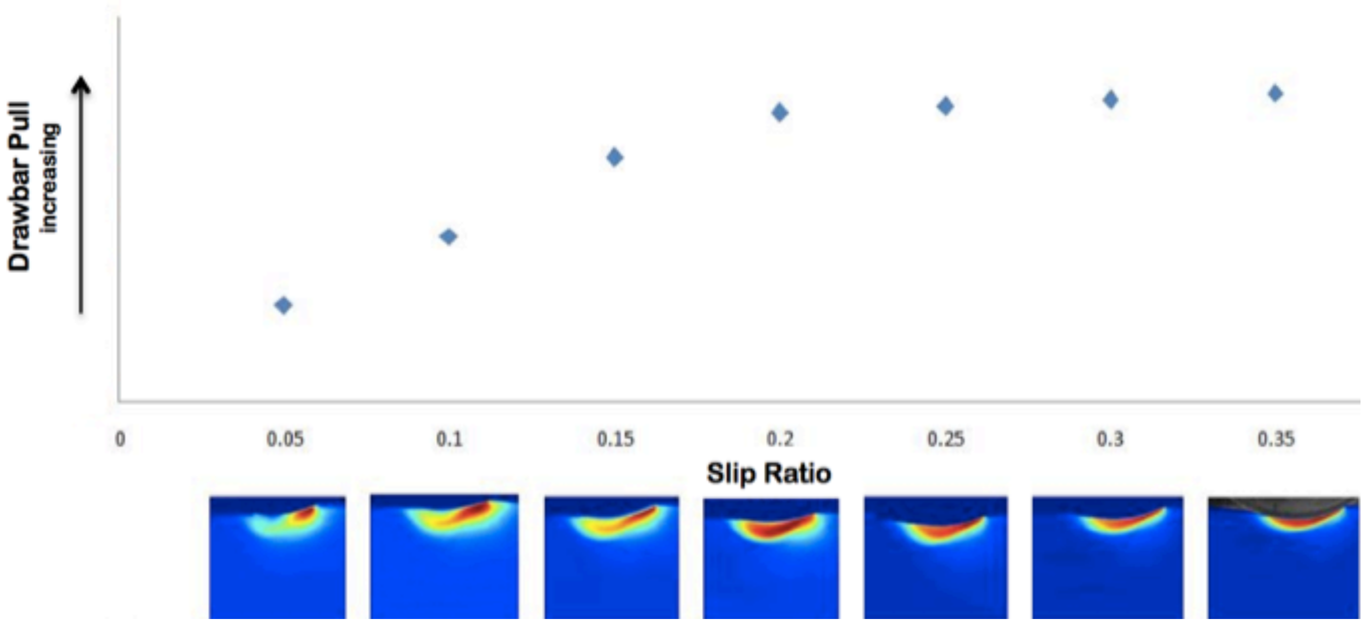

Figure 37: Drawbar-Slip curve with corresponding soil velocity magnitude plots at 5% slip intervals (see value above inset plots). Distinct changes in soil shearing behavior at key slip (0.2) and load points are observed. Wheel motion is to the right.

The degree of wheel slippage affects not only the net traction produced, but also the soil behavior below a wheel. Figure 37 shows the drawbar-slip curve for a small diameter rigid wheel. The shape of the curve is typical of many wheels in loose, granular soil relevant to planetary vehicles. A common trend is a knee in the curve that occurs near 20% slip, where afterwards, the rate of increase in drawbar pull declines. The shape of the curve is still highly dependent on the specific wheel design and currently there is no method to predict the shape.

There are distinct changes of the wheel induced soil motion at key points of the drawbar-slip curve shown in Figure 37. Three important observations can be made: (1) the shear interface size and shape do not change between 0.05 and 0.20 slip ratio, although the drawbar pull produced quadrupled. (2) From 0.05 to 0.20 slip ratio, the soil motion velocity, within the shear interface, transitions from a low gradient motion (implying shearing) to a region with near zero gradient inside the shear interface (moving as a whole) and to a sharp gradient at the shear interface. (3) Above 0.20 slip ratio, the forward flow appears to diminish while the shearing zone (region within shear interface) begins to reduce in depth (see Figure 38 for a clearer example). There are a number of hypotheses that can be made from these observations. First, the shear interface (outer extent of soil affected by shearing) might primarily be governed, not by the applied drawbar pull load, but by the shearing induced by the rotation of the rim. Also, the extent of the soil shearing even at low slip and low thrust load (0.05 slip and lower), is similar to that at 0.20 slip ratio. Therefore, it may not be the horizontal thrust loads that produce the soil failure planes, but rather the forced displacement due to the rim curvature and sinkage.

A second hypothesis states that the knee in the drawbar-slip curve (at 0.20 slip in this example) might occur when the soil shearing is fully developed within the shear interface. Operating at a slip ratio above 0.20 appears to transition, from a thrust generation type behavior of the wheel and to an excavation behavior at increasing slip. Further slip, beyond 20%, might result in increased drawbar pull by a different mechanism other than from thrust generated within the shear interface. Additional slip might reduce motion resistance due to soil transport at the wheel leading edge.

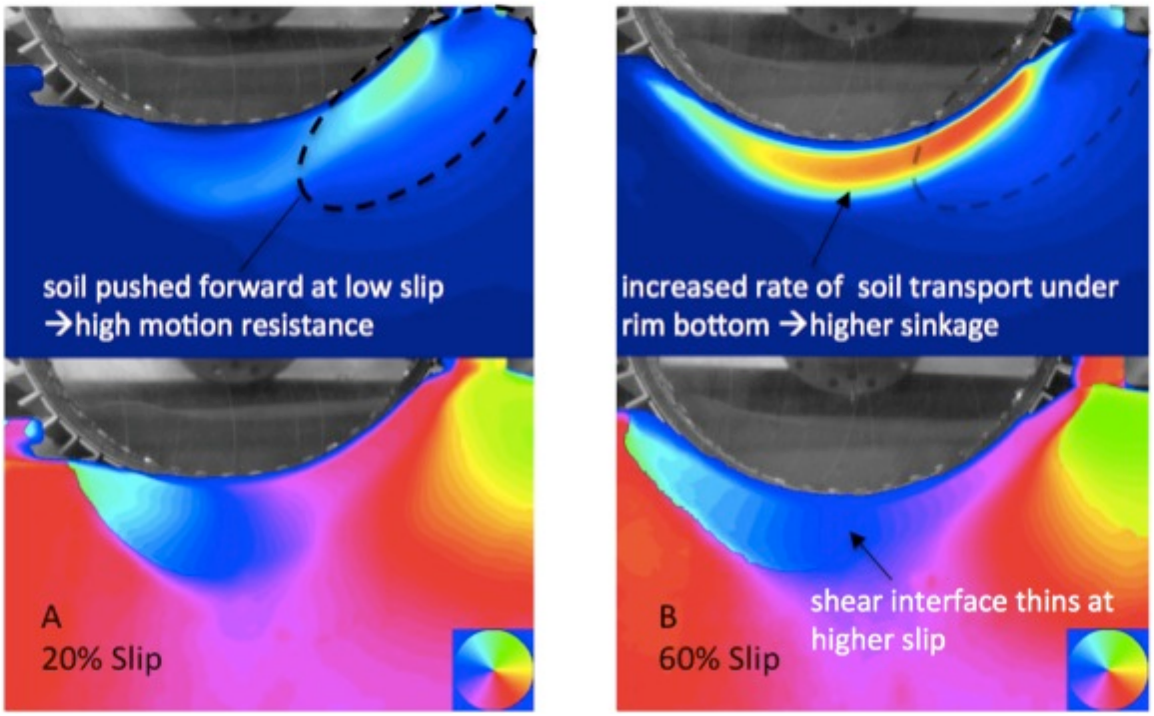

Figure 38: Major observations of effects of slip on shear interface and soil motion. A wheel operating at a medium and high slip rate are shown. The wheel velocity magnitude plots are normalized by ground speed and are at equal scale, allowing for direct comparison.

It is observed that the soil at the leading edge of a wheel that is pushed forward, reduces in magnitude and in the amount of soil engaged with increased slip. The wheel, operating at 20% slip (Figure 38), appears to push forward more soil, at a higher velocity, than the same wheel at 60% slip. Soil transport is a function of slip due to the fact that rim rotation, relative to stationary ground can cause soil motion. That fact and the observation of reduced forward soil motion, lead to the conclusion that soil transport due to increasing slip is a mechanism which slip can reduce motion resistance. There are other considerations, such as sinkage, when discussing mechanisms affecting motion resistance. However the realization that slip induced soil transport has a strong influence cannot be understated.

Both Figure 37 and Figure 38 show soil transport at the bottom of the wheel, increasing with slip. Soil transport, at the wheel bottom, would have an effect on traction as well as increasing sinkage by excavating below the rim. This trend was observed during all tests, over a range of slip values. An ideal wheel design would remove soil from the wheel leading edge while simultaneously not creating excessive soil transport from underneath the rim. A grousered wheel can be configured to address these two issues.

Soil transport is not accounted for in terramechanics theory, and there are few investigations of sub-surface soil motion induced by a wheel. Bekker and Wong have conducted a small number of tests, looking at sub-surface soil motion, using long exposure film [5] [14]. This measurement method had low fidelity and could not produce visualizations that allow for many of the observations presented in this thesis. However, Wong concluded that the performance, of a wheel and the soil motion below a wheel, are closely related and that theory must be established to reflect soil motion.

4.2.7 High Sinkage

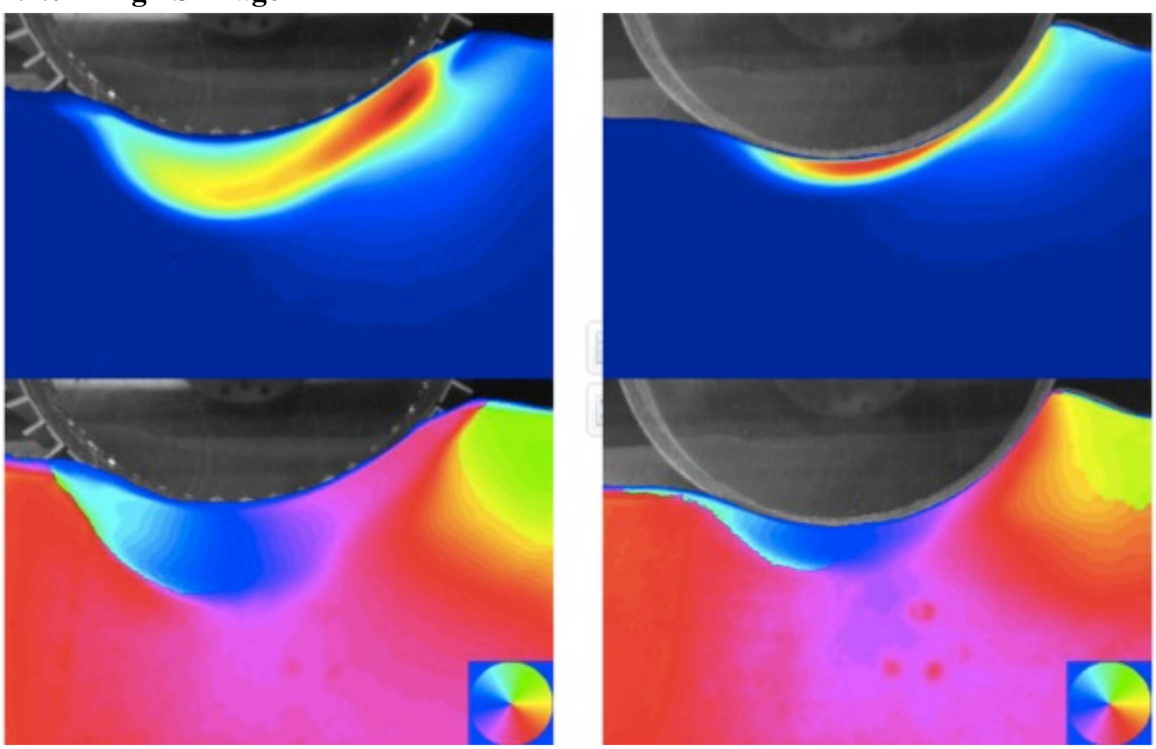

Figure 39: A material of very weak bearing and shear strength (Fillite) was used to demonstrate a high sinkage scenario where self-propelled travel is difficult. The grousered and grouserless wheels travel at 30% and 60% slip respectively (zero drawbar pull, self-propelled equivalent). High slip and sinkage resulted. The process of soil transport, at the wheel leading edge, can be observed and plays an increasingly important role in a high sinkage state.

It is evident from the SIIA plots, in Figure 39, that the soil in front of a wheel plays an important role in the traction process under high sinkage. These wheels are operating in the self-propelled state where the magnitude of thrust and motion resistances are equal and opposite. This is a scenario where self-propelled motion is not trivial since sinkage is significant enough to result in immobilization. It can be seen that soil in front of the wheel leading edge could create significant resistance to forward travel, therefore a wheel must manage this wall of soil since it is the only external force to overcome (when in a self-propelled state).

Two different wheel types are shown in Figure 39. Both wheels, grousered and grouserless, are operating in a self-propelled state but at different slip rates. These tests are conducted without slip control or any external load, therefore the resulting slip is naturally occurring. The grousered wheel, being more capable of transporting soil from in front of the rim (due to grouser sweep), appears to have lower magnitude of soil pushed forward at the wheel leading edge. This may be the mechanism that results in lower slip in a self-propelled state.

Although not fully supported by these experiments, a wheel, already operating at high slip (>20%), likely has to increase slip in order to reduce soil being pushed forward to match the thrust that has been generated.

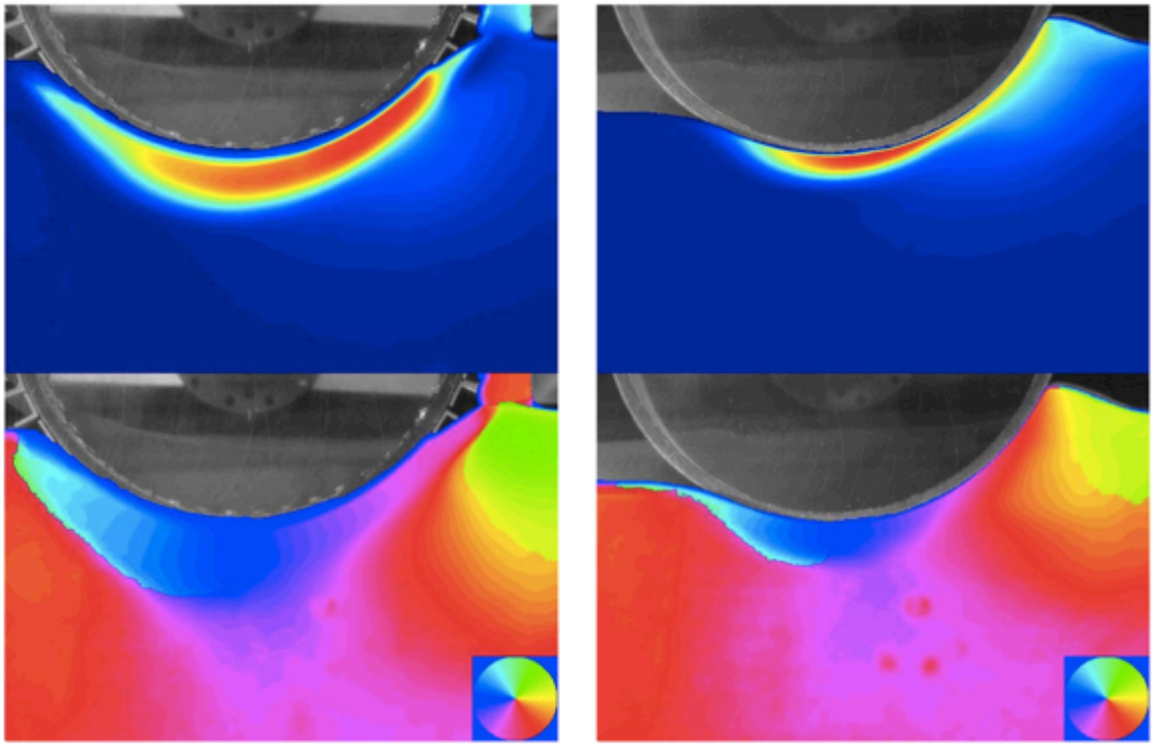

Figure 40: Constant slip tests, in a high sinkage material (Fillite), with groused and grouserless wheels both operating at 60% slip. Soil velocity magnitudes for both wheels are equally scaled.

It is evident, from the two wheels in Figure 40, that the soil motion, in front of a wheel (leading to motion resistance), is governed primarily by rim feature design (such as grousers) and operating point (such as slip) and not by solely by sinkage and wheel radius as terramechanics theory states [4].

The SIIA plots, shown in this section, provide another example of a sub-surface soil motion due to the influence of a wheel that has not before been directly observed. Previous soil imaging work did not look at soil motion due to different wheel designs [5]. The soil transport, that affects pushing forward of soil, is poorly understood and is not accounted for in terramechanics models. Soil transport is seemingly very important as it could account for the difference in self-propelled slip of the two wheels shown in Figure 39 and Figure 40.

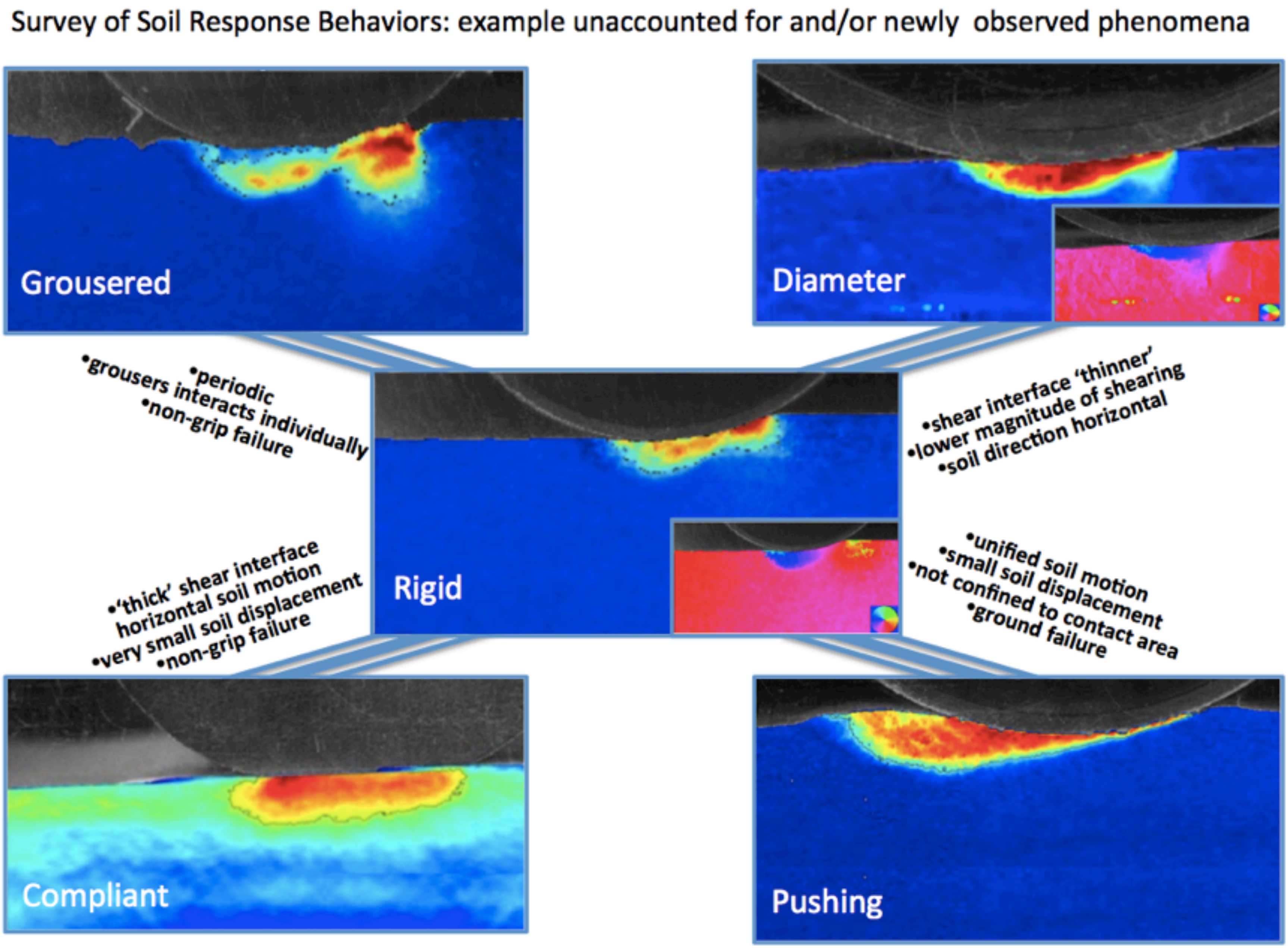

Figure 41: Soil motion behaviors can be observed between wheel types shown in this figure. These are not accounted for in terramechanics analytical models and generally have not been studied in the past.

4.3 Conclusion and Discussion

4.3.1 Conclusion

The survey of sub-surface soil motion behaviors due to the influence of common wheel types were revealed to be varied, generally inadequately understood and to possibly have significant influence on traction. The examples provided show that because most soil motion behaviors are either inconsistent with the literature, have not been observed before and are usually not accounted for in terramechanics models, that there is a general lack of understanding of how they affect traction. The objective of this chapter and the survey of soil behaviors, was to show the nature of these behaviors and that there is motivation to investigate specific phenomena. The discussion of some of these soil motion behaviors observable using SIIA, shows that soil motion must be taken into account if accurate prediction of performance is expected and if reasonable assumptions are to be made.

This is a strong impetus for further work that studies what happens underneath a wheel operating in loose, granular materials. The experimental results in the next chapter show that by, example of the grousered wheel type and a locomotion mode (push-roll), how research into wheel induced soil motion leads to the explanation of mechanisms by which they govern traction. This information is then used to improve design and traction device performance.

4.3.2 Discussion

The experimental results of this chapter present some interesting information about how wheels might operate and highlight a general lack of understanding about specific processes governing traction. Also, it is obvious that details about wheel stiffness, tread geometry, diameter, operating point (e.g. slip, sinkage) and many other aspects, have a profound affect on soil shearing, which in turn must influence thrust and resistance.

We see that results vary from the canonical simple wheel case, yet this is used to represent all wheels. Assumptions that only discriminate between contact area, are not truly accounting for the actual contacting surface (e.x. round, flat, lugged). Also, aspects commonly thought of as being of much higher importance than other wheel parameters, such as contact area and payload, do not appear to have the most overpowering effect on soil shearing structure.

It is also important to realize some of the many specific results. Studying wheels under varying slip rate and at high sinkage highlights soil transport, due to wheel rotation, as a mechanism that might play a major roll in traction; sinkage induced by slip affects resistance, while similarly, soil transport at the front of the rim can reduce traction by moving soil out of the wheel path. The shear interface shape of the rigid wheel is vastly different from that of the compliant, flat contact wheel and from that of the pushed wheel. Creating designs that could somehow achieve the shear interface of a high drawbar pull device, such as the pushed wheel, may produce wheels of extraordinary performance. These examples illustrate how studying soil motion behaviors could forward understanding and give insight into wheel-soil mechanisms that play important roles in traction.

5 Study of Soil Behaviors Governing Traction and Application to Design

5.1 Introduction

To show that behaviors of observed sub-surface soil motions influence traction and are important in understanding the operation of wheels in loose, granular material, the study of a wheel type and a locomotion mode are presented. Section 5.2, Grouser Mechanics, presents the study of the function of grousers and introduces design guidelines to achieve high performance based off SIIA observed traction processes. Section 5.3, Push-Roll Locomotion, investigates a non-typical locomotion mode to discover the sources of traction gains measured during full vehicle experimentation. The findings explain how this locomotion mode is able to produce high thrust and how best to implement for difficult surface materials.

The findings presented in this chapter highlight the importance of recognizing these insufficiently understood soil motion behaviors and show that better design can be achieved by accounting for specific wheel induced soil motions during analysis.

5.2 Grouser Mechanics

5.2.1 Introduction and Background

The use of features on the rim of wheels, such as grousers, has been relied upon for increasing traction of planetary rover mobility platforms in a wide range of applications. Performance measurements for use in loose, granular soil, have shown tractive gains for many implementations of these features [59] but little empirical data exist on the mechanisms present in the soil that contribute to increases in mobility capability. Additionally, there exists no well-supported theory pertaining to the soil failure characteristics created by wheel operations with grousers. As such, grousers are a poorly understood but commonly implemented design aspect of wheels for planetary rovers and other systems traversing loose, granular soil. Of theory that exists, no direct empirical evidence has been offered to validate the soil failure that governs how thrust is generated by grousers.

Figure 42: Rigid wheels with grouser implementations deployed to Mars. From left to right: Mars Exploration Rover, Sojourner, Mars Science Laboratory. Image credit [54].

The two soil failure types, shown in Figure 43, are commonly accepted and used in modeling of wheels with grousers. The left diagram, (A), shows soil shearing between immediately neighboring grouser tips. As soil has filled the spacing between the grousers, the effect on soil interaction below the wheel, is that of a slightly larger diameter wheel with an increase equal to two grouser heights. Bekker illustrates this soil failure type as a curved line of radius of the wheel radius, plus grouser height. He refers to the soil failure as a “grip” type failure [4]. The expected effect on traction would be to increase the rim-soil coefficient of friction (immediate rim to soil contact) and to have gains associated with a larger wheel diameter. It has been previously shown that the traction gains, when utilizing grousers, exceeds that of a larger diameter wheel due to the additional height of the grousers [60] [61]. Therefore, it has been previously concluded that the wheel with grousers does not simply increase drawbar pull by increasing the effective diameter.

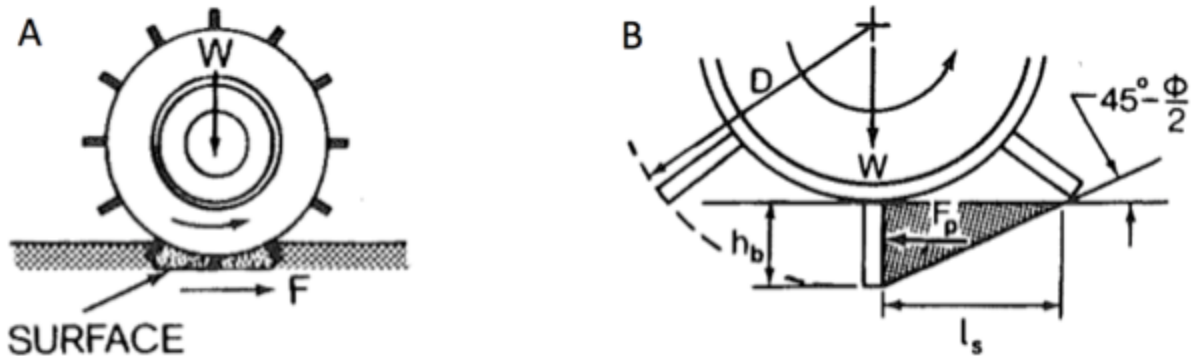

Figure 43: Theory of the mechanics of grouser interaction with the ground is shown. Wong and Bekker describe two types of soil failure processes a wheel with grousers follow. (A) Soil shears along a straight line that occurs from grouser tip to tip. (B) Passive soil stress region, of which soil failure follows a line from tip to ground surface along a line of angle 45° - φ/2. Shown here are figures from [9]

Diagram (B), of Figure 43, represents the passive soil stress state from conventional soil mechanics theory derived for bearing capacity and retaining walls [58]. Applying this method to a wheel, implies a failure plane along a line from the grouser tip to the soil surface at an angle of 45° - ϕ /2 from the horizontal (where ϕ is the internal angle of shearing resistance). The angle of the failure plane is constant and is dependent of soil properties. For loose GRC-1 this angle is as low as 30°. It should be noted that, for this type of failure to occur, very large grousers with large spacing would have to be implemented, to allow for a passive soil stress state to occur.

As these two failure types are simple to describe, the soil response plots from Shear Interface Imaging Analysis should allow for easy identification of either of the characteristic shearing types if present during actual wheel operation.

5.2.2 Approach

The experimental approach was conducted in two stages. First, preliminary tests to survey general grousered wheel soil behavior were conducted. These tests were used to identify major differences in characteristics compared to a wheel without grousers. Additionally, large changes in spacing were examined to determine what major sub-surface soil motion behaviors changed with the spacing parameter. The preliminary results were used to assist experiment design of the second stage of the grouser mechanics research.

The second stage was a comprehensive experimental campaign to associate changes in wheel induced soil motions with changes in grouser parameters: height and spacing. Twenty-five different wheel/grouser configurations were evaluated using SIIA and wheel force measurements (Table 5). These results were used to identify possible grouser induced traction mechanisms and were used to associate these mechanisms with configurations of high measured drawbar pull.

5.2.3 Methodology

The test configuration, for single wheel force measurements and SIIA sub-surface soil motion analysis varied only in wheel configuration and soil type. For all experiments, a slip controlled test type was applied. The wheel tangential rim velocity was 1cm/s and slip was held at 20% (carriage speed varies to control slip). A 23cm and 41cm diameter wheel, each 5.72cm wide (11.43cm effective width), were the two wheel sizes utilized in experimentation. These wheels were both rigid, flat rim profile, and with a sandpaper surface. Grousers, fabricated from aluminum angle stock ('L' shaped), were mounted to the wheels to form many different configurations. The total vertical load on both wheel types was 10kg (consisting of added deadweight, plus weight of the wheel module). The 10kg payload was applied to the wheel creating an average ground pressure of 22kPa for the small, 23cm diameter wheel in GRC-1 soil simulant (by measuring contact area at 20% slip, without grousers). This ground pressure is relevant to planetary vehicles, such as the NASA Mars Exploration Rovers [62]. The single wheel imaging test bed was prepared with GRC-1 lunar soil simulant or Fillite material before each test run. The soil is loosened to a state of lowest relative density and slightly compacted by use of a drop tamper method to produce repeatable soil properties. Shear strength measurements were taken after each soil preparation to verify consistent strength properties. Specific strength values were not required for the research type experimentation conducted. A torsional shear strength tester, modified for constant normal pressure control was utilized [63]. The Fillite did not undergo any compaction after loosening, as the very low density, due to hollow particles, would create dust hazard to health. Shear strength, for this material, was not measured the as strength is too low for in-situ measurement tools available.

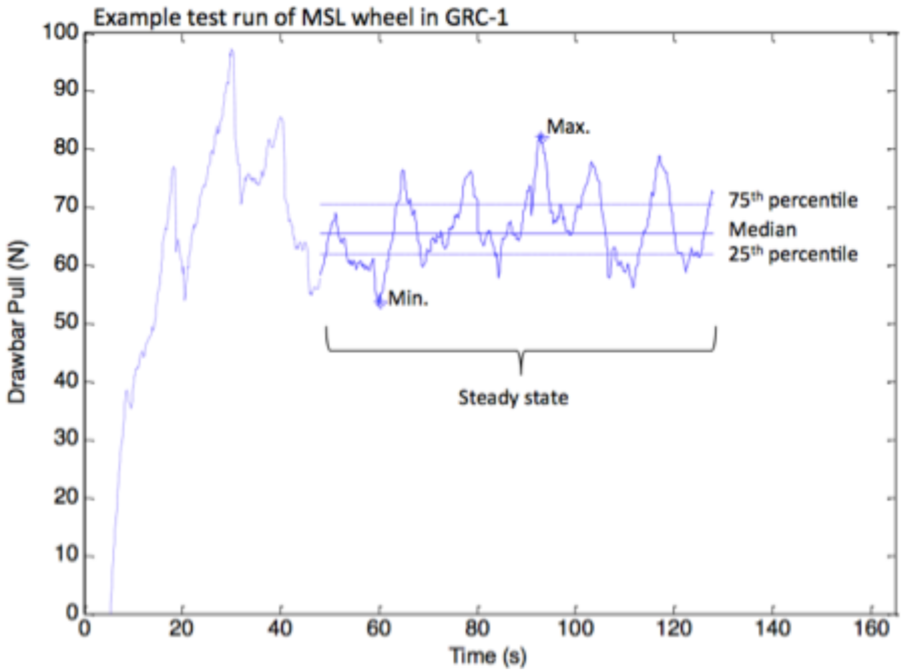

Figure 44: Example rigid wheel with grousers in GRC-1 soil simulant at 20% controlled slip in the single wheel test apparatus. The median value during the steady state region of measured drawbar pull is used for evaluation to compare amongst grousered wheel configurations.

Wheel reaction forces were measured using a 6-axis force/torque sensor [64]. The horizontal force in the direction of travel, called drawbar pull, was used for evaluation of traction performance. The median value of drawbar pull, during steady state response, was the value used to compare amongst different wheels (see Figure 44). The median value is a simple method for direct comparison of the groused wheels since a similar drawbar pull-time response type of periodic response occurs. Using the median value to compare to other wheel types that do not have large amplitude, periodic responses such as a compliant wheel, could be problematic. Using the median drawbar pull value is not an appropriate method to compare very different wheel types or to estimate vehicle performance, such as slope climbing ability. The 25th percentile would be a suitable and more conservative method for estimate of vehicle performance.

5.2.4 Experimental Results

5.2.4.1 Preliminary Experimental Results

Preliminary experiments were conducted to look at wheel induced soil motion that occurs from grouser interaction. A single wheel diameter (23cm), two grouser spacings and a non-grousered wheel were compared. Basic soil responses were observed that resulted in important conclusions.

Two wheels, with different grouser configurations, are shown in Figure 45. One wheel was selected to represent a design following a common spacing rule of thumb where at least two grousers are in contact with the ground. The other wheel had a closely spaced configuration that might force 'grip' soil failure. Both wheels have grousers of 13mm height.

There are important observations, made from Figure 45, regarding the understanding of grousered wheel function. Periodic soil motions, induced by wheel rotation and a periodic response in drawbar pull are measured (Figure 46). The distinct periodic soil motion events and the major peaks of the drawbar pull have a period proportional to grouser spacing. The periodic nature of the soil motion response and the measured reaction forces suggest that the 'grip' type soil failure behavior, as suggested by Bekker, is probably not the dominant behavior in governing grousered wheel traction. Non-periodic soil and drawbar pull response would be expected, if a wheel simply acted as larger diameter wheel when grousers are added to a rim.

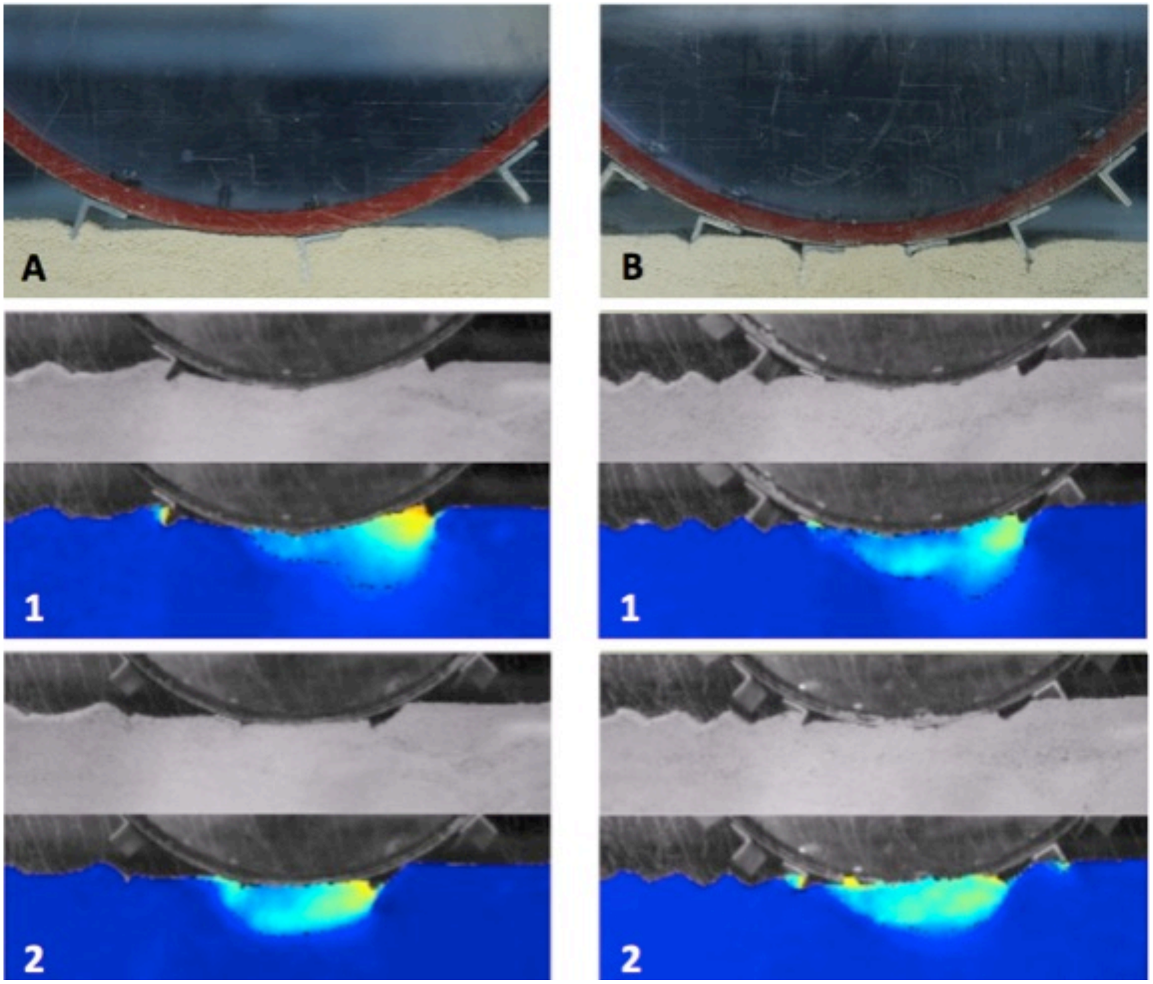

Figure 45: Wheel ‘A’ has 12 grousers and at least two are in contact with the ground at any time. Wheel ‘B’ has 24 grousers and at least 4 are in contact with the ground at any time. Wheel motion, is to the right (clockwise wheel rotation) and is at 20% slip. Soil motion velocity magnitude plots, of major soil shearing events in a cycle, are shown; denoted as ‘1’ and ‘2’. Frame 1 is when the leading edge grouser first fully engages the soil and full rim contact occurs. Frame 2 is shortly after when this grouser displaces the soil due to slip. These two distinct soil motion characteristics repeat periodically.

The two wheels, in Figure 45, exhibit similar soil motions throughout the cyclic processes. A cycle consists of the duration when a grouser engages new soil, to the time the next grouser meets the ground. The only difference between the two wheels, when assessing the SIIA magnitude plot, is the period of the soil response. This observation is important, as the measured mean drawbar pull of the two wheels is significantly different. Figure 46 shows a higher mean drawbar pull for the wheel with more grousers (pull coefficient of 0.24 versus 0.17). There is no mechanism observable, from these experiments to suggest why one wheel might generate more traction than the other. There is no obvious mechanism of increasing thrust due to the grouser implementation of higher drawbar pull. Evidence of increased thrust would likely take the form of a larger shear interface that engages more soil. However, these observations do not preclude the existence of a mechanism to increase thrust that results in the two wheels having different drawbar pull characteristics.

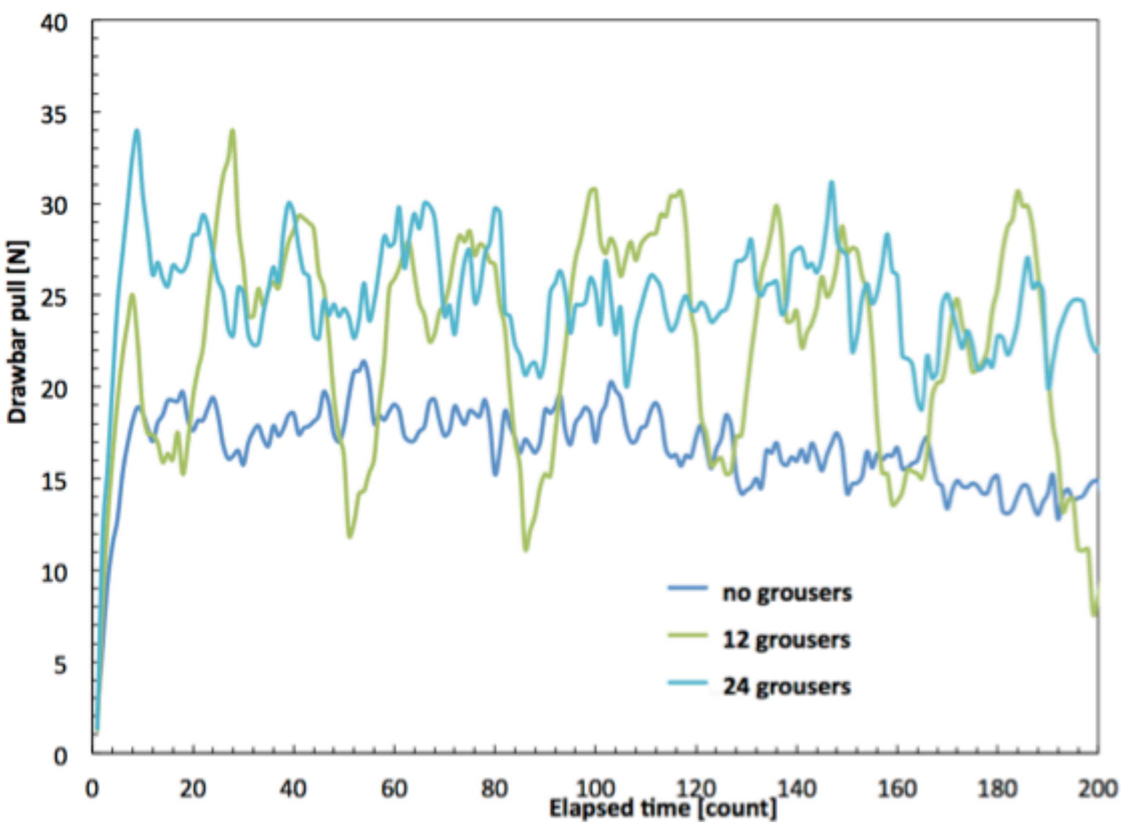

Figure 46: The drawbar pull is shown to be periodic for wheels with grousers. For these wheels, major period is observed to be proportional to grouser spacing. A large peak and trough occurs with each grouser. The period of response is proportional to the number of grousers. This means each grouser might have an individual effect on traction.

The periodic response of the reaction loads (drawbar pull versus time shown in Figure 46) is a key observation. There is a major peak for each grouser entering the soil for all spacing's tested. The relationship of period of drawbar pull and number of grousers is an important realization as it shows that each grouser has an individual effect on drawbar pull. There is also an observable decrease in variation (amplitude of periodic curve) of the drawbar pull as a function of time as the spacing decreases. Although only two spacing's are shown in Figure 46, this trend is maintained for all spacing's tested later and is presented in the next section. A physical explanation, for the cause of these observations, increased mean and lower variation of drawbar pull for smaller spacing, was sought when conducting the second part of the grouser mechanics study.

Comparing a wheel with grousers to a wheel without grousers also yielded important findings. The concept that a wheel with grousers might act similarly to a slightly larger wheel because the grousers fill with soil is logical. SIIA results of a groused and grouserless wheel (Figure 47) show that this concept might be valid, although still does not explain sources of drawbar pull gains due to grousers.

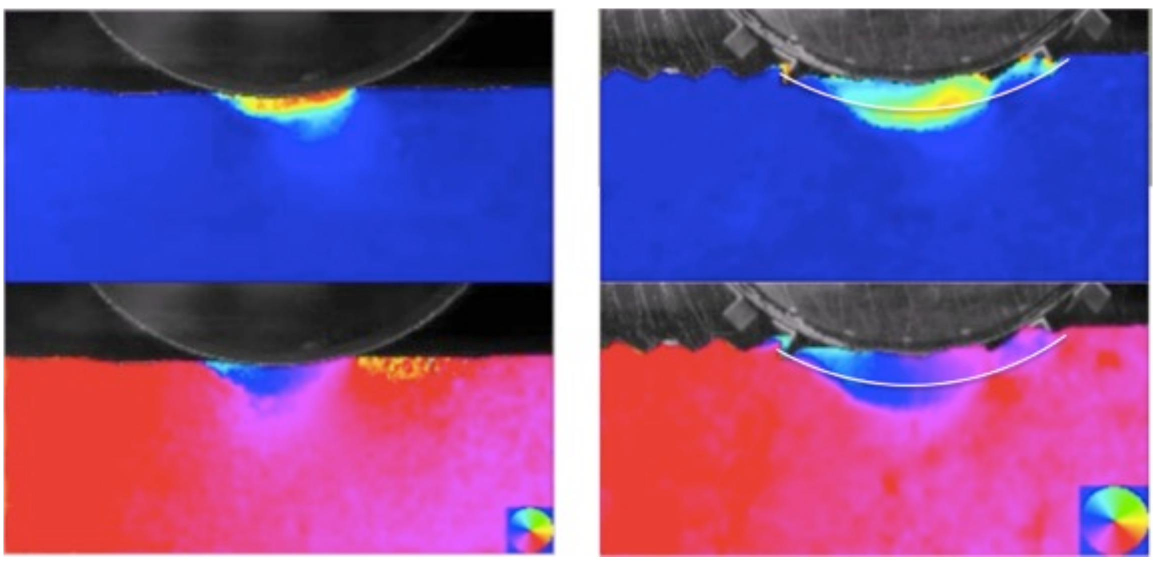

Figure 47: Similarities between the grouserless wheel and groused wheels are observable. The depth of the grouser tips is indicated by a white curve in the figure with the groused wheel. The shear interface beyond the grouser tips is similar in thickness, magnitude of soil displacement and shape to that of the grouserless wheel. Soil velocity magnitudes for both wheels are equally scaled.

Although there are periodic soil motion events, the snapshot of the soil motion shown in Figure 47, is representative of the longest duration of the cycle that soil motions go through. That is, there appears to be an underlying soil shearing plane and periodic bursts of motion, at the wheel front, occurring for each grouser (although not necessarily when the grouser interacts). The underlying shear interface is easier to observe in Figure 53 which shows two cycles and four time steps per cycle.

It can be seen that the shear interface of the grousered wheel in Figure 47 is similar to the shear interface of the grouserless wheel. That is, the shape of the slip plane at the outer extent of significant soil motion might be identical to that of the grousered wheel. The shear interface is offset by the height of the grousers. Although the shear interface is deeper in the soil, it has the same size and shape. Additionally, the soil motion magnitude and direction along (and within) the shear interface are the same. These similarities suggest that the region of the wheel where the grousers are full of soil, creates a shear interface similar to that of a grouserless wheel. Therefore, the net traction created by a grousered wheel, would not change significantly compared to that of a grouserless wheel in terms of this region of the wheel (the contact region except for the front where grousers are yet to be filled with soil). This suggests that the front contact region might be of more importance to study.

Figure 51 is another example, where an offset of grouser height of the shear interface compared to that of a non-grousered wheel is evident. For a more dramatic comparison, a 48-grouser wheel that has a significantly higher drawbar pull than that of the same wheel without grousers (sandpaper surface), is compared in Figure 49. The wheel and grousers are blacked out to aid in direct comparison of SIIA plots to that of the grouserless wheel. For reference, Figure 49 shows a picture of the grousered wheel in this comparison. It can be seen that the shear interface and soil motions are remarkably similar between the two wheels except for the front contact region. This finding supports the hypothesis that the wheel front region for a grousered wheel is of importance for explaining grousered wheel mechanics.

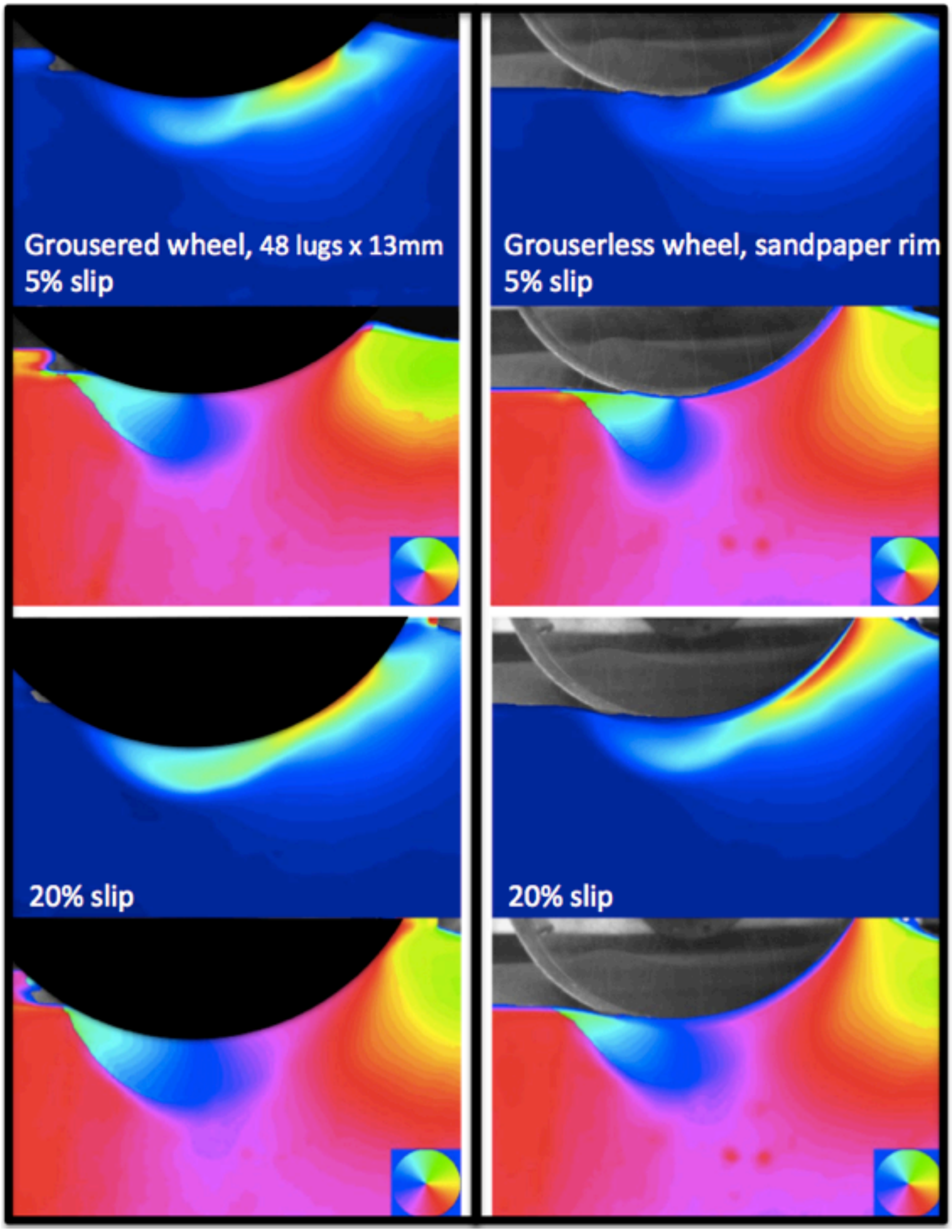

Figure 48: Grousered and grouserless wheels are shown operating at 5% and 20% slip. The arc formed by the grouser tips is indicated by the blacked out region for ease of comparison. The shape of the shear interfaces below both wheel types is similar for the region outside the grouser tips. These similarities might suggest that once the grouser is full of soil, that part of the wheel acts simply as a larger diameter wheel with increase due to grouser height. See Figure 49 for picture of groussered wheel used in these tests.

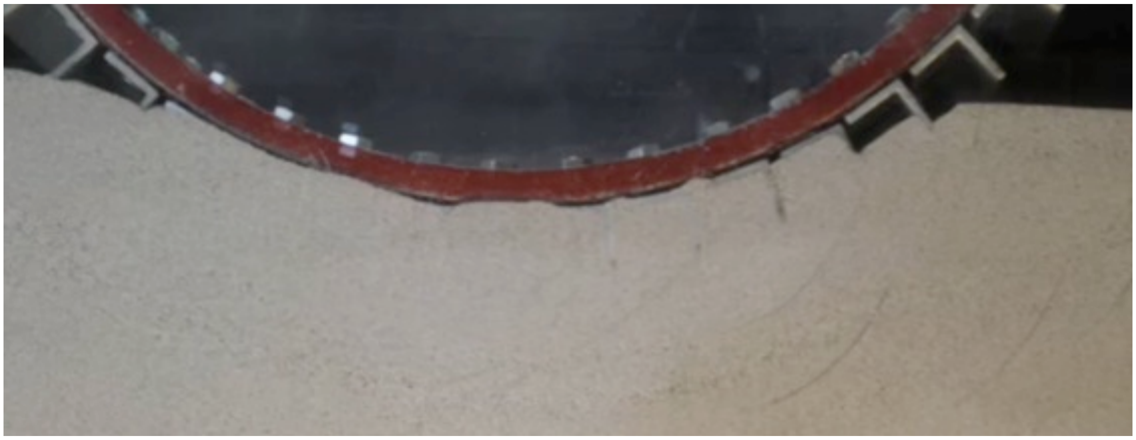

Figure 49: Grousered wheel used in tests shown in Figure 48. This wheel has 48 grousers that are 13mm in height.

5.2.4.2 Summary of Preliminary Results

There are three main observations from the preliminary experiments. First, the soil and drawbar pull response are periodic. Since the period tracks directly with the number of grousers, it is probable that each grouser has an individual effect on traction. The second observation is that there is no evidence, in terms of soil motion, of a mechanism to produce higher thrust for a wheel with grousers of higher drawbar pull versus that of a grousered wheel of lower drawbar pull. Similar shear interfaces are seen for both grouser configurations studied via SIIA. The length, thickness and general shape are similar. The similarity might suggest, that for like wheel types of differing drawbar pull, looking for evidence of increased thrust in the form of soil mass engaged or different type of soil failure might not yield useful results. The third observation is that, other than the region at the wheel front where the grouser first engages the soil, the shear interface characteristics of grousered and non-grousered wheels are similar. The sources of traction might be associated with differences in soil motions at the front of the wheel where major dissimilarities are apparent.

5.2.4.3 Grouser Configuration Experimental Results

A comprehensive experimental campaign, consisting of twenty-five different wheel/grouser configurations, was conducted. SIIA and wheel force measurements were collected for these configurations and are outlined in Table 5. The goal of the grouser configuration experimental campaign was to identify changes in wheel induced soil motions with changes in grouser parameters. Soil motion behaviors then could be associated with measured performance gains. As the soil behaviors are informative of actual traction processes, an effort to use wheel induced soil motions to explain the mechanisms behind grousered wheel traction was undertaken.

Table 5: Grouser Configurations Tested.

t =tested (telemetry collected), i = SIIA processed

Wheel Diameter [cm]	Grouser Height [mm]	Number of Grousers						
		6	12	16	24	32	42	48
23	13	t, i	t, i	t, i	t, i			t, i
	9.5	t, i	t, i	t, i	t, i			t, i
	6	t	t, i	t, i	t, i			t
	0	t, i						
41	25		t, i	t, i	t, i			
	13				t, i	t, i	t, i	t, i
	9.5				t, i			
	6							
	0	t, i						

The drawbar pull of many grouser configurations is plotted in Figure 50. It shows that grousers can be configured to increase drawbar pull. There is a trend of increasing traction with larger height and smaller spacing. Additionally, there is a plateau in drawbar pull as the number of grousers increase for a fixed height.

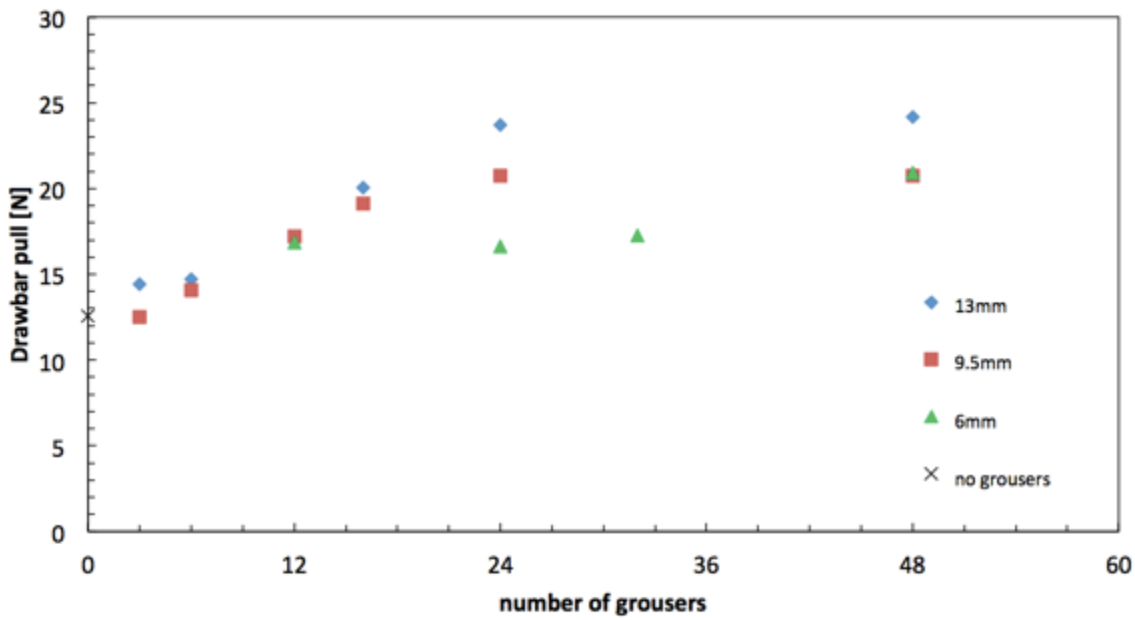

Figure 50: Drawbar pull results for 23cm diameter rigid wheel with grousers at six spacing's and four heights. These results are evaluated at 20% slip and averaged over the steady state portion of response. The use of grousers shows significant increase in drawbar for some configurations. A plateau in performance is visible for two grouser heights.

It is desirable to identify the specific mechanism due to grouser/wheel interaction with the ground that results in the observed soil failure, leading to specific trends such as the plateau in drawbar pull with respect to spacing. A similar plot, Figure 59, displays more grouser configurations and show the same trends.

The traction performance, of the 23cm diameter wheel without grousers (sand paper rim) and of the same wheel with 48 grousers at 13mm height, act as extremes of the grouser configurations and drawbar pull measured. Studying SIIA plots (Figure 51) of these two cases leads to an important realization. The soil behavior of the grouserless wheel and of the 48-grouser wheel are very different at the leading edge of the rim. Figure 51A is a direction plot that shows a yellow patch of soil in front of the wheel that moves in a horizontal direction forward. The soil forward motion is evidence of wheel motion resistance as the soil is likely being pushed forward and reacting against the rim. This motion resistance would reduce the drawbar pull of the wheel. However, the wheel with highest drawbar pulled tested (48 grousers, 13mm height), does not display forward soil motion.

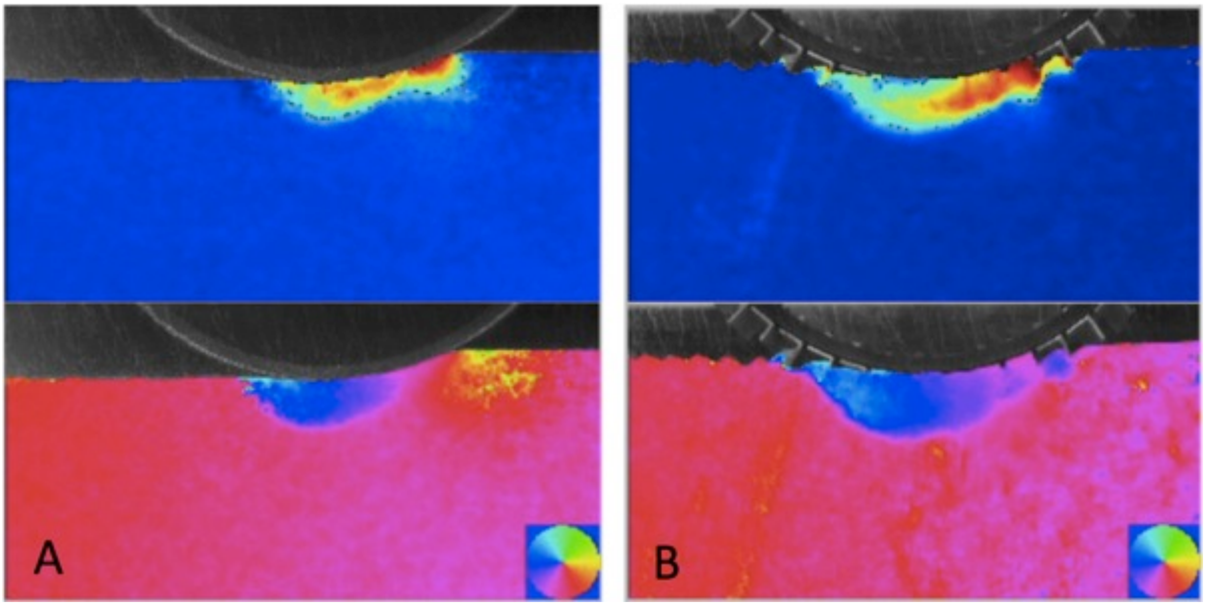

Figure 51: Forward flow is the most evident difference in soil motions between the lowest and highest drawbar pull wheels tested. (A) The wheel without grousers (sandpaper surface) does exhibit for forward motion at the wheel leading edge. (B) The wheel with 48 grousers at 13mm height does not display soil pushed forward at the wheel leading edge. Soil velocity magnitudes for both wheels are equally scaled.

For small diameter rigid wheels operating at ground pressures and in soils relevant to planetary surface vehicles, motion resistance is usually in the range of 10% to 50% of available thrust, thus drastically reducing drawbar pull available. It is reasonable to conclude, from the lack of soil forward motion of the wheel in Figure 51B, that the grouser implementation can lead to reduced motion resistance, and thus higher drawbar pull. This can potentially account for the significant difference in drawbar pull between the two wheel types.

This experimental result highlights forward soil motion at the wheel leading edge as a key behavior that can be linked to measured traction, theoretical drawbar pull gains and grouser interaction with the ground.

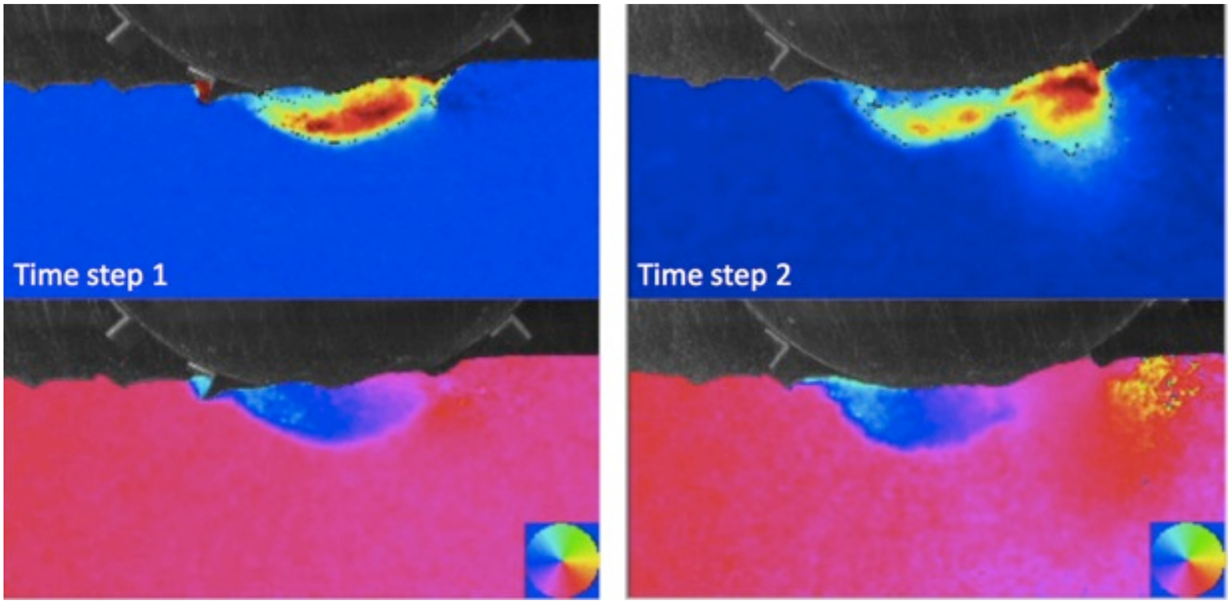

Figure 52: Periodic forward motion of soil at the wheel leading edge is evident. The ‘yellow patch’ at the right side of the wheel, at Time Step 2, is evidence of periodic motion resistance. A 23cm diameter wheel, with 12 grousers of 13mm height, is shown.

The forward motion of the soil, at the wheel leading edge, is periodic for most wheels with grousers. As the drawbar pull of groused wheels is also periodic and of the same frequency as the forward soil motion, the two behaviors might be related (based off drawbar pull major peaks, see Figure 46). The periodic presence of motion resistance can account for the periodic drawbar pull measured. The conclusion that periodic motion resistance accounts for variations in drawbar pull does not preclude any additional thrust generated by a grouser, however, little experimental evidence was found to support possible gains due to thrust.

Forward soil motion can only be affected by the interaction of the ground with the wheel leading edge; a mechanism should exist by which the grouser prevents soil forward motion and/or creates a periodic forward soil motion response. Looking for the wheel-soil interaction that forces or reduces soil forward motion, leads to the results in Figure 53.

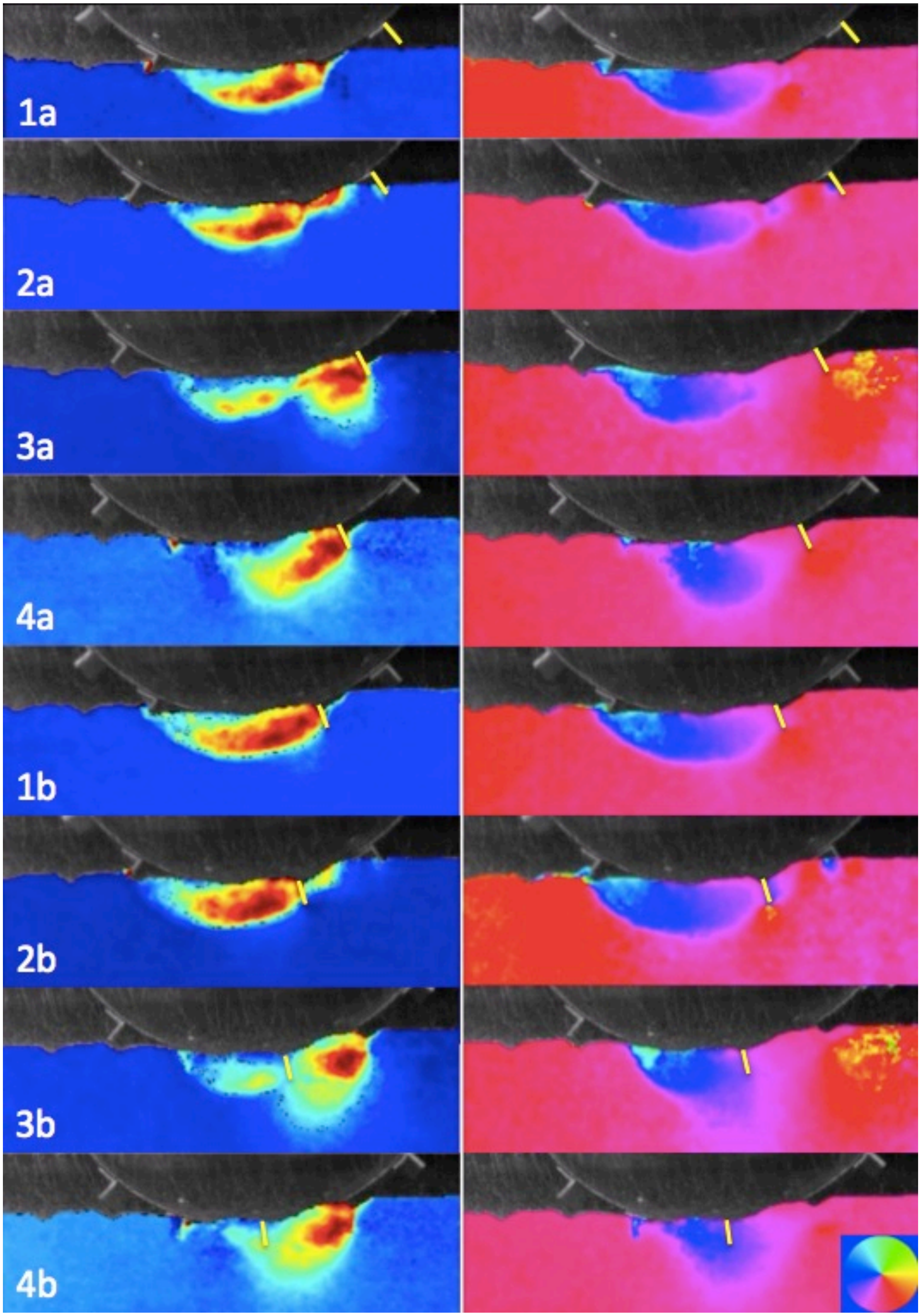

Figure 53: Time lapse of two grouser engagements (two cycles). Rim interaction at the leading edge of the wheel creates periodic forward motion (motion resistance) that is reflected in the drawbar-pull versus time plot (Figure 46, 12 grouser curve). The periodic 'yellow' patch of soil, at wheel front, is evidence of grousers affecting soil forward motion and wheel motion resistance.

All grousered wheels that displayed periodic forward soil motion (these all also had periodic drawbar pull) had a common behavior of rim interaction with the ground. When the rim first contacts the ground and pushes on the soil, forward motion of soil in front of the wheel is evident (Figure 53, 3a and 3b direction plots). This process is periodic as the grouser sweeps in front of the wheel and, therefore, the rim is not always in contact at the leading edge (in the region where it would contact on a grouserless wheel). During these non-contact times, the forward soil motion does not occur, as the rim is not pushing against the soil at the wheel front.

This process can be seen in Figure 53. In direction plot 2a, the rim leading edge has just contacted the soil. Then, in direction plot 3a, the rim starts to push against the ground resulting in forward motion of the soil. At this point, motion resistance likely occurs and the drawbar pull momentarily drops. As the grouser continues to sweep (direction plot 4a), soil at the leading edge is transported away from the very front contact point (now no longer in contact) and the motion resistance drops, resulting in an increase in drawbar pull. This cyclic process of the grouser at the leading edge transporting soil away from the rim front reduces the soil the wheel must push through and is the mechanism by which motion resistance is reduced. The effects of this process are evident by the reduction of measured forward soil motion. This simple mechanism can be seen as a result of tracking sub-surface soil motion by SIIA.

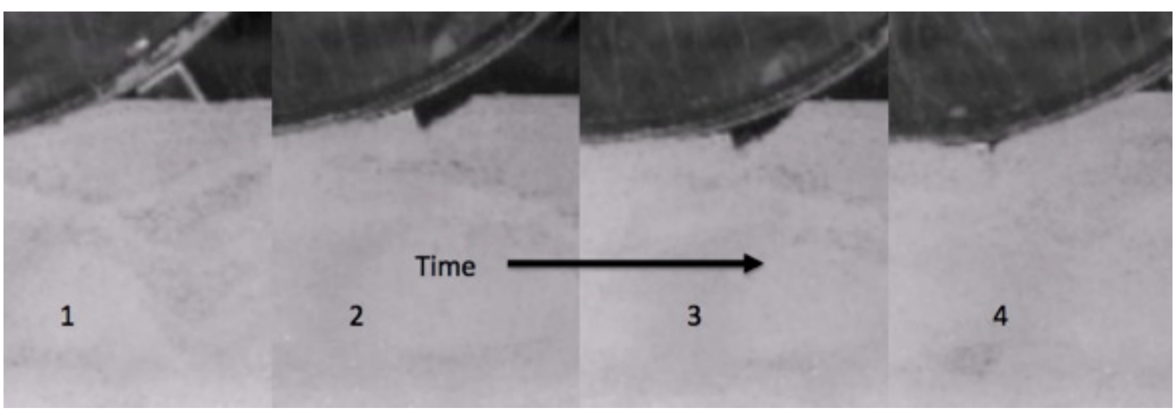

Figure 54: Closer look at grouser sweeping action shown for a wheel operating at 20% slip. At step 4, the rim pushes soil forward similar to a wheel without grousers.

Figure 54 provides a closer look at the sweeping action that results in the grouser transporting soil underneath the rim before it can contact at the leading edge of the wheel. If a wheel is operating at non-zero slip, the rim will rotate faster than the forward motion of the wheel, thus creating a rearward motion of the rim with respect to the ground. When grousers are implemented, soil is transported away from the front of the wheel, removing soil that would normally be resisting forward motion.

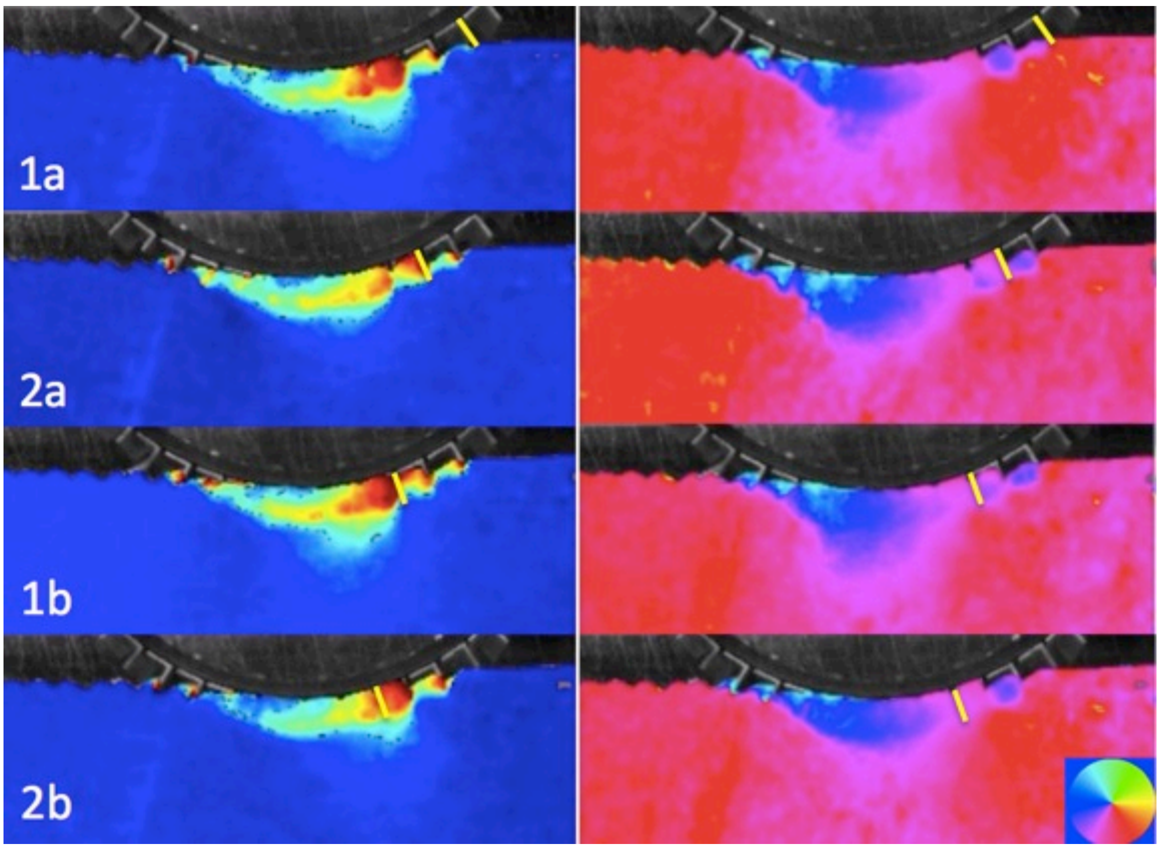

Figure 55: Time lapse of two grouser engagements (two cycles, a & b). The wheel shown does not exhibit forward motion of soil at wheel leading edge. This wheel generates the highest drawbar pull of the wheels tested and has a periodic response of lowest amplitude (i.e. low variation in drawbar pull).

The 23cm diameter grousered wheel tested that had the highest drawbar pull is shown in Figure 55. This wheel does not show evidence of motion resistance and has a relatively high drawbar pull compared to other grouser configurations. The lack of soil forward motion and high drawbar pull demonstrates that wheels with grousers can be configured to significantly reduce motion resistance.

The height and spacing of the grousers on this wheel (Figure 55), must promote a reduction of forward soil motion, thus reduce motion resistance. Looking closely at the front contact of the wheel with the ground (similar to area magnified in Figure 54), it can be seen, in Figure 55, that the rim of this wheel can never push soil at the very front of the wheel since a grouser always sweeps the soil before it can touch the rim (as occurs in Figure 54, step 4). The soil at the very front, that would contact the rim and resist wheel travel, is instead confined by a grouser and transported away from this region. By transporting the soil out of the wheel path, the effective contact angle is reduced and less soil must be pushed on during forward travel.

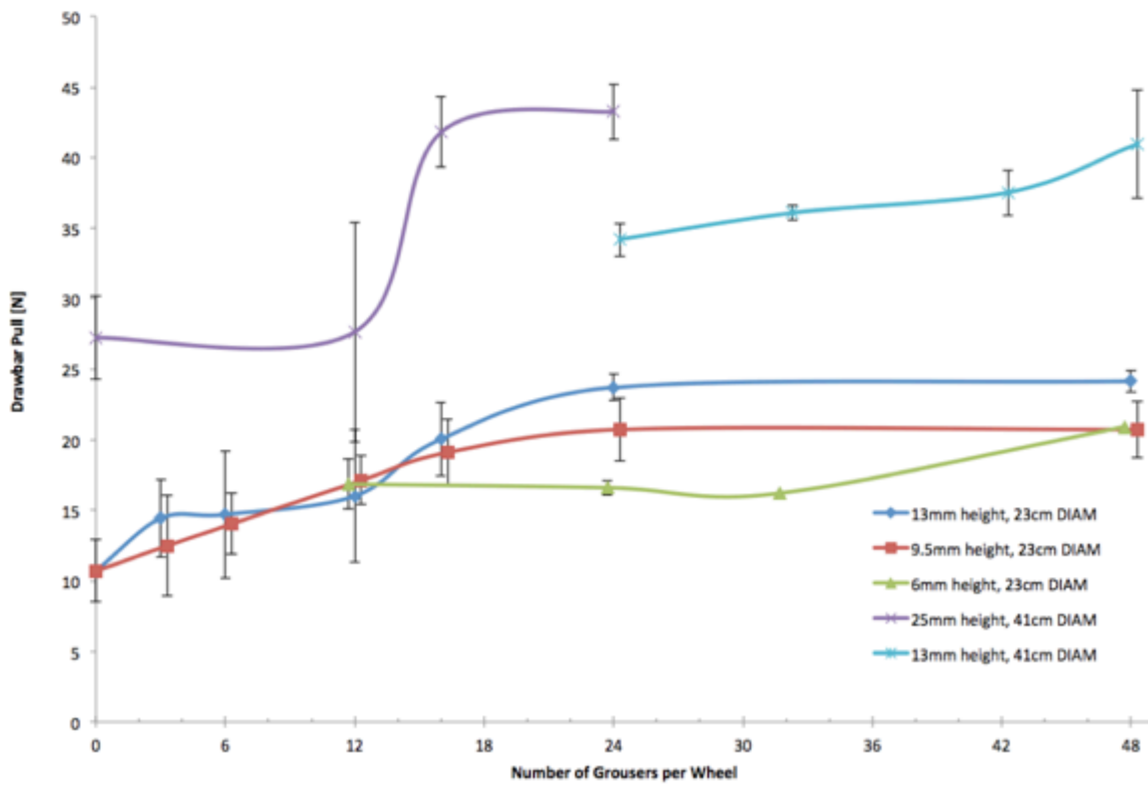

Figure 56: Drawbar pull measurement for two different wheel diameters with multiple grouser spacing's and heights. These are evaluated at 20% slip. A plateau in drawbar pull can be identified for three of five curves. The plateau might occur due to the grouser configuration achieving a minimum motion resistance; therefore no additional gains can be achieved. Error bars indicate two standard deviations.

Proper selection of length and spacing of grousers enhances these effects. If length and spacing are chosen properly so that the rim does not contact the soil surface before a grouser confines and transports soil, then motion resistance will be reduced.

There is a plateau in drawbar pull, as the number of grousers increase for a fixed height, observable in Figure 56. The plateau occurs, due to the fact that the grouser spacing/height combination is such that grousers are able to effectively remove soil at the wheel front before it can resist wheel travel. Since the contact at the wheel leading edge has been eliminated, decreasing grouser spacing to achieve higher drawbar pull yields no gains. The two different soil contact behaviors that occur either before the plateau and on the plateau, are confirmed by looking at SIIA plots on either side of the knee in the curves. See Figure 53 and Figure 55 for configurations before and on the plateau respectively. It can be observed that there is periodic rim contact leading to forward soil motion for the lower drawbar pull wheel, while no rim contact at the leading wheel edge occurs for the wheel on the plateau.

Wheels with drawbar pull values lying on the plateau have grouser configurations that effectively reduce motion resistance and, therefore, yield higher performance. Formulating design guidelines to achieve low motion resistance, was undertaken by recognizing the grouser sweeping behavior, to reduce motion resistance as the mechanism that increases drawbar pull.

5.2.5 Grouser Height/Spacing Relationship

The mechanism of reducing motion resistance by confining and transporting soil from the wheel front can be used to guide design. Selection of proper grouser height and spacing can enhance the clearing effect and increase drawbar pull.

A mathematical derivation of the grouser height/spacing relationship was introduced by C. Skonieczny and S. Moreland based off the SIIA results presented in the previous section [65]. This section covers the research of these authors.

Parameters, relevant to the deriving an expression relating grouser spacing and height for high performance are summarized in Table 6. The length parameters are normalized with respect to wheel radius, r, for simpler derivation. Figure 57 diagrams relevant parameters related to the wheel and ground. Two protrusions from the rim of height, $\hat{h}$, indicate the grousers central in describing the rim contact process.

Table 6: Wheel parameters used in minimum grouser spacing relationship.

Parameter	Symbol	Symbol for normalized parameter
Wheel radius	r	1
Grouser height	h	$\hat{h}$
Wheel sinkage	z	$\hat{z}$
Wheel linear velocity	v	$\hat{v}$
Wheel angular velocity	ω	n/a
Angular grouser spacing	ϕ	n/a
Wheel slip	i	n/a

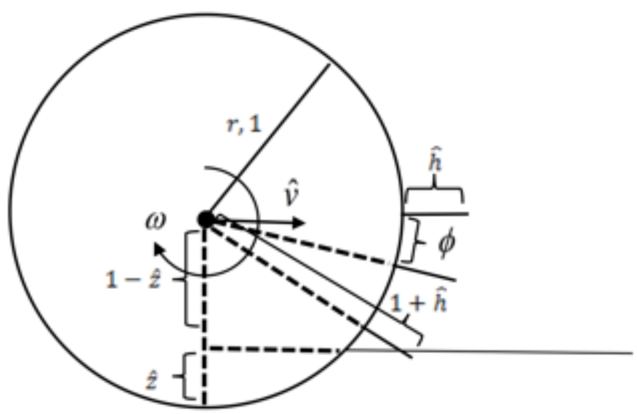

Figure 57: Diagram of parameters used in grouser spacing/height relationship. These are normalized with respect to wheel radius.

Figure 58 indicates important geometric points in deriving the grouser configuration expression. The grouser at the leading edge of a wheel, that is moving forward and rotating with a non-zero slip rate, will sweep in front of the wheel, clearing a space in front. The wheel will not encounter the soil until it translates horizontally forward a distance $\overline{BC}$ (Figure 58). To ensure that the next grouser sweeps the ground in front of the wheel before the rim can contact this point the rim must rotate a minimum angle, ϕ.

Equating the rotation and translation times gives the expression:

$$\frac{\phi}{\omega} < \frac{\overline{BC}}{\hat{v}} \quad \text{or} \quad \phi < \frac{\omega \overline{BC}}{\hat{v}} \qquad \text{Equation 7}$$

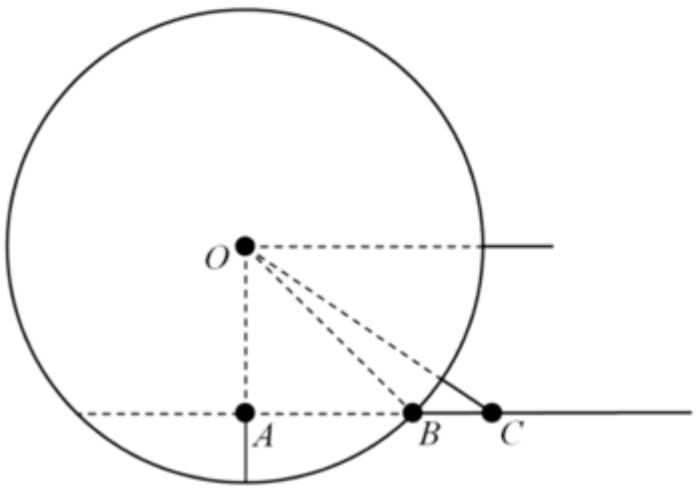

Figure 58: Geometry used in derivation of grouser height/spacing relationship.

Applying Pythagoreans theorem to triangles OAC and OAB gives an expression for $\overline{BC}$ in terms of wheel parameters:

$$\overline{BC} = \overline{AC} - \overline{AB} = \sqrt{(1+\hat{h})^2 - (1-\hat{z})^2} - \sqrt{1-(1-\hat{z})^2} \qquad \text{Equation 8}$$

As slip relates rotational and translational velocities, it is useful in the form:

$$i = 1 - \frac{v}{r\omega} = 1 - \frac{\hat{v}}{\omega} \quad \text{or} \quad \frac{\omega}{\hat{v}} = \frac{1}{1-i} \qquad \text{Equation 9}$$

Substituting Equation 8 and Equation 9 into Equation 7 results in:

$$\phi < \frac{1}{(1-i)}\left(\sqrt{(1+\hat{h})^2-(1-\hat{z})^2}-\sqrt{1-(1-\hat{z})^2}\right) \qquad \text{Equation 10}$$

Equation 10, calculates the minimum grouser spacing so that the rim does not contact the ground before a grouser removes soil that would normally contribute to motion resistance. Equation 10 relates grouser configuration (height and spacing) to wheel parameters (wheel radius) and operational parameters (sinkage and slip).

The purpose of this equation is to predict the grouser geometry that determines the behavior of periodic forward motion of soil at the wheel front as seen in SIIA plots. Lack of this behavior correlates to high drawbar pull, therefore, use of this equation is expected to yield high performance for a given wheel size.

5.2.5.1 Comparing Predicted Grouser Height/Spacing to Measured Data

The grouser height/spacing expression can be corroborated, in terms of traction performance, by comparing predicted spacing values to the measured data in Figure 59. As the derivation of the equation is based off wheel geometry, operating parameters and the assumption of a motion resistance reducing mechanism, the measured drawbar pull curves are an independent check of the equation's prediction capability.

The values in Table 7 are fixed other than sinkage and the calculated grouser spacing (ϕ or minimum number of grousers). The two operating parameters are slip and sinkage. As the single wheel testbed allows for slip control, the slip rate was held at 0.20. The sinkage value was measured during single wheel tests of the rim with grousers and a sandpaper surface. With the soil type used and at slip rates tested (i.e. 0.20), the sinkage of the rim was similar with and without grousers and with different grouser configurations. This is due to the fact that at the wheel bottom grousers are already filled with soil and therefore do not contribute to additional soil transport from below the wheel.

Table 7: Parameter values used to calculate minimum grouser spacing.

Wheel Diameter	Grouser Height [mm]	$\hat{h}$	z [mm]	$\hat{z}$	i	φ	**Calculated minimum # of grousers**
23cm	13	.11	13	.13	.2	.259	**24**
	9.5	.08	13	.13	.2	.200	**31**
	6	.05	13	.13	.2	.130	**48**
41cm	25	.12	12	.06	.2	.343	**18**
	13	.06	12	.06	.2	.191	**33**

The predicted grouser spacing (expressed as number of grousers per wheel), for each wheel diameter and grouser height tested, is shown in Figure 59 as a diamond shape. For the three wheel configurations (diameter and grouser height) that display a plateau, the predicted minimum number of grousers is consistent with its purpose. The 41cm diameter wheel with 25mm height grousers and the 23cm diameter wheel with 12mm and 9.5mm height grousers both display plateaus in drawbar pull with respect to spacing. The calculated minimum spacing values indeed predicts correctly for these three examples. The closest data points are all in the higher drawbar pull range and near the knee in the curve (therefore acting as a minimum value). This result demonstrates the usefulness of the grouser spacing equation from a design perspective, as the equation will predict the minimum number of grousers that must be implemented to achieve high drawbar pull (i.e. above the knee in the curve). In this sense, the equation serves to optimize a design for either a fixed grouser height or spacing.

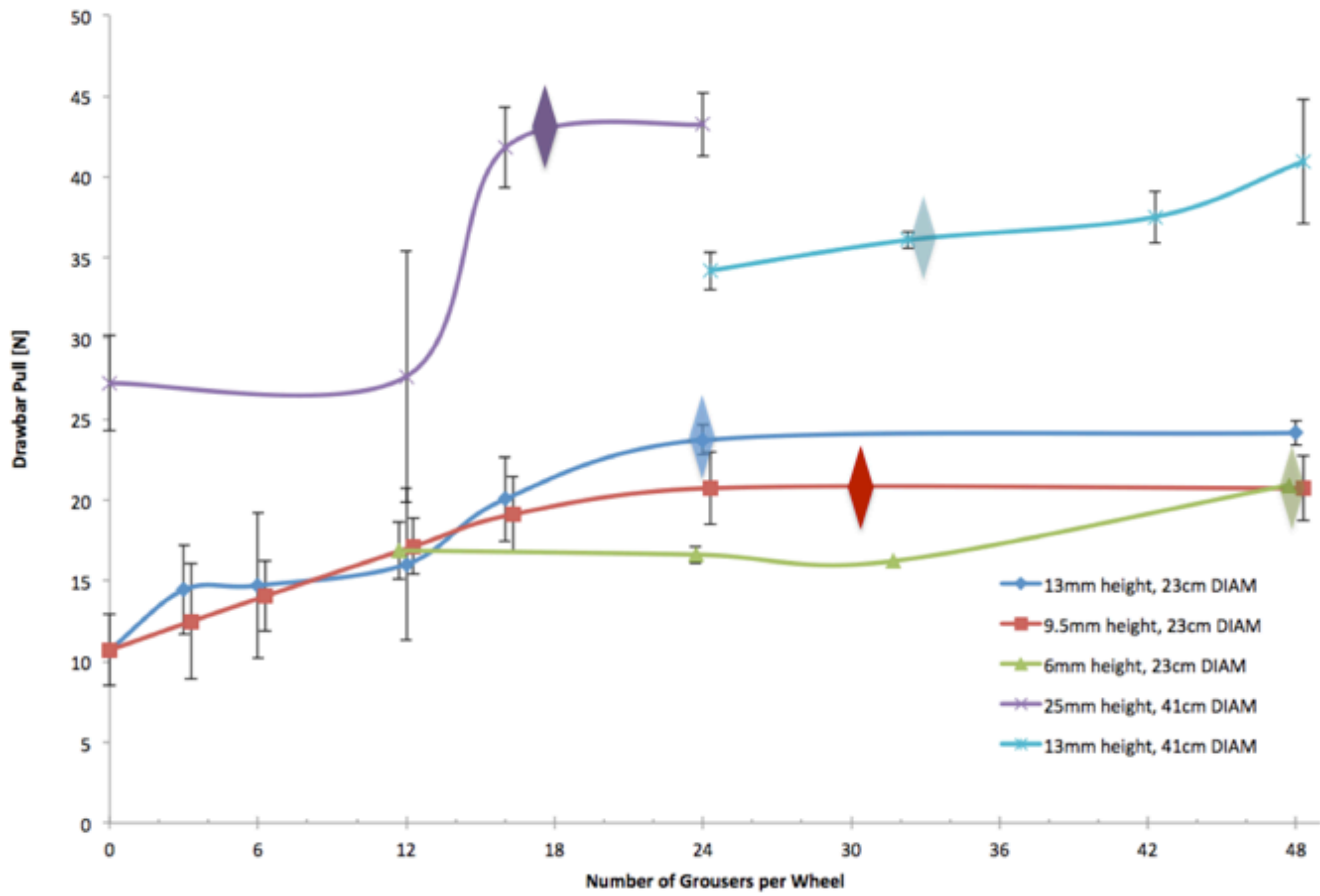

Figure 59: Drawbar pull performance for many grouser and wheel configurations. The diamond shape on each curve denotes the predicted value for minimum number of grousers for the height and wheel diameter (From Table 7).

For the two curves, where an obvious plateau does not exist, one might have a knee outside the experiment space (23cm diameter wheel with 6mm height grousers) while the other might not have been tested to a suitable low value for the number of grousers (41cm diameter wheel with 13mm height grousers).

The grouser spacing and height are dependent on wheel diameter, sinkage and slip. A range of slip values was not tested with varied grouser configuration to validate the expression with respect to the slip parameter. Future experimentation should be conducted to validate the effects of slip. However, from a strictly design perspective, slip might have little importance and is discussed in the next section. As sinkage is related to slip it is treated in a similar manner and discussions of these parameters follow in the next section. Extreme values, of either grouser height or spacing, will probably result in inaccurate predictions. The 6mm to 25mm range of heights was considered a reasonable range that covers most implementations of standard rigid wheels to date.

The reduction of motion resistance might not be the only traction process affected by grouser parameters. There is a measured difference between the maximum drawbar pull for some of the grouser heights (e.g. 23cm diameter with 9.5mm and 13mm height grousers). Despite this drawbar pull difference, the equation for the height/spacing relationship of grousers is still very useful. It does appear that the change in drawbar pull with grouser spacing, is larger than changing height only (for all tested configurations). Therefore, motion resistance might still be the dominating process in governing drawbar pull with respect to grouser implementations.

5.2.5.2 Use of Grouser Height/Spacing Expression

The minimum grouser spacing equation can be useful to aid design. The equation introduced is a relationship of the height and spacing, so from a design perspective it allows for flexibility. If there were design constraints such as maximum height (i.e. for structural reasons), use of more grousers can be relied on to achieve the desired soil transport process. Also, the equation is inherently useful because a grouser height or spacing can be calculated and a factor of safety can be applied. Applying a factor of safety is applicable because the equation predicts the minimum spacing or height required, not an exact value. For example, if the minimum spacing equation predicted 24 grousers for a given wheel, adding additional grousers beyond 24 would not degrade performance. This is due to the fact that the grousers would still transport soil from the wheel front before the rim contacts the ground surface level. The flexibility to add more grousers than necessary (from a loose, granular material traction perspective) is an important realization as additional grousers may be required for other aspects of mobility such as rock climbing or bedrock slopes. There is a practical limit, however, that will be reached when the soil transport mechanics is disrupted when spacing becomes too small between grousers. This limit was not investigated in this research, therefore, if closely spaced grousers are desired (with a height to space ratio >1:1), then verification of soil transport behavior should be undertaken.

To calculate a minimum spacing, sinkage and slip must be prescribed. If nominal values are chosen (measured sinkage at 0.20 slip, and slip value of 0.20), the result is still a robust design choice (i.e. if conditions degrade, the grouser implementation is still applicable to the situation). The minimum required number of grousers, predicted by the equation, decreases with increasing slip, therefore if a wheel were to enter higher slippage, as routinely occurs, the number of grousers would still satisfy the minimum required. When slip increases, the soil transport rate from the wheel front increases, as there is an increased rearward velocity of the grousers with respect to the ground. However, the number of grousers (or height) required does increase with increasing sinkage, but in reality, the effects of slip usually dominate the equation, since sinkage does not occur without slip increasing substantially. The relationship of slip and sinkage (i.e. slip induced sinkage) is complex and is beyond the predictive capability of current models. To demonstrate that the increase in wheel sinkage does not invalidate the usefulness of the grouser spacing equation, experimental data is used.

Table 8: Measured slip and sinkage of Ø31cm by 16.5cm width rigid wheel with 30 grousers of 15mm height operating in dry sand [59]. Predicted minimum number of grousers required for reduced motion resistance using Equation 10 is provided.

Measured		Predicted
Slip ratio	Sinkage [mm]	Minimum # of grousers required
0.1	6	23
0.2	8	22
0.3	12	21
0.4	16	20
0.5	23	19
0.6	27	16

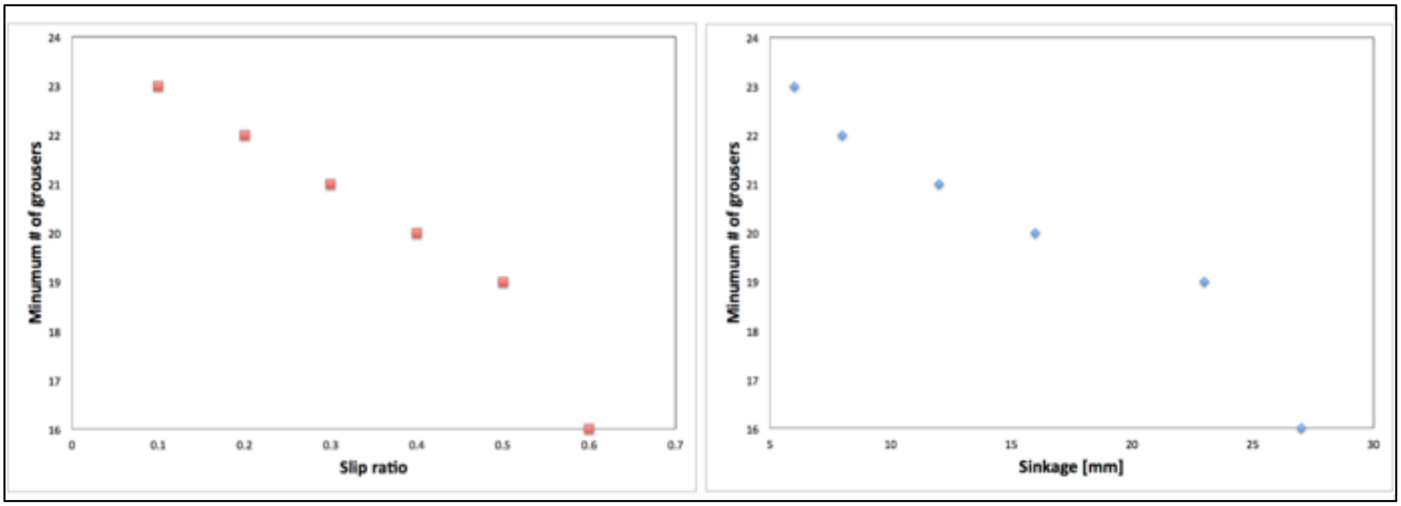

Figure 60: Trend of predicted minimum number of grousers required to maintain low motion resistance with respect to slip and sinkage. The slip and sinkage are dependent on each other. Data of measured slip and sinkage of Ø31cm by 16.5cm width rigid wheel with 30 grousers of 15mm height operating in dry sand from [59].

The predicted minimum number of grousers required for a wheel configuration to maintain low motion resistance, does not increase with degrading conditions such as increase slippage and sinkage. Table 8 and Figure 60 show the predicted minimum number of grousers utilizing Equation 10 due to measured wheel sinkage and slip values during single wheel tests (sinkage and slip data from Ding, et. al [59]). This demonstrates that if nominal values from a low slip operating point (such as 20%) and the corresponding sinkage are utilized, the grouser configuration will still be above the minimum number of grousers to reduce motion resistance. It is possible that material types exist were the slip-sinkage relationship would cause an increase number of grousers to be required with degrading conditions. However, even for Fillite (fly ash), a material with extremely high initial sinkage (static sinkage), the effects of sinkage were still dominated by slip in terms of number of grousers required.

There are many other considerations when utilizing Equation 10 for design applications. The grouser spacing equation predicts the clearing behavior that minimizes forward soil motion in front of a wheel, therefore, minimizing motion resistance. Since this mechanism was discovered via SIIA experimentation, it is recommended that a grousered wheel implementation undergo soil imaging validation to make sure that soil, pushed forward, is minimal and the correct behavior is achieved.

Outside the parameter space that the grouser equation was validated, the designer should consider the underlying soil behavior of transporting soil away from the wheel front, instead of relying on the equation. Again, validating the design via soil motion analysis is recommended. For example, if wheels were to be designed for very high sinkage application, the soil transport process should be directly observed to see if adequate removal of soil in front of the wheel occurs. The concept of reducing motion resistance by transporting soil away from the wheel front, and the method of selecting proper grouser geometry to promote adequate clearing is still correct, however, the minimum spacing equation may be altered to reduce resistance further.

For example, if it were desired to have a low motion resistance at low slip while operating in a high sinkage material, one of the requirements for the formation of the equation could be altered. A requirement in forming Equation 10 is that the grouser sweeps soil away so the rim will never contact the soil at ground level (as described by Equation 7). If a configuration was desired that is most appropriate for high sinkage at low slippage, than Equation 7 should take the form that relates initial rim contact at a prescribed depth (absolute or percentage of wheel radius). This will actually produce a design that creates an effective reduced sinkage value, with respect to motion resistance processes, that is chosen by the designer. The initial point of contact may also be better described by a prescribed entrance angle (angle between rim tangent and ground plane at the point of initial contact). This relationship encompasses the effect of wheel radius on motion resistance and since it is a function of wheel radius, it is generalizable over wheels of different sizes.

The gains of implementing grousers might be small for some wheel types. As this research hypothesizes that much of the expected gains are a result of reducing motion resistance, wheels that already have low resistance will not see much improvement in drawbar pull. Large diameter wheels and highly compliant wheels are examples where grousers might yield little traction benefits. Also, in scenarios where when motion resistance is not the most significant source of resistance, such as slope climbing, a grouser implementation may not aid significantly in steepness of slopes ascendable. This often occurs on very steep slopes where the gravitational resistance is high compared the wheel sinkage.

In traction scenarios that are not the intended focus of this research, such as ground materials outside the scope, the importance of the grouser spacing equation might lessen. This is due to the fact that grousers could increase thrust, resulting in a contribution to drawbar pull that should not be ignored during design. In cohesive materials (organic soils, clay, non-dry sand) grousers may cause direct increase in drawbar pull due to engagement of soil deeper in the ground with increased strength or due to increased amount of soil engaged. However, even in soils outside the scope of this research, the motion resistance reducing effect of grouser induced soil transport, is expected to provide traction benefits in the same manner as a planetary rover provided that non-trivial slip and sinkage occur. The design changes suggested by this thesis might still be valid with respect to reducing motion resistance only. Nevertheless, making design changes based off the concept of motion resistance reduction only (as this thesis suggests) is ill advised for materials outside the intended scope. Design changes might adversely affect the thrust producing ability of grousers unless it is separately determined that grousers do not have a significant effect on thrust. For traction scenarios within the scope of this research, thrust was found to be independent of the grouser configuration, therefore design changes suggested in this chapter are likely valid.

5.2.6 Grouser Mechanics Summary and Conclusion

The empirical study of sub-surface soil motion provides new information relevant to fundamental terramechanics and traction device design. SIIA was able to show that grousered wheels have a mechanism to reduce motion resistance, leading to higher drawbar pull. The mechanisms identified provide design guidelines for improved performance.

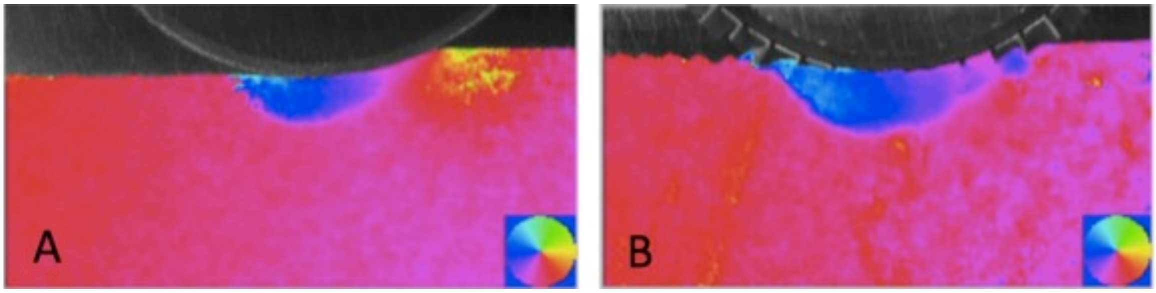

Figure 61: Key behavior identified using SIIA, that grousers can be implemented to reduce motion resistance. (A) A wheel without grousers and (B) a wheel with high performance grouser configuration is shown.

Soil forward motion, at a wheel leading edge, was identified as a key behavior for the grousered wheels (Figure 61). The soil motion behaviors correlated with drawbar pull response and, therefore, were shown to have a strong influence on traction. In depth analysis of how a grousered wheel interacts with the soil led to the mechanics behind reducing motion resistance via soil transport. Furthermore, an equation for the implementation of high performance grouser configurations was developed and values predicted by the equation were corroborated by measured data.

5.3 Push-Roll Locomotion

5.3.1 Introduction

A study investigating a non-typical locomotion mode, called push-roll, was conducted to assess possible increases in traction compared to conventional rolling locomotion. Push-roll locomotion utilizes non-rotating wheels in conjunction with the rolling wheels of a vehicle, in order to produce forward travel. This research consisted of two parts. First, full vehicle experimentation was conducted to measure potential traction gains (drawbar pull metric) provided by the hybrid locomotion mode, push-roll. Preliminary experiments showed an approximate doubling in drawbar pull for push-roll locomotion relative to traditional rolling for the vehicle that was tested. The source of the traction gains was not readily identifiable and since the non-rotating and the rolling wheels have a different interaction with the ground, SIIA was conducted to provide insight. The push-roll vehicle motions were mimicked in a single wheel testbed, while individual wheel reaction forces were measured and sub-surface soil motions were recorded. The Shear Interface Imaging Analysis plots revealed different failure modes between the rolling and pushing wheels.

5.3.2 Push-roll Background

Vehicles with a variety of articulation types are being developed for exploration of the Moon and of other planetary bodies [25] [26] [21] [66]. These vehicles are capable of modes of locomotion and methods of operation unlike that of previously deployed planetary rovers. Systems that are capable of conventional rolling, walking, hybrid push-roll and center of gravity control, are continuously being developed.

Push-roll is a hybrid locomotion mode where the vehicle wheelbase is actively expanded and contracted in a controlled manner using onboard actuation. By this action, a set of rolling wheels can be assisted by pushing or pulling off of a set of non-rolling wheels (not rotating with respect to ground). Net traction gains have been measured, which have been attributed to either a decrease in motion resistance or to an increased thrust available from the non-rotating set of wheels. Therefore, in push-roll mode, a vehicle could potentially climb higher slopes or tow a greater payload than in conventional rolling mode. Also, the vehicle could lower its slip rate during self-propelled operation (no external horizontal load) and/or escape from an entrenched state in loose terrain. The analysis of push-roll locomotion has been previously undertaken for both planetary exploration [67] and for terrestrial vehicles [68]. At the Army Land Locomotion Laboratory, segmented vehicles were tested and showed mobility improvements [69]. It was determined through theoretical analysis, that eliminating resistances on one or more segments by remaining stationary was the source of measureable net traction gains. The assumption that motion resistances likely account for the differences in drawbar pull between push-roll and rolling vehicles, comes from the use of conventional terramechanics models relying on shear displacement theory to predict pushed wheel thrust. The research presented in this chapter supports an alternate conclusion.

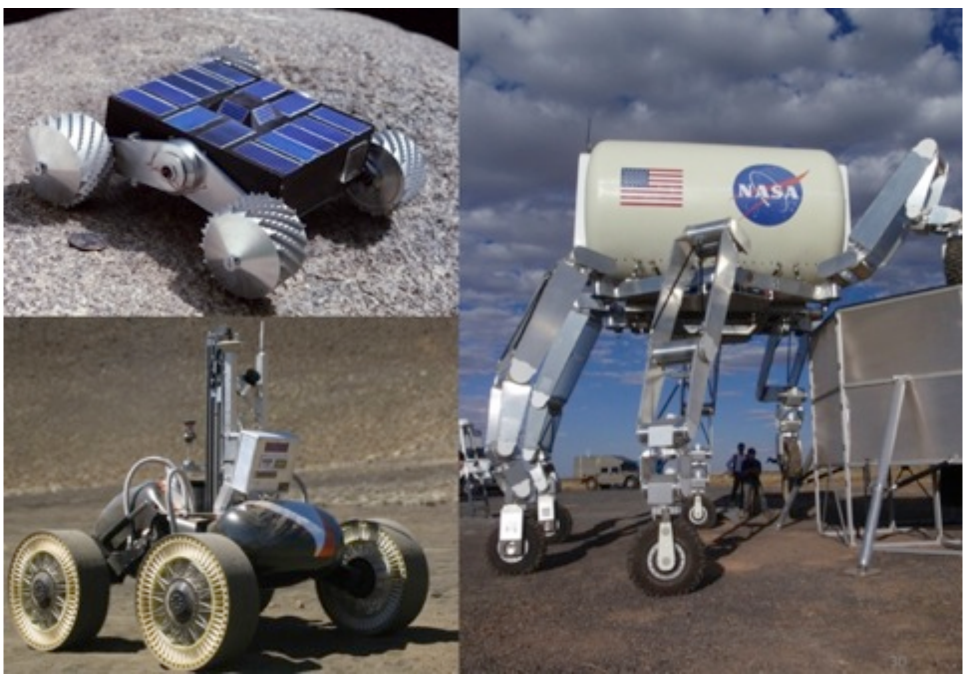

Figure 62: All vehicles shown are kinematically capable of push-roll locomotion. Clockwise from top left: NASA MUSES-CN Nanorover, NASA ATHLETE rover and CMU Scarab rover. The ATHLETE rover can also walk; walking is another form of pushing locomotion. Top left image credit JPL [55].

A study of the European Space Agency (ESA) ExoMars rover system provides the latest example of a mobility system that benefits from push-roll like locomotion [21] [70]. Other recently developed vehicles that are capable of push-roll are the JPL ATHLETE system and the NASA Space Exploration Vehicle (SEV). Both are highly articulated.

However, there is not enough information to determine how to best take advantage of all the modalities available. Figure 62 shows the JPL ATHLETE rover and other push-roll capable vehicles.

5.3.3 Full Vehicle Experimentation

An existing system capable of push-roll locomotion was utilized for full vehicle traction measurements. Push-roll mode of locomotion can be achieved by the Scarab rover (Figure 63), a concept vehicle developed at Carnegie Mellon University. This system has demonstrated, on a full-scale prototype, push-roll locomotion in laboratory and in field settings that are analogous to lunar terrain [66].

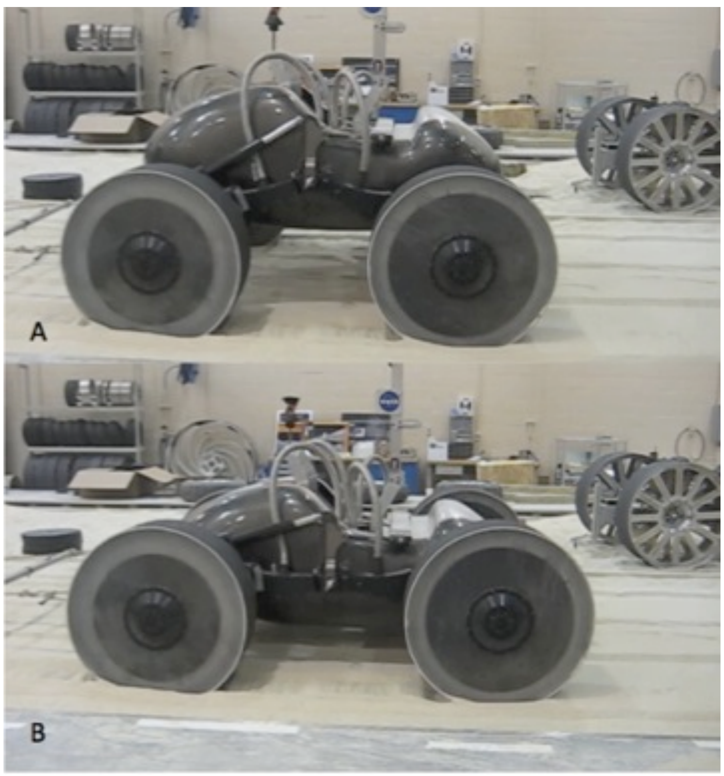

Figure 63: The Scarab prototype rover capable of push-roll locomotion. This vehicle was utilized for drawbar pull measurement comparison of push-roll versus conventional rolling. In step 'A,' the vehicle is at nominal driving height and wheelbase. At step 'B,' the wheelbase is fully extended. Non-rotating and rolling wheels are used in conjunction with wheelbase change to produce forward motion.

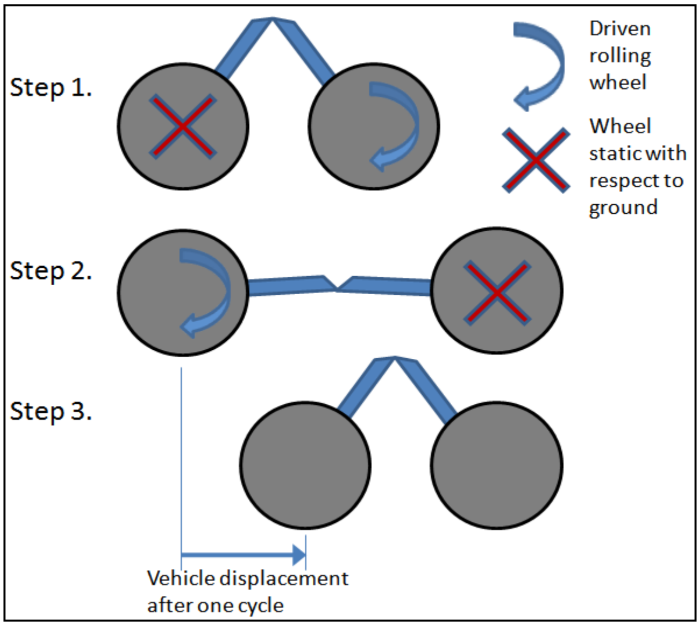

Figure 64: Simplified kinematics of the Scarab rover showing push-roll motion. One wheel is held static in rotation with respect to the ground while the wheelbase is actively extended (or retracted) and the other wheel rolls in a rotating driven fashion.

To begin the cycle of push-roll on Scarab, the wheelbase expands while rolling the front wheels forward and keeping the rear wheels fixed in rotation relative to the ground (Figure 64). Once the limit of body expansion is reached, the wheel base contracts while the rear wheels roll forward and the front wheels remain fixed with respect to the ground (other than slight sliding motion). Note that the fixed wheel actuators must counter-rotate in synchrony with the wheelbase expansion or contraction. If the wheels were to be locked, they would rotate in the direction of vehicle displacement and thereby induce slippage associated with a rotating wheel. These non-rotating wheels can provide extremely high thrust. To achieve these benefits, push-roll locomotion not only eliminates the wheel motion resistances on two of the four wheels by not travelling forward, but the non-rotating wheels also generate higher thrust than a conventional rolling wheel, thus adding to traction gains.

Laboratory drawbar pull testing of Scarab was conducted to assess the tractive capabilities of the rolling push-roll mode of locomotion. Drawbar pull, as a metric, is quite informative when comparing different aspects of wheel and suspension designs but also can be used for estimating the slope that a vehicle can continuously ascend for a specified material [10]. In experimentation, a towed load considered the drawbar pull, is equivalent to the net traction potential (thrust available in excess of wheel motion resistance) of the vehicle for the specific surface material being traversed.

In the gathering of drawbar pull data, a range of external loads that resists vehicle travel is applied in steps resulting in a vehicle response ranging from low to high slip. The drawbar load is held constant for a set distance of vehicle travel (minimum two vehicle lengths) to allow steady-state slip to be achieved. Then the load is stepped up to a higher value to gather a subsequent data point.

In the case of push-roll locomotion, the wheel angular speed and rate of wheel base expansion are predetermined. During steady-state response (after a full vehicle length), the vehicle speed is measured to determine slippage. As the vehicle velocity varies throughout the push-roll cycle, only full cycles are used in speed calculation. The average value of speed, v_{SP}, is used in the calculation of a slip metric. The meaning of slip, is ill defined for the non-rolling wheels, therefore a similar metric called “travel reduction” was utilized. Travel reduction is the percentage by which the vehicle ground speed is reduced compared to that of the vehicle at a nominal travel speed. A near zero load case, in which only self-propelled motion resistances are present, is utilized as the baseline speed. This is measured while the vehicle is driving (rolling or push-roll) on flat ground, with no external load and is used as the reference speed, v_{SP}. Travel reduction is defined as follows:

$$TR = 1 - \frac{v_{measured}}{v_{SP}} \qquad \text{Equation 11}$$

Where TR is travel reduction,

$v_{measured}$ is the measured speed of the vehicle during a drawbar pull test,

v_{SP} is the self-propelled speed of the vehicle in the soil simulant.

Drawbar pull tests were conducted at the NASA Glenn Research Center's Simulated Lunar OPErations laboratory (SLOPE). A cable payout mechanism, with variable tension control (via a magnetic brake), was used to apply the drawbar load to the vehicle (Figure 65) while vehicle velocity was determined using a 3-axis laser tracking system.

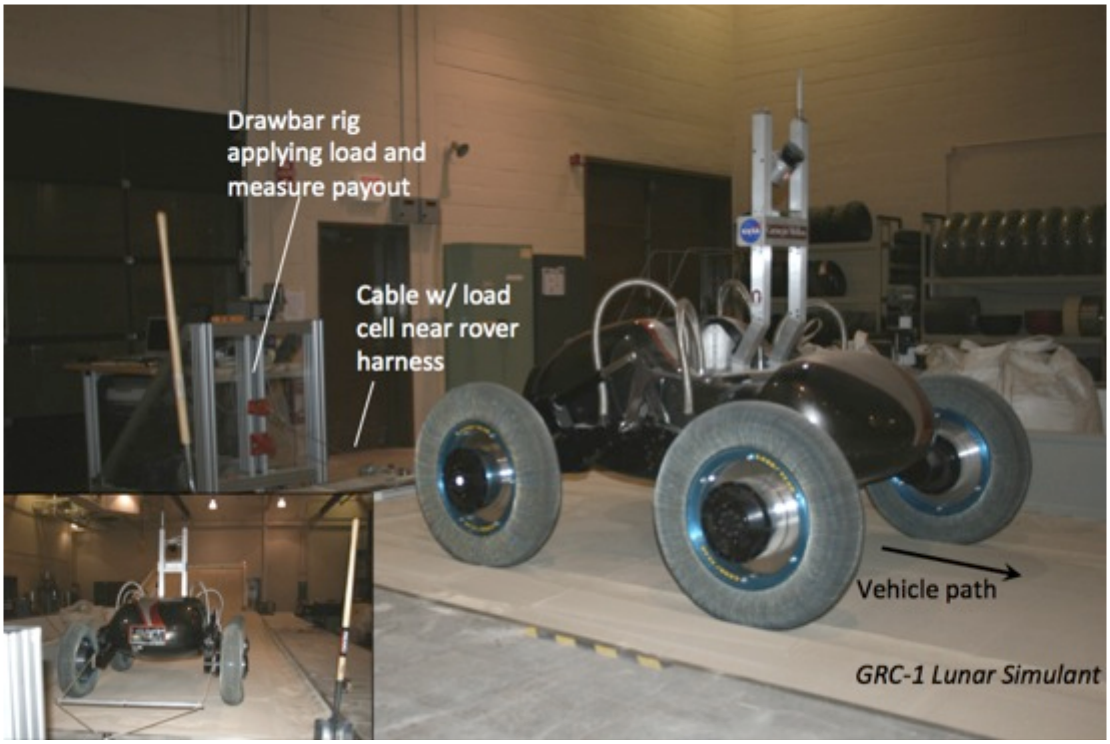

Figure 65: Scarab rover undergoing drawbar pull test to evaluate net traction. The drawbar rig applies a constant controlled load via a magnetic brake, while a laser ranging system measures vehicle speed.

The vehicle was configured at 400kg mass, with Ø71cm x 25cm wide rigid wheels (shown in Figure 63) and operated in GRC-1 lunar soil simulant. This soil was prepared before each test to achieve consistent strength values. Prior to each drawbar pull test, the soil was fully loosened (to 45cm depth) and then compacted with a heavily loaded roller. Cone penetration resistance measurements taken before each drawbar pull test, were used to check that the compaction gradient fell with in an allowable range. A description of the soil preparation process is given by Woodward [50].

5.3.3.1 Full Vehicle Traction Results

The results of the drawbar pull experiments, Figure 66, show that for the nearly the entire range of travel reduction evaluated, push-roll produces approximately 100% more drawbar pull than conventional rolling. For example, at a travel reduction of about 0.3, the rolling locomotion drawbar pull is 11%, while the push-roll drawbar pull is 21%.

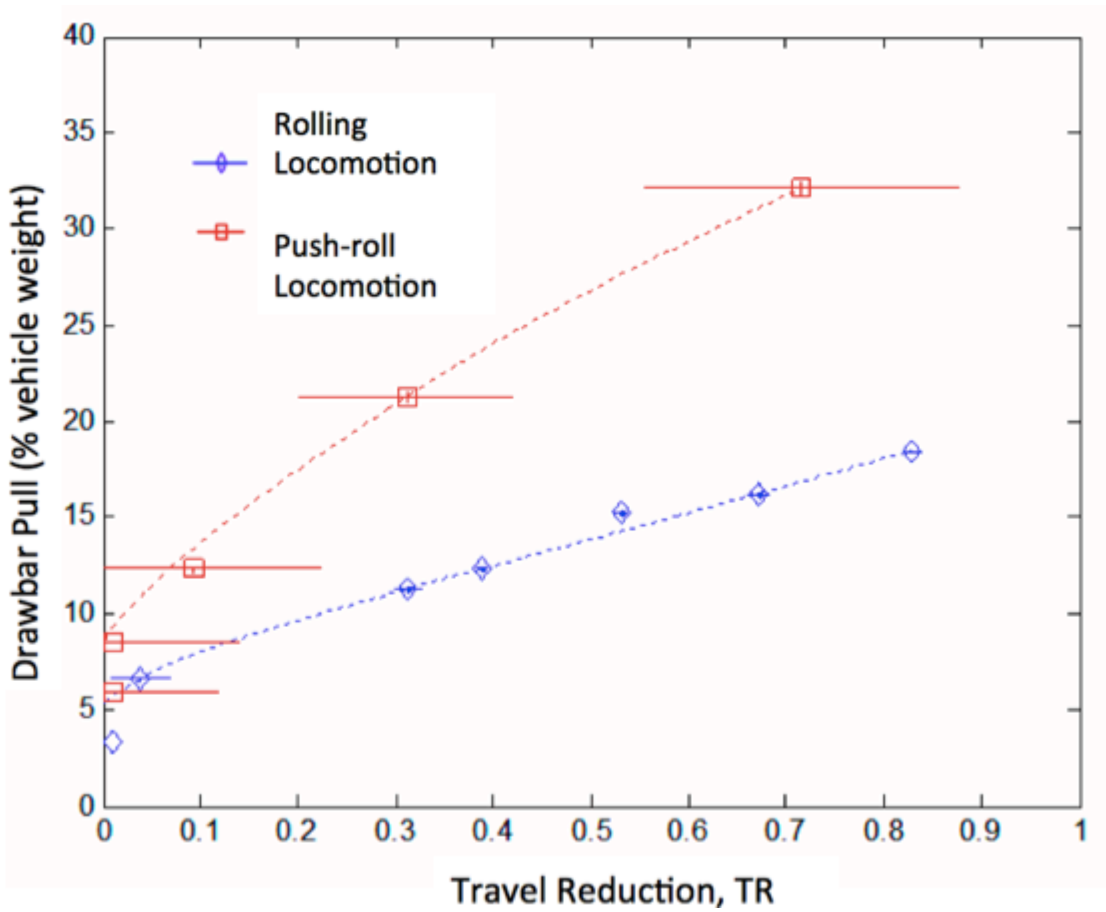

Figure 66: Drawbar pull-travel reduction curves comparing conventional rolling to push-roll locomotion. Results indicate an approximate doubling of drawbar pull for almost the whole range of travel reduction.

Increases in drawbar pull of this magnitude cannot be explained solely by reductions in wheel motion resistance. Therefore, it was hypothesized that there is a significant difference in the thrust potential between rolling and non-rolling, pushed wheels. This observation motivated the comparative study of the sub-surface soil response of the two types of wheel interaction with the ground that represent rolling and push-roll locomotion.

5.3.4 Shear Interface Imaging Analysis

The Shear Interface Imaging Analysis study conducted was intended to investigate possible differences in soil structure or in soil failure modes between conventional rolling and push-roll locomotion. This research was not meant to replicate the Scarab rover vehicle in a scaled manner. For the results given in the next section, test parameters are as follows. A 23cm diameter wheel (5.72 cm width) with a 10kg payload was tested in GRC-1 for both rolling and pushing wheels. The rolling wheel was evaluated at 20% slip, while the pushed wheel underwent constant rate horizontal displacement of 1mm/s. For all SIIA plots, the equivalent wheel vehicle motion is to the right. For the pushed wheel, the wheel actually displaces slightly to the left.

5.3.4.1 Push-Roll Compared to Rolling Results

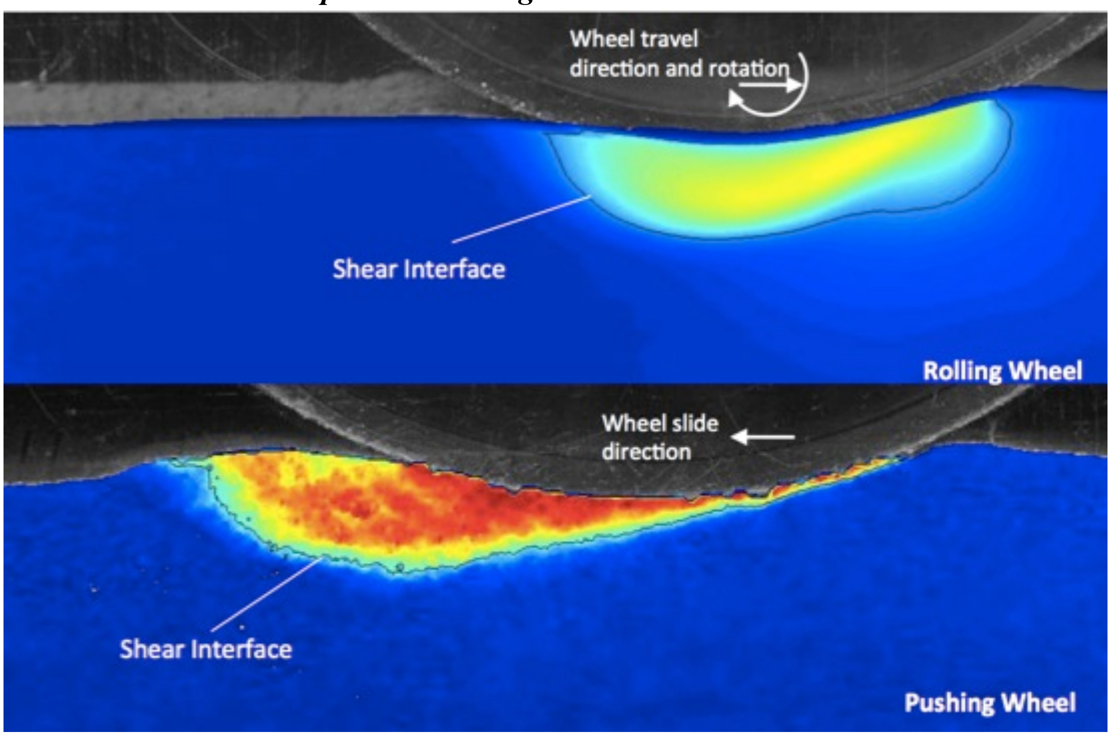

Figure 67: Soil velocity magnitude plots of a rolling wheel at 20% slip and a pushed (non-rotating) wheel sliding at constant rate. Note that the magnitude plots are different scales. "Ground failure" type response of the soil is observed for the pushing wheel, identifying a likely source of tractive gains. The rolling wheel soil velocity magnitude is averaged over 20 seconds since the soil undergoes steady-state response. The pushed wheel velocity is an instantaneous measurement since steady-state will not occur with increasing displacement. All pushing and rolling magnitude plots in this chapter are at different scales, therefore, the values cannot be directly compared.

The SIIA plots, of Figure 67 and Figure 68, indicate that the soil failure patterns of the rolling and pushed wheels are very different. Differences in the direction and shape of the shear interface and soil motions are evident. The soil beneath the rolling wheel appears to follow the shape of the wheel in a direction somewhat tangential to the wheel rotation and is confined to the wheel contact area. Large variations in soil motion direction are apparent Figure 68. However, the pushing wheel produces a much different soil response that might be contributing to a larger thrust than the rolling wheel can achieve. The soil displacement occurs as a unified mass moving together in the same direction, opposite the direction of thrust. The consistent magnitude and direction shows that the soil moves as a whole. The shear interface extends well beyond the wheel contact region and has a shape of that of a logarithmic spiral slip plane common in soil mechanics theory. This type of soil response is called “ground failure” [58]. Bekker describes how this fundamental difference in soil failure mode, enables traction devices producing ground failure, to generate thrust significantly higher than that of a conventional wheel or track [14].

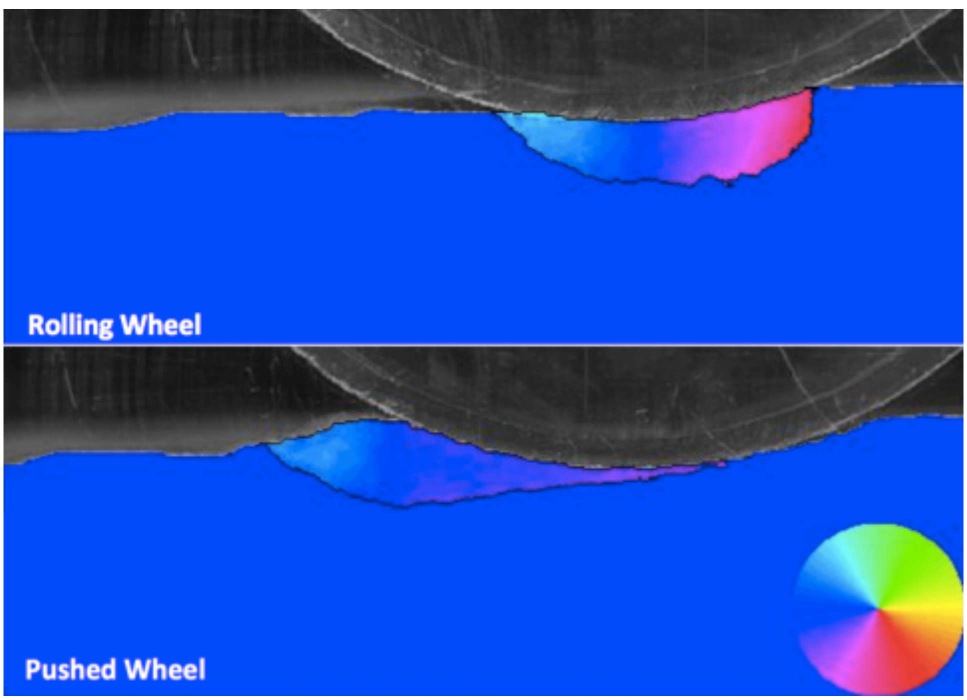

Figure 68: Soil motion direction plots with thresholding and shear interface indication.

The soil failure pattern formed by the pushed wheel, as seen in Figure 67, is fundamentally stronger than that of the rolling wheel (i.e. shear interface can support higher thrust loads). The unified soil motion created by a pushed wheel in the direction of slide and the resulting long slip plane (shear interface), accounts for increased thrust. This soil motion behavior is very different from the shear interface of the rolling wheel where soil is undergoing constant change in direction and where confinement is limited to the contact length.

Bekker provides analytical analysis for the ground failure type soil response. The Spaced-Link Track was experimentally shown to produce the same type of soil failure mode of the pushed wheel investigated in this thesis research [14]. Bekker's theoretical analysis, for the Spaced-Link Track, is adapted from Terzaghi's bearing capacity theory for footings [58], not from conventional terramechanics models. Previous analysis of push-roll locomotion [67] [68] [69] assumed conventional wheel mechanics to model the non-rolling pushed wheel. The use of conventional wheel-soil models led to incorrect application of models and to the incorrect assumption that there is little difference between rolling and pushed wheel maximum thrust. Sub-surface soil analysis, provided by SIIA, allowed of the identification of the correct soil failure mode and for an explanation for the increased thrust ability of the pushed wheel.

An analytical theoretical analysis, similar to Bekker's Spaced-Link Track, was not undertaken in this thesis research. However, Bekker's research provides compelling evidence showing the gains attainable by a traction device undergoing ground failure versus grip failure (the latter is the model utilized for rolling wheels). The comparison of the thrust of a Spaced-Link Track versus that of a conventional track is analogous to application of analytical models of ground failure mechanics versus conventional terramechanics models for a rolling wheel. Figure 69, shows both the predicted thrust and measured thrust for both soil failure types. The thrust of the Spaced-Link Track, that produces ground failure, is up to 1.5x that of a conventional track that is governed by the same mechanics of a rolling wheel. The difference in thrust demonstrates that the correct model and assumption of soil failure type for the pushed wheel must be applied. If not, a large underestimate in the predicted thrust will occur. Bekker's Spaced-Link Track research also provides an explanation for the increased drawbar pull measure by the

Scarab vehicle operating in push-roll mode compared to conventional rolling locomotion. Further single wheel experimentation, measuring individual wheel reaction loads, confirms the thrust capability of a pushed wheel.

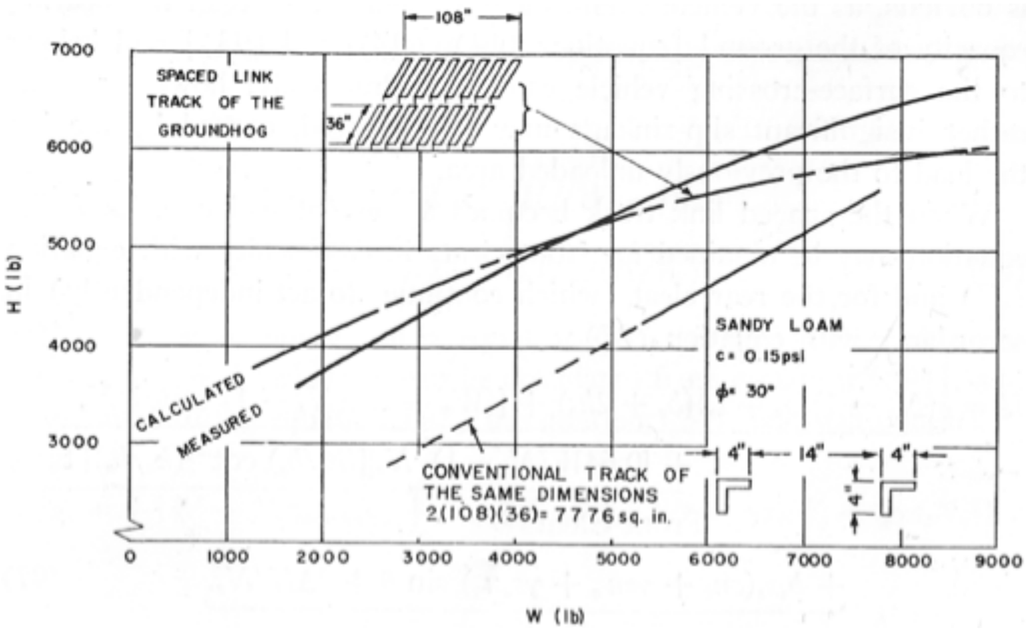

Figure 69: Thrust of Spaced-Link Track and conventional track. These track types correspond respectively to ground failure and grip type soil failure. H is thrust, while W is vehicle weight. Image credit [14].

The realization that the pushed wheel, utilized in push-roll locomotion, relies on ground failure is quite important. The fact that the pushed wheel relies on ground failure means that little slide is needed to generate thrust, as no accumulation of soil is required (i.e. bulldozing). The pushed wheel, in Figure 67, generates a pull coefficient of 0.5 for the displacement shown in the image (approximately 4mm horizontal wheel motion). There are many beneficial implications of utilizing ground failure. First, the pushed wheel needs to contact only the soil below the wheel and does not need to create a rut from which to push off. Secondly, since high thrust is created at low horizontal displacement, the wheel undergoes little sinkage (see Figure 70). In terms of vehicle safety, low sinkage operation is highly desirable.

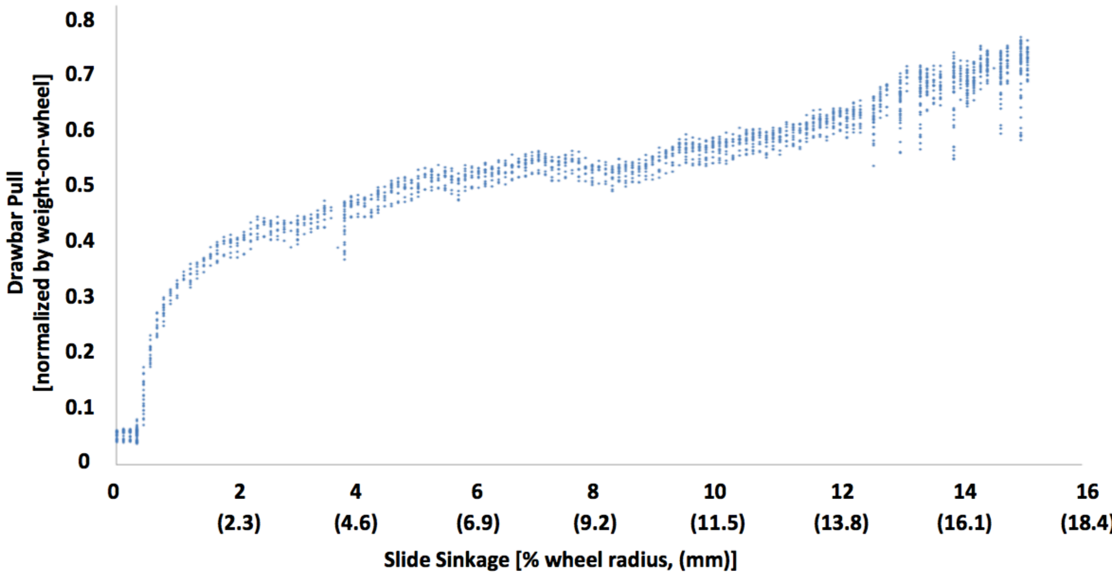

Figure 70: Slide-sinkage metric is used to evaluate the pushed wheel. As the slip metric is meaningless for a sliding wheel, a useful safety metric is sinkage. The 23cm diameter wheel, with sandpaper rim, is pushed horizontally at constant speed (1mm/s) while carrying a 10kg payload. Like all previous SIIA plots in this chapter, GRC-1 was the soil simulant utilized.

For a single wheel test, slip and travel reduction cannot be used as a metric to evaluate the pushed wheel as slip has no meaning for sliding motion. Sinkage is an alternative metric that is related to vehicle safety as excessive sinkage can lead to entrapment. Figure 70 provides a look at the sinkage characteristics of a pushed wheel. A high drawbar pull, with 0.4 pull coefficient, was measured before moderate sinkage occurs. Even for 0.7 pull coefficient, the sinkage is not problematic. For comparison, the rolling wheel only generates a pull coefficient of 0.11 for the 20% slip metric, a standard evaluation point for drawbar pull. This comparison of thrust available at a reasonable operating point of the pushed wheel and rolling wheel, results in a thrust of up to 7x for the pushed wheel.

5.3.4.2 Push-Roll High Sinkage Scenario Results

For both the subsystem (SIIA) and full-vehicle experimentation, research was conducted to evaluate mobility in extremely weak soil (Fillite) that would entrap many wheeled vehicles. The mechanics of push-roll in nominal materials (GRC-1) on flat ground and in slope climbing (using drawbar pull metric) were studied in the previous section. However this study, as documented in the previous section, was conducted in an inherently low sinkage material. In GRC-1, push-roll is able to achieve increased drawbar pull due to the high thrust capability of the pushing wheel. High thrust is most useful on steep terrain where high drawbar pull is needed to overcome gravity. Extremely weak materials on flat ground, such as fine, wind-blown materials on Mars, provide different challenges. In this scenario, a vehicle must overcome a potentially high motion resistance due to high sinkage. Push-roll can be used to operate in this scenario while maintaining high performance. High-slippage, high-sinkage operating point SIIA tests in Fillite, showed that motion resistance can be significantly reduced by controlling slip. High slip, with appropriate wheel types, can reduce motion resistance by directing soil underneath the wheel instead of it compacting and pushing against the rim. A push-roll vehicle can control the slip rate of the rolling wheel as wheel base extension and wheel rotation speeds are controlled. As such, the rolling wheel of a push-roll vehicle, can be controlled to operate at high slip and, therefore, low motion resistance. This feature was studied in an extremely loose material, Fillite, at both subsystem (SIIA) and full-vehicle levels.

In Figure 71 the pushing wheel, operating in soft ground, shows a quite prominent example of ground failure type soil response. The commanded motion of the pushed wheel, is to roll forward for two wheel lengths at 20% slip and then begin to push backwards while rotation is locked. This mimics the motions of a push-roll vehicle. The sinkage visible in the pushing wheel plot is almost solely due to static sinkage and to the wheel roll before the pushing is initiated. It should be noted that all SIIA plots of pushing and rolling are conducted independently and are not coupled in any manner.

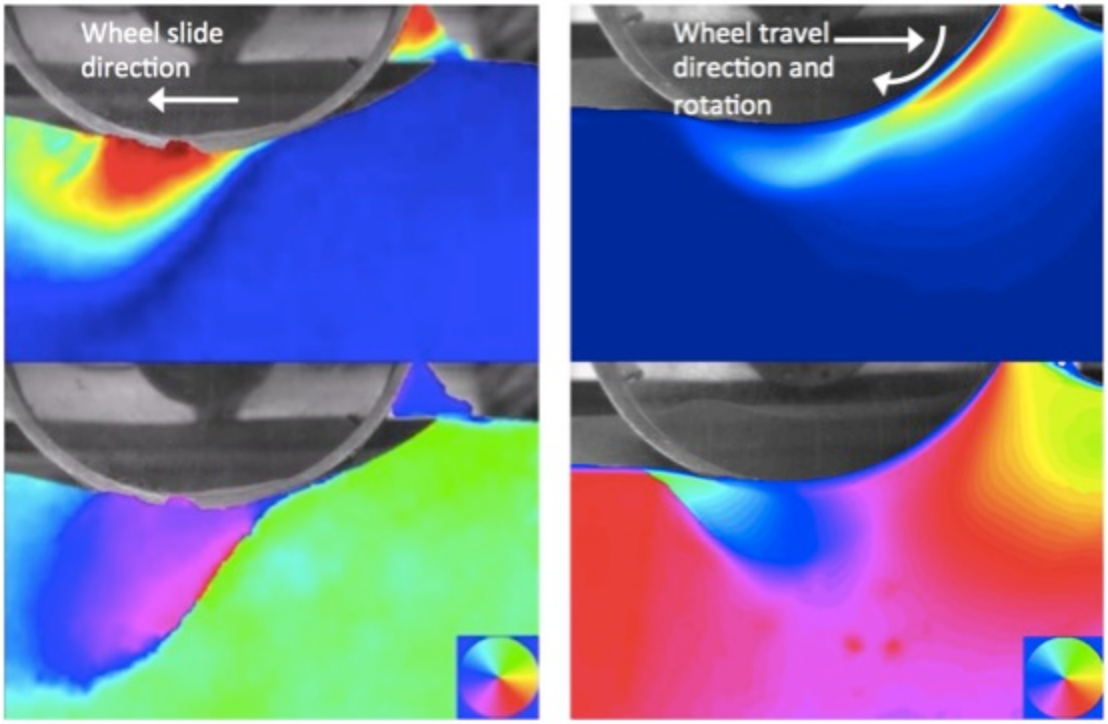

Figure 71: Pushing wheel shown with a rolling wheel to represent a push-roll vehicle in soft ground (Fillite). The pushing wheel has a horizontal displacement of 6mm and a 0.8mm sinkage generating a pull coefficient of 0.32. The rolling wheel is at 20% slip, 25mm slip induced sinkage and generates a pull coefficient of -0.10. Soil velocity magnitude plots are scaled differently between the pushed and rolling wheel.

Controlling the wheelbase expansion rate and the wheel speed, determines rolling wheel slip. It should be noted that there is a slight increase in slippage differing from the commanded value due to the slide of the pushed wheel, however this difference is insignificant unless the pushed wheel slides excessively. As slip rate is predetermined by vehicle motion commands, the rolling wheel response can be thought to determine the vehicle state. That is, in a self-propelled scenario, the pushed wheel drawbar pull will be the opposite value of that of the rolling wheel drawbar pull (as a net zero drawbar pull is required). Therefore, it responds to overcome resistance created by the rolling wheel. Thus, varying the rolling wheel slip rate, changes the thrust requirement of the pushed wheel.

The pushing wheel, in Figure 71, has a horizontal displacement of 6mm, slide sinkage of 0.8mm and a pull coefficient of 0.32. The rolling wheel is operating at a commanded 20% slip rate, has a pull coefficient of -0.10 (i.e. creating net resistance) and a slip sinkage of 25mm. Slide sinkage refers to the sinkage induced by the sliding (pushing) operation, while slip sinkage refers to sinkage induced by rolling wheel slippage. As a rolling wheel, of a push-roll vehicle, can be arbitrarily commanded to operate at any slip point, 20% slip was chosen to begin discussion. Figure 71 provides a look at how a push-roll vehicle might operate in Fillite, a high sinkage material where self-propelled motion is difficult. It can be concluded that utilizing the pushed wheel in conjunction with the rolling wheel (e.g. at 20% slip) that a positive net drawbar pull can be achieved and, therefore, forward, self-propelled motion occurs. Adding the measured pull coefficients of the pushed and rolling wheels results in a net positive (0.22), thus guaranteeing forward travel. In the case described above, the rolling wheel will still create a -0.10 pull coefficient, while the pushed wheel will operate at an equal but opposite thrust (0.10), leading to a lower slide sinkage than the measured 0.8mm at 0.32 pull coefficient.

SIIA and external force measurements confirm that the pushed wheel can still operate in the ground failure regime and provide high thrust in the difficult material. A pull coefficient of 0.32, in the Fillite material, is quite high considering the rolling wheel, at 20% slip, generates a negative drawbar pull (-0.10 pull coefficient). Also, the pushed wheel induces little sinkage compared to the rolling wheel. As the sinkage induced by the pushing wheel is much lower then the net sinkage of the rolling wheel, the additional sinkage caused by this motion has little effect. The rolling wheel recovers the small sinkage that the pushing adds when the rolling cycle begins (example shown in Figure 72).

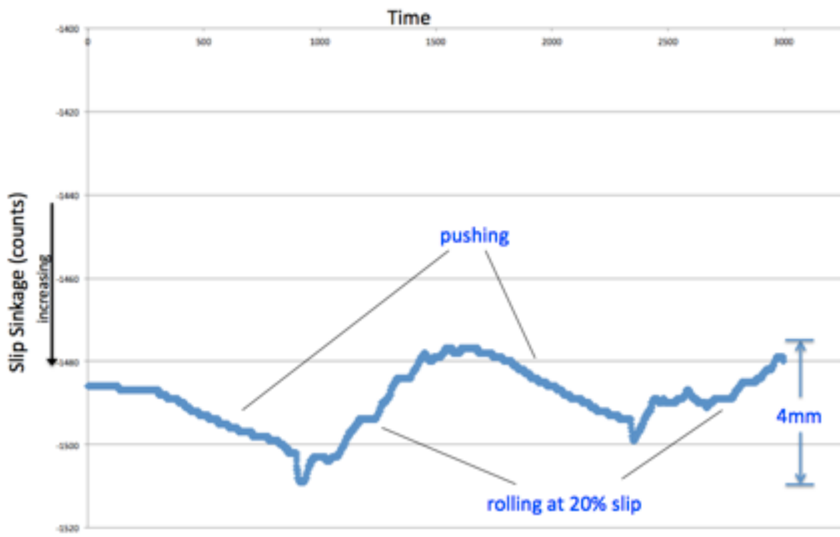

Figure 72: Slip sinkage time trace plotted for a roll-push-roll-push-roll motion of a single wheel. As slide induced sinkage is very small for pushed wheel, the rolling wheel easily recovers the sinkage, reducing the net value.

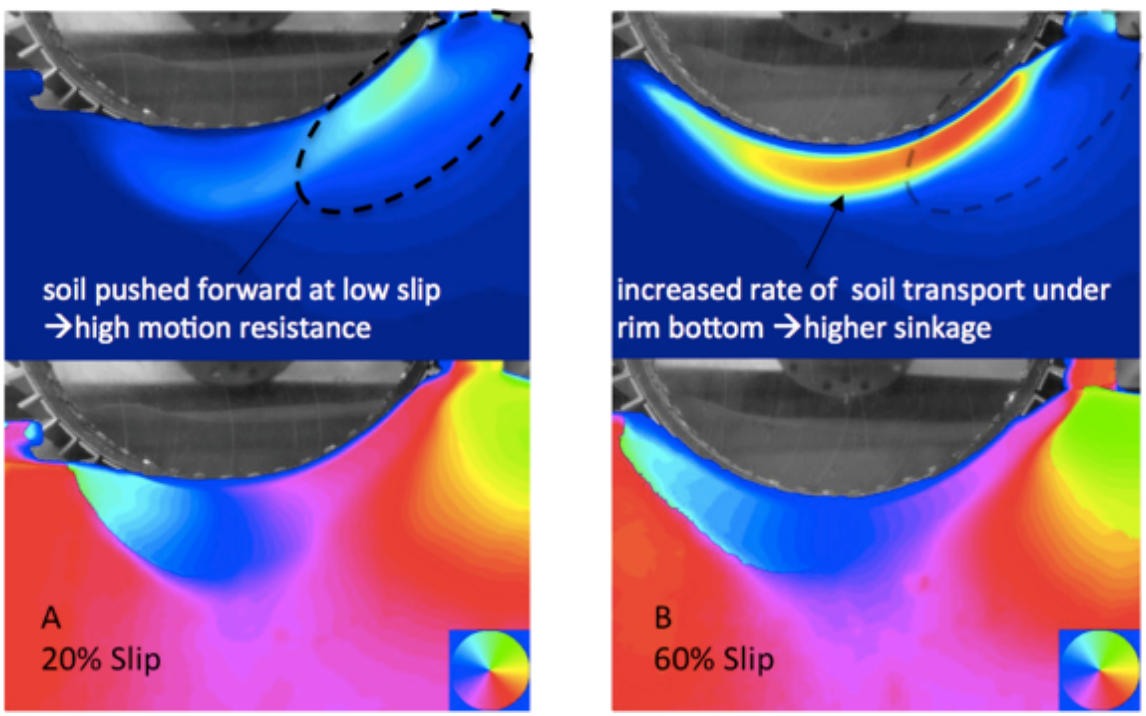

Figure 73: Example of slip induced soil transport at wheel leading edge and wheel bottom. The wheel velocity magnitude plots are normalized by ground speed and are at equal scale, allowing for direct comparison.

The reduction of soil forward motion is affected by increasing slip rate (Figure 73B) because slip induced soil transport can move soil away from the wheel front. As a rolling wheel slip rate of a push-roll vehicle can be controlled, entering high slip to achieve higher drawbar pull can be used to a vehicle's advantage. Similarly, reducing soil transport from underneath a wheel by lowering the slip rate, enables sinkage of the rolling wheel to be managed by a push-roll vehicle (Figure 73A).

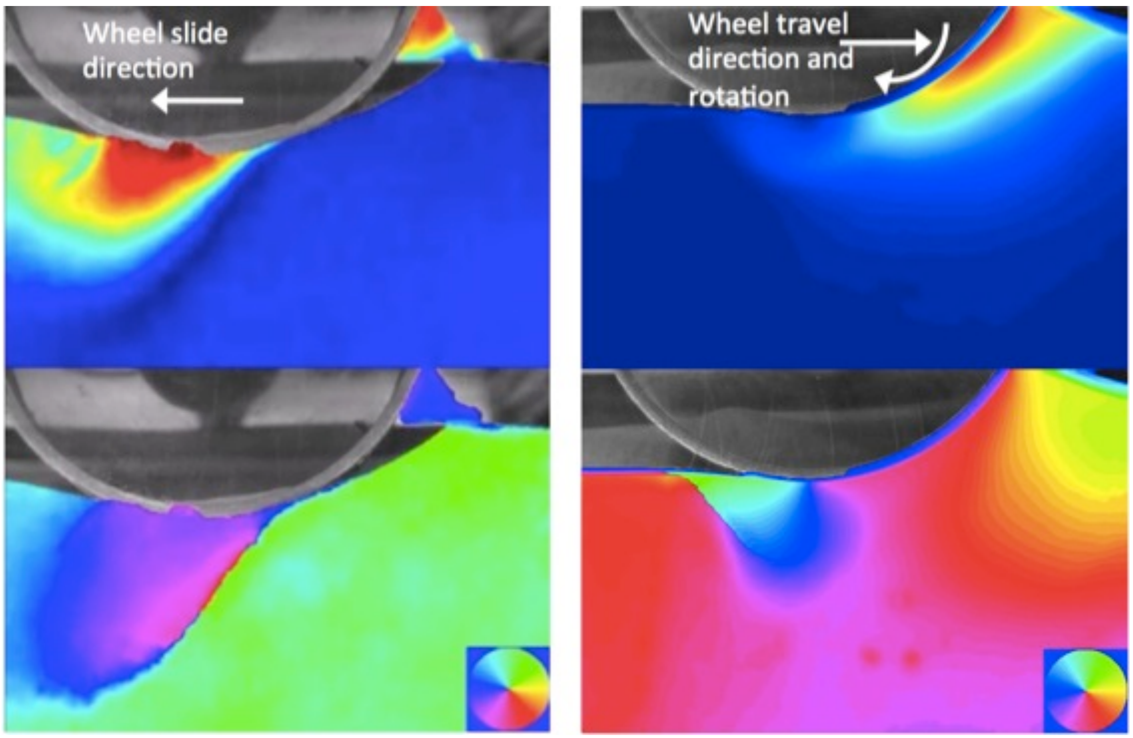

Figure 74: The pushing wheel generates substantial drawbar pull and, therefore, can work in conjunction with a rolling wheel that generates significant negative drawbar pull (from high motion resistance). The rolling wheel drawbar pull is -0.15 (pull coefficient), which is a considerable resistance. As an example, a wheel operating at 5% is chosen resulting in lower sinkage than the nominal 20% slip wheel (Figure 71). The 5% slip rate results in a slip induced sinkage of 5.2mm (compared to 25mm of 20% slip wheel). The soil velocity magnitude plots are scaled differently between pushed and rolling wheel.

An example representing use of a commanded low slip rolling wheel in conjunction with a pushing wheel is shown in Figure 74. The sinkage of the rolling wheel is much less then that of the push-roll example, in Fillite, given in Figure 71. By lowering the slip rate from 20% to 5%, the slip sinkage changes from 25mm to 5.2mm. As a consequence, the pull coefficient of the rolling wheel drops from -0.10 to -0.15. This trade off, of higher motion resistance, is manageable as the pushed wheel still generates 0.20 pull coefficient with only 0.4mm slide sinkage.

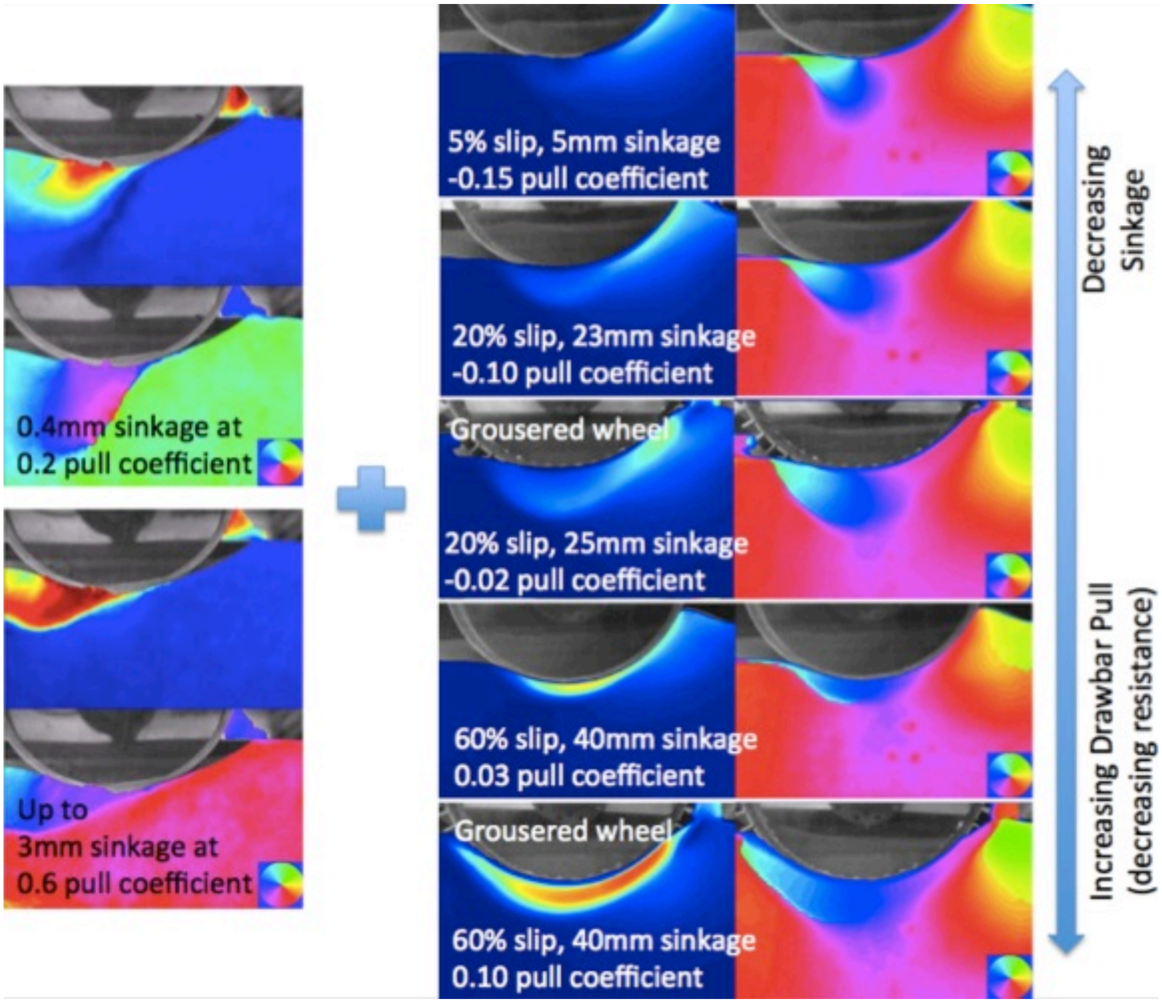

Figure 75: Example operating range of push-roll locomotion in soft ground. Push-roll locomotion can control the rolling wheel slip, therefore it can operate at a predetermined point to manage drawbar-pull and sinkage. Sinkage is expressed in terms of slide induced or slip induced sinkage (not static). Soil velocity magnitude plots are scaled differently between pushed and rolling wheel. The rolling wheel velocity magnitude plots are normalized by ground speed and are at equal scale, allowing for direct comparison.

A visualization, of a possible range of operating points of push-roll in soft ground is given in Figure 75 for discussion purposes. Figure 75 can be looked at as first choosing a wheel slip rate (which would be controlled by the vehicle) and then a pushed wheel that provides adequate thrust. Two examples of a pushed wheel are provided; one high thrust and one medium thrust. Although the lowest pushed wheel thrust provided in the figure, is greater than that of the lowest rolling wheel net resistance; the two points are provided to give a look at the relative influence the two points have on soil motion.

A wheel operating at a low slip rate must roll over the soil that is it encounters at its leading edge. At higher slip rates, a wheel is more capable of transporting soil away from the leading edge, resulting in a reduction of the resistance the soil in front of a wheel might produce. The increased pushing on soil, at low slip rates, reduces drawbar pull and an example of this process is evident in the 5% and 20% slip rolling grouserless wheels in Figure 75. At a low slip rate of 5%, the rate of soil removal below the grouserless wheel is reduced, however the rate of removal at the wheel front is also reduced. The lowered rate of soil transport, leads to decreased sinkage, but also a higher motion resistance (greater negative drawbar pull). This might be desired for flat ground in difficult materials where high margin against entrapment is warranted. As excessive resistance due to sinkage is the primary cause of vehicle entrapment, sinkage is a safety metric commonly utilized to asses full-vehicle mobility.

As the slip rate may be commanded at a high rate to intentionally reduce motion resistance by transporting soil from the wheel front, the use of grousers is quite appropriate for the task. At 20% slip, the grousered wheel can be seen to remove a large volume of soil from the wheel front, thus reducing motion resistance. However, the soil transport due to grousers actually tends not to increase the rate of soil removed below the wheel. The grousers don’t increase sinkage due to the fact that the space between the grousers is filled by the soil from the wheel front (now acting like larger diameter wheel). For this reason, the wheel with and without grousers at the same slip rate has very similar sinkage. A major difference between the two wheel types is the drawbar pull. Therefore, using grousers on a push-roll vehicle, is a quite useful configuration of locomotion mode and wheel type when slip is intentionally increased to reduce rolling wheel resistance. This combination provides higher drawbar pull without increased sinkage.

If high drawbar pull is desired for ascending an incline of high sinkage material, further slip might be required to reduce motion resistance to increase drawbar pull. This requirement comes from the need to overcome gravity due to the incline and motion resistance due to high sinkage material. The incline increases the total drawbar pull required to travel uphill, while reducing motion resistance might lead to more available drawbar pull, especially in soft ground. The wheel at 60% acts as an example of this case. It can be seen in the SIIA plots that less soil is being pushed forward and, therefore, motion resistance is decreased. The increased drawbar pull measured reflects this reduction of motion resistance.

Single wheel force measurements, sinkage measurements and sub-surface soil analysis show that push-roll might provide high mobility in high sinkage materials such as Fillite where many wheeled vehicles would become entrapped. The pushed wheel is still able to provide high thrust with little increase sinkage. When combined with a rolling wheel of high resistance, a net positive drawbar pull can still be achieved. A control strategy for prioritizing sinkage or drawbar pull can be implemented on a push-roll vehicle in soft ground by controlling the rolling wheel slip rate.

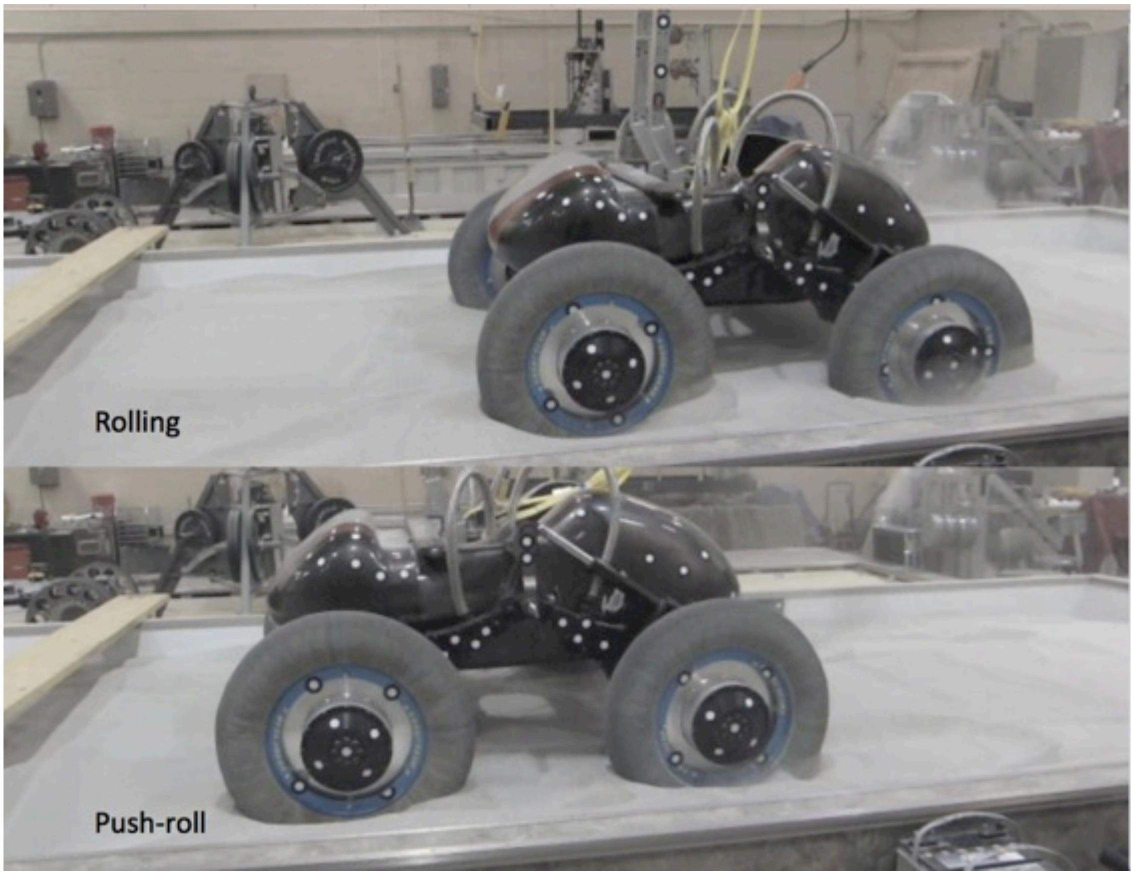

Figure 76: Full vehicle demonstration in soft ground (Fillite) in self-propelled state. The rolling locomotion is at high slip, substantial sinkage and near entrapment. The push-roll locomotion travels under much lower travel reduction (slip) and lower sinkage. State of sinkage after one vehicle length of travel is shown. The vehicle is not near entrapment and easily makes forward progress. The reduced sinkage is because the rolling wheel is able to operate at negative drawbar pull. The rolling wheel slip was estimated to be 10%.

A full-vehicle demonstration of push-roll locomotion in Fillite was conducted to verify that increased performance would be achieved over conventional rolling as was concluded from sub-system SIIA results. By visual inspection, the Scarab vehicle operating in push-roll mode, was able to make forward self-propelled progress under what appeared to be low travel reduction (however travel reduction was not measured). Rolling locomotion resulted in high slip (greater than 90%) and in high sinkage of the vehicle rear wheel (Figure 76). While in conventional rolling locomotion, the vehicle was near entrapment. Alternatively, while operating in a push-roll mode, entrapment seemed unlikely as little wheel slide or slippage occurred. These experiments show that there is potential use for push-roll in extreme scenarios such as the weak fly-ash material, Fillite, which would cause most wheeled vehicles to become entrapped.

5.3.5 Design for Improved Traction

The experimental results of this chapter can inform design in numerous ways; two examples are provided. First, identifying ground failure as the main source of traction gains, allows a designer to rely on high thrust in the development of a system using a pushing element. This not only enables better design of vehicles that may use a pushing element but also offers it as a design option to increase mobility through higher drawbar pull and lower sinkage. For example, a pushing element could be used on a tracked vehicle that already has very low sinkage (i.e. low motion resistance) and because thrust would be the additional source of drawbar pull gains, the design change might still yield significant mobility increases. Adding the pushing element would increase thrust and the ability to tow a larger load. On the contrary, if the assumption of previous works were made, that reduction of resistance is the most significant source of gains, then adding pushing to a vehicle with low resistance, would be expected to yield little gains. These implications are not true and lead to poor assumptions regarding use of pushing in vehicle design.

Second is an example specific to push-roll implementation (i.e. guiding push-roll vehicle development). A design aspect realized from this thesis work is that push-roll provides an opportunity for unique control strategies to prioritize for drawbar pull or sinkage. As is revealed by SIIA, soil forward flow and soil transport, causing sinkage of wheels in soft ground, varies with slip. Since the rolling wheel of a push-roll vehicle can be set to an arbitrary slip rate, soil transport phenomena can be exploited. If high drawbar-pull is desired, for example, to climb a slope of weak material (with moderate-high sinkage), the rolling wheel slip can be commanded to increase to reduce soil trapped at the wheel front. The will reduced motion resistance, resulting in higher drawbar-pull. If entrapment is of concern, for example in a flat ground sand-trap scenario with very high sinkage, low rolling wheel slip can be commanded to minimize sinkage. The lower slip will reduce soil being transported from underneath the wheel.

The two examples provided show how the push-roll locomotion, which is supported by sub-surface soil motion analysis, can directly inform design for improved performance and mobility.

5.3.6 Conclusions

The major findings of the push-roll locomotion research are:

- Push-roll locomotion generates thrust resulting in high drawbar pull that can aid in mobility. The pushing wheel produces this high degree of thrust as a result of ground failure. This soil failure mode is fundamentally different to that of a rolling wheel.

- Demonstration of a full-vehicle push-roll implementation on the Scarab rover platform was measured to produce approximately double the drawbar pull of conventional rolling for an equal travel reduction. The measured traction gains support the conclusion that push-roll can be used for steep slope ascent where high drawbar pull is required to overcome gravity. Also, push-roll in a high sinkage material (Fillite) was demonstrated and showed traction gains compared to conventional rolling in this scenario. In this material, most wheeled vehicles would face entrapment.

- High thrust is achievable without pushing off a wall of soil because of ground failure, not because of soil accumulation. This finding was experimentally proven in both loose material at low sinkage (GRC-1) and in extremely weak, high sinkage material (Fillite). The measured sinkage and horizontal displacement (slide) of pushed wheel was very low for both material types. These results show the overall feasibility of push-roll as it can gain high drawbar in many applications while still maintaining low sinkage.

- Soft ground control strategies, via push-roll, offer low sinkage and high margins against entrapment. By coupling a high thrust pushed wheel and a negative drawbar low slip rolling wheel, low sinkage can be achieved in high sinkage materials. Alternatively, operating at higher rolling wheel slip achieves lower motion resistance. As such, a push roll vehicle might be able to gain high drawbar pull in high sinkage materials. High drawbar pull in this scenario would be useful to ascend inclines of materials of high sinkage.

A prime example of a study of sub-surface soil behaviors leading to increased understanding and design improvement is the fact that a pushed wheel was determined to undergo ground failure using SIIA. Previous to this work, it was assumed that the mechanics of a pushed wheel are the same as that of a rolling wheel. This assumption resulted in misunderstanding regarding the traction ability of push-roll locomotion and possibly to poor implementation. The understanding that a push-roll vehicle generates high drawbar pull by pushed wheel thrust has design implications, as was discussed in the previous section (5.3.5, page 128).

5.4 Experimental Results Summary

The results of the study of grouser mechanics and push-roll locomotion were presented to show that behaviors of observed sub-surface soil motions influence traction and that employing an empirical method for analysis of these behaviors leads to explanation of previously unknown traction processes. Shear Interface Imaging Analysis provided unique data in these studies and resulted in novel findings confirming the importance that detailed sub-surface soil behaviors should play in terramechanics research, analysis and design.

Section 5.2, Grouser Mechanics, presented the study of the function of grousers and introduced design guidelines to achieve high performance based off a traction mechanism discovered by sub-surface soil motion analysis. Section 5.3, Push-Roll Locomotion, investigated a non-typical locomotion mode for the discovery of sources of traction gains measured during full vehicle experimentation. The findings explained how this locomotion mode is able to produced high thrust and how to implement for difficult terrain such as extremely weak surface materials.

Both the grouser wheel and push-roll studies resulted in guidelines for implementation for high performance. Examples of implementation for improved design are the minimum grouser spacing equation and slip control of push-roll for low sinkage.

The studies highlight the importance of recognizing the insufficiently understood processes underneath a wheel and that better design can be achieved by accounting for specific wheel induced soil motions. If a common approach of terramechanics research were undertaken which relies solely on force and sinkage measurements, none of the major findings of this thesis research could have been made.

6 Conclusion

6.1 Summary

This research has shown that the behavior of soil under a rolling wheel was poorly understood, and that such understanding is important in the design and analysis of planetary rovers operating in loose, granular material. Empirical analysis of sub-surface soil motion exposes traction processes too complex for current models and theory to describe.

The study of common wheel types, and a range of operating points, revealed soil motion behaviors that were previously unobserved, that were inconsistent with the literature and that were not accounted for in terramechanics models. These results motivated further investigation of specific soil motion behaviors. Examination of these soil behaviors show that accounting for soil behaviors is needed if accurate prediction of traction is expected and if reasonable assumptions regarding traction mechanics are to be made.

The two major studies of this research, the investigation of grouser mechanics and the investigation of push-roll locomotion, show that the empirical method of observing sub-surface soil motions can lead to new explanations of traction processes of wheels. This method led to improved wheel design and control strategy, during the research of grousered wheels and push-roll locomotion, respectively. The study of grousers led to an explanation of how they influence traction and introduced design guidelines to achieve high performance based off traction processes discovered by sub-surface soil motion analysis. The push-roll locomotion study, investigated a non-typical locomotion mode for the discovery of sources of traction gains measured during full vehicle experimentation. The findings explained how push-roll locomotion mode is able to produce high thrust and how to implement control for difficult terrain such as extremely weak surface materials.

As a result of sub-surface soil motion analysis, a new explanation of traction mechanics of grousered wheels was formed, and design guidelines for improved performance were developed. Soil forward motion at a wheel leading edge was identified as a crucial soil behavior associated with grousered wheels. The forward motion correlated with drawbar pull response and, therefore, was shown to have a strong positive influence on traction. In-depth analysis of how grousers interact with the ground resulted in the formation of the concept regarding reduction of motion resistance via grouser induced soil transport. The selection of proper grouser height and spacing enhances the soil transport clearing effect and can increase drawbar pull. As a result, an equation for grouser height/spacing relationship to achieve high performance grouser configuration was developed and partially validated. This equation predicts the minimum grouser spacing such that the rim does not contact the ground before a grouser removes soil that would normally contribute to motion resistance. This expression relates grouser configuration (height and spacing) to wheel parameters (wheel radius) and operational parameters (sinkage and slip).

Sub-surface soil motion analysis of push-roll locomotion revealed new potential for the mobility mode. Full vehicle traction measurements quantified mobility gains and confirmed feasibility in low bearing strength materials.

The pushed wheel is able to produce large thrust as a result of ground failure. This soil failure mode is fundamentally different than that occurring below a rolling wheel. It was revealed that high thrust could be achieved without requiring an accumulation of soil behind the wheel due to the nature of a ground failure response. This result was experimentally proven in both loose material at low sinkage (GRC-1) and in high sinkage material (Fillite). Measured sinkage and horizontal displacement (slide) of a pushed wheel was also very low for both material types. These findings confirm the overall feasibility of push-roll as a locomotion mode as it can gain high drawbar pull at low horizontal displacement, thus maintaining low sinkage.

It was discovered that push-roll provides an opportunity for unique control strategies to prioritize for drawbar pull or sinkage. As was revealed by sub-surface soil motion analysis, soil forward flow and soil transport, causing sinkage of wheels in soft ground, varies with slip. Since the rolling wheel of a push-roll vehicle can be set to an arbitrary slip rate, soil transport processes can be exploited. By coupling a high thrust pushed wheel and a negative drawbar pull, low slip, rolling wheel, low sinkage can be achieved in high sinkage materials. Alternatively, operating at higher rolling wheel slip achieves lower motion resistance. As such, a push roll vehicle might be able to gain high drawbar pull in high sinkage materials. Soft ground control strategies via push-roll offer low sinkage and high margins against entrapment or high drawbar pull to ascend slopes of materials of high sinkage.

Push-roll implementation, on the Scarab rover platform, produced approximately double the drawbar pull of conventional rolling. This large traction gain might allow for increased steepness of slopes ascendable as high drawbar pull is required to overcome gravity in this scenario. Push-roll in a high sinkage material (Fillite) was demonstrated and showed mobility performance gains, such as lowered sinkage and slip, compared to conventional rolling. In this material, most wheeled vehicles would face entrapment.

In summary, the results of the experimentation campaigns of this research, verify all aspects the thesis statement asserted in this document.

6.2 Contributions and Significance

The research of this thesis advance planetary rover mobility and the study of terramechanics in the following ways:

- Introduced a method of empirical terramechanics investigation based on observation and analysis of design prototypes. The general approach, utilized in the two major studies included in this research, show how empirical observation of sub-surface soil motion utilized for analysis can be an insightful method of studying both terramechanics fundamental traction processes and specific wheel prototype designs. This method for research can be used in the formation of principles describing wheel-soil mechanics and aid in developing a wheel or operating a vehicle. Direct analysis of soil motion provides knowledge of the soil failure planes, soil transport processes and many other aspects of traction. This analysis leads to insight into complex traction processes not described by current theory, and can lead to improved mobility performance through design changes. This research also introduces the concept of validating design via subsurface soil motion analysis and designing for specific sub-surface soil response behavior. Design using this approach is an alternative to typical evaluation by reaction forces and theoretical analysis.

- Created the Shear Interface Imaging Analysis (SIIA) method as a new tool for terramechanics research. The SIIA method utilizes the optical flow computer vision techniques to measure sub-surface soil motion underneath a wheel for the first time. This method produces high fidelity, spatially dense soil displacement fields. The SIIA method differs from other methods of investigating sub-surface soil motion by not needing specialized equipment, such as high-speed cameras, pulsed lasers, multi-phase LED lamps, or the alteration of the soil specimen via reference markers or coloring. Other methods also had lower resolution, accuracy and spatial density of information than the optical flow implementation utilized by SIIA. Shear Interface Imaging Analysis (SIIA) does not require special soil preparation or alteration of the soil sample and relies on an inexpensive consumer digital camera and readily available software. The high fidelity soil displacement fields produced by SIIA were demonstrated to provide useful data during both the research and in guiding design by enabling sub-surface soil motion analysis as described previously. Other research groups have already adopted this technique as a result of this work [71]. The high fidelity soil particle motion fields, generated by the novel soil tracking approach for terramechanics, also has many other uses such as validation of DEM models and possible hybrid methods to infer soil stress/strength.

- Observed that different wheel types and devices generate traction in different ways. Empirical evidence showing unexplained phenomena of sub-surface soil motions between wheel types, gives direction for much potential research. This thesis provides a framework that may be followed to conduct the research. A need to validate basic assumptions that underpin conventional terramechanics theory and models is also highlighted. The validity of many assumptions can be called into question as a result of this research and by the empirical results presented.

- Investigated empirically the sub-surface soil mechanisms related to grousered wheel traction. As a result, design guidelines for improved performance are offered based on a new explanation of grousered wheel traction. Analysis of grousered wheel-soil interaction led to the mechanics behind reducing motion resistance via soil transport. An equation for the implementation of high performance grouser configurations was developed and demonstrated to predict useful values compared to measured data. Also, highlighted is the importance of validating aspects of traction devices that are not explicitly part of model. Fine details, such as rim surface features, have a profound effect on soil shearing, and in turn, on traction.

- Revealed the soil mechanisms behind push-roll locomotion and demonstrated high drawbar pull (slope climb) and soft ground (high sinkage) applications. SIIA analysis provided unique insight to confirm ground failure type soil response that provides high thrust used by push-roll locomotion. This thesis research provides the most comprehensive empirical study of wheel-soil interaction of push-roll locomotion to date. Confirmation of the high thrust capability due to the type of soil failure and the implementation for operation in soft ground brings forward the mobility gains of this non-typical locomotion mode and as a possible use for future planetary missions.

- Provided insight into traction processes of wheels operating in loose, granular soil. Although numerous novel findings were made (see Table 4), three key examples are worth highlighting. The extent of the role soil transport processes play in traction was shown. The observation that the shear interface is almost always confined to wheel contact, and the drastically different shape of soil failure planes for different wheel types are important findings. The former observation is important as it suggests that the soil failure planes may be governed by the path the soil is forced to take due to wheel geometry and is not only a function of loading. Studying wheels under varying slip rate and at high sinkage highlights soil transport, due to wheel rotation, as a mechanism that plays an important role in traction; sinkage induced by slip affects resistance, while similarly, soil transport at the front of the rim can reduce traction by moving soil out of the wheel path. The shear interface shape of the rigid wheel is different from that of the compliant, flat contact wheel and from that of the pushed wheel. The drastically different shape of the shear interfaces (soil failure planes) is an important finding as it suggests that the thrust producing mechanism varies between wheel types. This finding motivates research into the different processes governing the different shear interface shapes. Creating designs that could somehow achieve the shear interface of a high drawbar pull device, such as the pushed wheel, would produce wheels of extraordinary performance.

6.3 Importance of Soil Transport

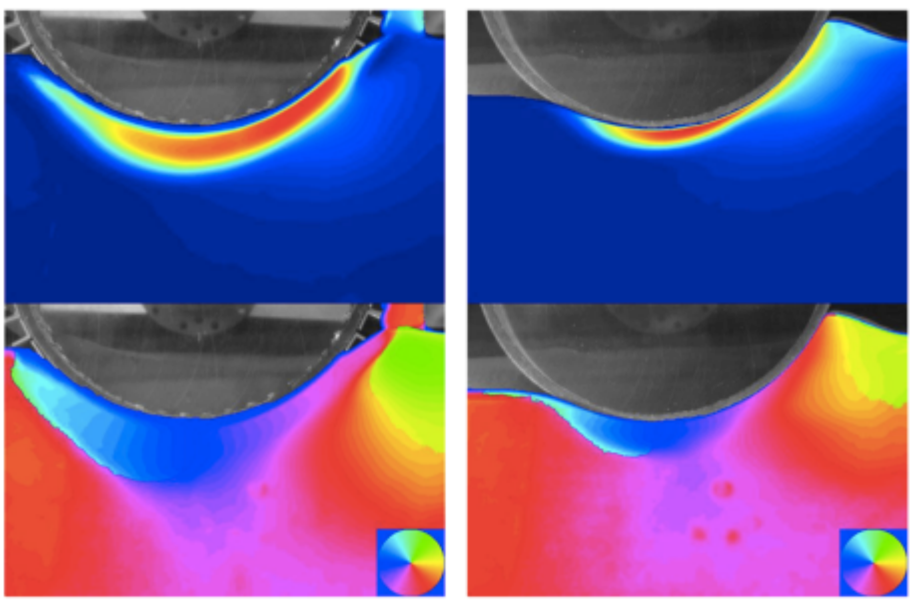

Figure 77: A grousered and grousereless wheel is shown operating in high sinkage material at 60% slip. The grousered wheel is generating 10N drawbar pull, while the grouserless wheel generates 2.5N. This experiment highlights multiple key insights into wheel operation in general. At the front of the wheels, the soil moves in a tangential direction for the grousered wheel, while the direction of the soil is near normal to the rim for the grouserless wheels. Soil velocity magnitudes for both wheels are equally scaled.

Soil transport is a key process highlighted by much of the experimental results. This process can explain many aspects of wheeled traction in loose, granular soil. However, it has received little attention in research and is not accounted for in terramechanics theory.

In Figure 77, wheels operating in high sinkage material are shown and are an example where soil transport can be seen to play a major roll in motion resistance. If soil is moved away from a wheel region of interest, the soil can no longer play a role in generating thrust or resistance with respect to that region. A clear example of the result of soil transport is seen in Figure 77. There is less soil visible in front of the wheel with grousers (a wheel type that transports soil well). This experimental result highlights soil transport as a key traction process that must be accounted for, if accurate predictions of performance are to be made.

6.4 Future Work

This thesis research developed improved PIV (Particle Image Velocimetry) tools and demonstrated a unique approach to conducting terramechanics research. The experiment space of the traction device types and range of parameters investigated was fairly limited. Although various wheel diameters and wheel types were tested, only grousers and push-roll were studied in depth. A comprehensive investigation of all wheel types, and of expanding the experiment space to include other traction devices, such as tracks, is expected to yield useful results. The results would not only lead to knowledge about a specific device studied, but also by accruing the results of many traction device types, a comparative study could be conducted. There is a lot to learn by identifying differences in traction processes between traction device types. For example, the study of the shear interface of a highly compliant wheel compared to that of a track, could inform how to better design the wheel to approach the high performance of a track. A deeper understanding of how the flat contact of a track affects soil transport and soil failure planes might direct efforts of compliant wheel design toward a flat contact or show if this feature is not importance. Another example from the study of push-roll locomotion is that research could be conducted to attempt to develop a rolling wheel that would produce ground failure of the soil, similar to that of the pushed wheel. There is no reason in principle why this could not be done, and traction gains would be extraordinary. However, a practical design of a rolling that interacts with the soil the same manner as the pushed wheel might not be feasible from a mechanical design perspective.

Many basic traction processes should also be the focus of investigation via a method like SIIA. As an example, a study of sinkage due to soil transport could provide insight about fundamental processes such as motion resistance and slip.

There is value in specifically investigating some of the underlying assumptions of terramechanics as applied to wheels in loose, granular material. This investigation might show limitations of current analytical models or provide insight into modifications and improvement. It might be possible to improve some aspects of existing analytical models by accounting for soil motion. For example, an effective sinkage and contact angle may be determined based on sub-surface soil motion analysis. An effective sinkage value could be utilized to calculate motion resistance while accounting for soil transport.

Analysis techniques and how to use soil displacement plots should be expanded upon. This research relied primarily on soil motion velocity magnitude and on direction fields. There are better indicators of both thrust and resistive forces such as total displacement. For example, manipulating the velocity data to calculate total displacement of soil in front of a wheel could be used to compare motion resistances between wheels. There are other ways to visualize the soil motion data that might be an informative output of SIIA. For example, tracking groups of particles and calculating the change in area particles are spread over can lead to measurement of change in density. This measurement can be useful as density strongly correlates to soil strength, therefore SIIA could be used to infer local changes in soil strength due to wheel influence.

The use of high fidelity soil displacement plots, to infer stress and strength could be powerful. Novel hybrid experiment-model methods might be achieved utilizing the SIIA data. This type of approach is motivated by the difficulty in predicting soil motion over long distances and by interaction with complex wheel geometries. An example of a hybrid approach, is the method introduced by Vlahinic, the author of this thesis, and others, that rely on high-fidelity soil displacement fields from SIIA experimentation, coupled with a physics-based computational framework to infer soil stress at high spatial density [53]. This hybrid method is an example of possible uses of sub-surface soil motion data that may open doors for new terramechanics research.

The study of wheels with grousers resulted in an alternative explanation of the processes leading to traction gains seen by wheels with these rim features. The process of reducing motion resistance and an explanation of the wheel interaction mechanism by which this occurs was discovered. An equation for high performance grouser configuration was also developed, based off the concept of reducing motion resistance via grousers. The transport of soil away from the wheel leading edge was found to reduce contact in this region, thus reducing resistance to forward wheel travel. As soil transport is the key process, there are many implications in terms of wheel design. This research solely investigated grousers that were straight, paddle like protrusions. Alternate shapes of grousers might promote more efficient clearing of soil from the wheel leading edge, or even reduce slip-induced sinkage. As soil transport plays a key role in both the grouser induced drawbar pull gains and slip sinkage, any wheel feature that has a significant effect on soil transport should be a focus of future research. For example, confining soil on all sides before forcing it to move might better transport all the soil from in front of the wheel without inadvertently pushing some to the side. The shape of the grousers is expected to have a significant effect on how well it contains the soil it initially engages (e.g. a U-shaped grouser would confine soil well). As more soil that is moved away from the wheel front will end up passing underneath the wheel, the slip induced sinkage might actually be lowered due to this grouser shape that better confines soil. There are many other considerations with regard to grouser shape and possible effects on traction due to soil transport. This aspect of grouser configuration has potential to influence traction and is a suggested avenue of future research.

The minimum grouser spacing equation for high performance presented in this thesis is a first of its kind and therefore might be overly simplified or not expressed in the most suitable manner. The formation of the equation resulted from an attempt to capture algebraically the basic mechanism by which grousers can reduce motion resistance. As such, it is in its simplest form. It is suggested that the wheel-ground interactions related to the soil clearing behavior be further investigated to reveal any secondary behaviors that influence motion resistance and that were not accounted for in the equation. Accounting for soil properties that have an obvious effect on the grouser soil transport behavior is expected to produce more accurate results. Soils that flow easily or are highly compressible will have less stringent requirements for grouser spacing and height, as soil transports more easily and resists forward motion less respectively for these soil types. Accounting for flowability and compressibility is expected to lead to a more refined form of the grouser spacing equation. Currently, a requirement in forming the grouser spacing equation is that the grouser sweeps soil away so the rim will never contact the soil at ground level. If a configuration was desired that is most appropriate for high sinkage at low slippage than the derivation of the equation could impose an initial rim contact at a prescribed depth (absolute or percentage of wheel radius). Prescribing an initial contact depth will actually produce a design that creates an effective reduced sinkage value, with respect to motion resistance processes, that is chosen by the designer. The initial point of contact may also be better described by a prescribed entrance angle (angle between rim tangent and ground plane at the point of initial contact). This relationship encompasses the affect of wheel radius on motion resistance and since it is a function of wheel radius, it is generalizable over wheels of different sizes. These types of improvements to the equation should be undertaken to produce a revision that can be broadly applied, thus of greater value for design.

7 Works Cited

[1] R. Arvidson, "Remote Sensing of Mars Focus on Relevance to Terramechanics ," in *KISS xTerramechanics Workshop*, Pasadena, 2011.

[2] (2013) [Online]. http://www.nasa.gov/mission_pages/mer/images/mer20090716.html

[3] M.G. Bekker, *Introduction to Terrain Vehicle Systems*. Ann Arbor: The University of Michigan Press, 1969.

[4] M.G. Bekker, *Theory of Land Locomotion*. Ann Arbor: University of Michigan Press, 1956.

[5] J. Wong, "Behaviour of Soil Beneath Rigid Wheels," *Journal of Agricultural Engineering Research*, pp. 257-269, 1967.

[6] S. Moreland, K. Skonieczny, D. Wettergreen, C. Creager, and V. Asnani, "Soil Motion Analysis System for Examining Wheel-Soil Shearing," in *17th International Conference of the ISTVS*, Blacksburg, 2011.

[7] S. Moreland, K. Skonieczny, H. Inotsume, and D. Wettergreen, "Soil Behavior of Wheels with Grousers for Planetary Rovers," in *IEEE Aerospace*, Big Sky, MT, 2012.

[8] J., Lindemann, R., Iagnemma, K., Trease, B., Vlahinić, I., Senatore, C., Andrade, "XTerramechanics: Integrated Simulation of Planetary Surface Missions ," 2012.

[9] J. Wong, *Theory of Ground Vehicles*, 3rd ed. New York: John Wiley & Sons, 2001.

[10] D. Freitag, A. Green, and K. Melzer, "Performance Evaluation of Wheels for Lunar Vehicles ," Vicksburgh, Summary Report 1970.

[11] M. Budhu, *Foundations and Earth Retaining Structures*. New York: John Wiley & Sons, 2008.

[12] M. Apfelbeck, S. Kub, B. Rebele, and B. Schafer, "A Systematic Approach to Reliably Characterize Soils Based on Bevameter Testing," *Journal of Terramechanics*, vol. 48, no. 5, pp. 360-371, October 2011.

[13] D. Freitag, "A Dimensional Analysis of the Performance of Pneumatic Tires in Soft

Soil," U.S. Army, W.E.S., 1965.

[14] M.G. Bekker, *Off-the-Road Locomotion*. Ann Arbor: University of Michigan Press, 1960.

[15] Y. Favaedi, A. Pechev, M. Scharringhausen, and L. Richter, "Prediction of Tractive Response for Flexible Wheels with Application to Planetary Rovers," *Journal of Terramechanics*, pp. 199-213, 2011.

[16] H. Shibly, K. Iagnemma, and S. Dubowsky, "An Equivalent Soil Mechanics Formulation for Rigid Wheels in Deformable Terrain, with Applican to Planetary Exploration Rovers," *Journal of Terramechanics*, no. 42, pp. 1-13, 2005.

[17] R. Irani, R. Bauer, and A. Warkentin, "A Dynamic Terramechanic Model for Small Lightweight Vehicles with Rigid Wheels and Grousers Operating in Sandy Soil," *Journal of Terramechanics*, May 2011.

[18] G. Meirion-Griffith and M. Spenko, "A Modified-Pressure-Sinkage Model for Small, Rigid Wheels on Deformable Terrains," *Journal of Terramechanics*, pp. 149-155, Jan. 2011.

[19] L. Ding, H. Gao, Z. Deng, K. Nagatani, and K. Yoshida, "Experimental study and analysis on driving wheels' performance for planetary exploration rovers moving in deformable soil," *Journal of Terramechanics*, pp. 27-45, 2011.

[20] R. Bauer, W. Leung, and T. Barfoot, "Experimental and Simulation Results of Wheel-Soil Interaction for Planetary Rovers," in *IROS*, 2005.

[21] N. Patel, R. Slade, and J. Clemmet, "The ExoMars Rover Locomotion Subsystem," *Journal of Terramechanics*, 2010.

[22] S. Michaud, L. Richter, T. Thueer, A. Gibbesch, and N. Patel, "Rover Chassis Evaluation and Design Optimisation Using the RCET," in *The 9th ESA Workshop on Advanced Space Technologies for Robotics and Automation* , 2006.

[23] D. Apostolopoulos, "Analytical Configuration of Wheeled Robotic Locomotion," Robotics Intitute, Carnegie Mellon University, 2001.

[24] T. Thueer and R. Siegwart, "Mobility Evaluation of Wheeled All-Terrain Robots," *Robotics and Autonomous Systems*, pp. 508-519, 2010.

[25] B. Wilcox, "ATHLETE: A Cargo and Habitat Transporter for the Moon," *IEEEAC*, 2009.

[26] D. Harrison, "Next Generation Rover for Lunar Exploration," in *IEEEAC*, 2007.

[27] K. Iagnemma and S. Dubowsky, *Mobile Robots in Rough Terrain: Estimation, Motion Planning, and Control with Application to Planetary Rovers*.: Springer, 2004.

[28] K. Yoshida, T. Watanabe, N. Mizuno, and G. Ishigami, "Slip, Traction Control, and Navigation of a Lunar Rover," in *I-SAIRAS*, 2003.

[29] L. Ding, Z. Deng, H. Gao, K. Nagatani, and K. Yoshida, "Planetary Rovers' Wheel-Soil Interaction Mechanics: New Challenges and Applications for Wheeled Mobile Robots," *Inttel. Serv. Robotics Special Issue*, pp. 17-38, 2011.

[30] W. Harrison, "Soil Failure under Inclined Loads," *Journal of Terramechanics*, pp. 11-50, 1973.

[31] M.G. Bekker, "Photographic Method of Determining the Soil Action Beneath Footings," in *Proc. of the 2nd Int. Conf. on Soil Mechanics and Foundation Engineering*, Rotterdam, 1948, pp. 193-194.

[32] R. Earl and A. Alexandrou, "Deformation Processes Below a Plate Sinkage Test on Sandy Loam Soil: Experimental Approach," *Journal of Terramechanics*, vol. 01, no. 38, pp. 153-162, 2001.

[33] R. Adrian, "Twenty Years of Particle Image Velocimetry," *Experiments in Fluids*, vol. 39, pp. 159-169, 2005.

[34] S. Raschke, R. Hryciw, and G. Donohoe, "Microdeformations in Sands by Digital Image Processing and Analysis," *Transportation Research Record*, no. 1548, 1996.

[35] R. Khot, M. Salokhe, H. Jayasuriya, and H. Nakashima, "Experimental Validation of Distinct Element Simulation for Dynamic Wheel-Soil Interaction," *Journal of Terramechanics*, pp. 429-437, 2007.

[36] P. Gachet, G. Klubertanz, and et al, "Interfacial Behavior of Unsaturated Soil with Small-scale Models and use of Image Processing Techniques," *Geotechnical Testing Journal*, pp. 12-21, 2003.

[37] A. Monismith, and S. Cowen, "A Hybrid Digital Particle Tracking Velocimetry Technique," *Experiments in Fluids*, vol. 22, no. 3, pp. 199-211, 1997.

[38] D. Take, W. Bolton, and M. White, "Soil Deformation Measurment Using Particle Image Velocimetry (PIV) and Photogrammetry," *Geotechnique*, vol. 7, no. 53, pp. 619-631, 2003.

[39] T. Gnanamanickam, E. Saldana, C. Chandrasekar, and S. Murthy, "Deformation Field in Indentation of Granular Materials," in *Int'l Conf. on Micromechanics of Granular Media*, 2009.

[40] G. Spenko, and M. Meirion-Griffith, "A Pressure-Sinkage Model for Small-Diameter Wheels on Compactive, Deformable Terrain," *Journal of Terramechanics*, vol. 50, no. 1, pp. 37-44, 2013.

[41] S. Okada, and N. Nemat-Nasser, "Radiographic and microscopic observation of shear bands in granular materials ," *Geotechnique*, vol. 51, no. 9, pp. 753-765, 2001.

[42] K. Hasan, and A. Alshibli, "Spatial variation of void ratio and shear band thickness in sand using X-ray computed tomography," *Geotechnique*, vol. 58, no. 4, pp. 249 – 257, 2008.

[43] S. Moreland et al., "Inching Locomotion for Planetary Rover Mobility," in *IEEE Aerospace Conference*, Big Sky, 2011.

[44] C. Creager et al., "Benefit of "Push-pull" Locomotion for Planetary Rover Mobility," in *Earth and Space Conference*, Pasadena, 2012.

[45] J. Wong and A. Reece, "Soil Failure Beneath Rigid Wheels," in *Proc. 2nd Int. Conf. of the International Society for Terrain-Vehicle Systems*, Quebec City, 1966, pp. 425-445.

[46] M. Black and P. Anandan, "The Robust Estimation of Multiple Motions: Parametric and Piecwise-smooth flow fields," *CVIU*, pp. 75-104, 1996.

[47] H. Oravec, V. Asnani, and X. Zeng, "Design and Characterization of GRC-1: A Soil for Lunar Terramechanics Testing in Earth-Ambient Conditions," *Journal of Terramechanics*, pp. 361-377, 2010.

[48] H. Orevac, "Understanding Mechanical Behavior of Lunar Soils for the Study of

Vehicle Mobility," Department of Civil Engineering, CASE WESTERN RESERVE UNIVERSITY, Thesis 2009.

[49] N. Murphy and A. Green, "Effects of Test Techniques on Wheel Performance," *Journal of Terramechanics*, vol. 6, no. 1, 1961.

[50] A. Woodward, "Experimental Analysis of the Effects of the Variation of Drawbar Pull Test Parameters for Exploration Vehicles on GRC-1 Lunar Soil Simulant," Mechanical Engineering, Virginia Polytechnic Institute and State Univeristy, Blacksburg, Masters Thesis 2011.

[51] Z. Janosi and B. Hanamoto, "The Analytical Determination of Drawbar Pull as a Function of Slip for Tracked Vehicles in Deformable Soils," in *1st International Conference on the Mechanics of Soil Vehicle Systems*, Torino, 1961.

[52] A. A. Rula and C.J. Nuttall, "An Analysis of Ground Mobility Models (ANOMOB)," US Army W.E.S., Vicksburg, 1971.

[53] I. Vlahinic, J. Andrade, K. Skonieczny, S. Moreland, and D. Wettergreen, "Rover Mobility on Granular Soil: Marrying Multi-scale Modeling and High Fidelity Experiments to Infer Soil Stresses Under the Moving Wheel," in *Earth and Space Conference*, Pasadena, 2012.

[54] (2013) [Online]. http://photojournal.jpl.nasa.gov/catalog/PIA10017

[55] (2013) Jet Propulsion Laboratory. [Online]. http://www.jpl.nasa.gov/news/facts/muses.pdf

[56] L. Karafiath and E. Nowatzki, "Traction Performance of Wheels in Soft Soil," Grumman Research Department, 1973.

[57] A.R. Reece, "The Effects of Grousers on Off-road Vehicle Performance," *Journal of Agricultural Engineering Research*, vol. 9, no. 4, 1964.

[58] K. Terzaghi, *Theoretical Soil Mechanics*. New York: John Wiley and Sons, 1943.

[59] L. Ding, H. Gao, K. Deng, K. Yoshida, and K. Nagatani, "Slip Ratio for Lugged Wheel of Planetary Rover in Deformable Soil: Defenition and Estimation," in *IROS*, St. Louis, 2009.

[60] M. Sutoh, J. Yusa, T. Ito, K. Nagatani, and K. Yoshida, "Travelling Performance Evaluation of Planetary Rovers in Loose Soil," *Journal of Field Robotics*, Jan. 2012.

[61] J. Gao, H. Deng, and Z. Liu, "Effect of Straight Grousers Parameters on Motion Performance of Small Rigid Wheel on Loose Sand," *Information Technology Journal*, pp. 1125-1132, 2008.

[62] M. Heverly et al., "Traverse Performance Characterization for the Mars Science Laboratory Rover," *Journal of Field Robotics*, 2013, In Review.

[63] humboltmfg. [Online]. http://www.humboldtmfg.com/c-1-p-43-id-1.html

[64] (2013) ATI Delta Specifications. [Online]. http://www.ati-ia.com/products/ft/ft_models.aspx?id=Delta

[65] K. Skonieczny, S. Moreland, and D. Wettergreen, "A Grouser Spacing Equation for Determining Appropriate Geometry of Planetary Rover Wheels," in *Intelligent Robots and Systems Conference (IROS)*, 2012.

[66] D. Wettergreen et al., "Design and Field Experimentation of a Prototype Lunar Prospector," *International Journal of Robotics Research*, 2010.

[67] H. von Sybel and F. Grosse-Scharmenn, "Increased Draft for Wheeled Vehicles Operating Outside the Roadway by the Thrust-Stride System," in *Proceedings of the First International Conference on Terrain-Vehicle Systems*, Torino., 1961.

[68] H. Zhongliang, "Study and Implementation of Wheel Walking for a Mars Rover," Department of Space Science, Luleå University of Technology, Masters Thesis 2007.

[69] T. Czako, "An Analysis of Multi-Element Inching Vehicles," Tank-Automotive Center, U.S. Army, Michigan, 1963.

[70] R. Bauer, W. Leung, and T. Barfoot, "Development of a Dynamic Simulation Tool for the Exomars Rover," in *Robotics and Automations in Space*, Munich, 2005.

[71] C. Senatore, M. Wulfmeier, P. Jayakumar, and K. Iagnemma, "Investigation of Stress and Failure in Granular Soils for Lightweight Robotic Vehicle Applications," in *NDIA Ground Vehicle Systems Engineering and Technilogy Symposium: Modelling and Simulation, Testing and Validation (MSTV) Mini-Symposium*,

Michigan, 2012.

[72] S. Moreland, D. Wettergreen, C. Creager, V. Asnani K. Skonieczny, "Visualizing and Analyzing Machine-Soil Interactions using Computer Vision," *Journal of Field Robotics* , (submitted).

[73] J. Wong and A. Reece, "Prediction of Rigid Wheel Performance Based on the Analysis of Soil-Wheel Stresses Part I: Performance of Driven Rigid Wheels," *Journal of Terramechanics*, vol. 4, no. 1, pp. 81-98, 1967.

[74] O. Onafeko and A.R. Reese, "Soil Stresses and Deformations beneath Rigid Wheels," *Journal of Terramechanics*, vol. 4, no. 1, 1967.

[75] L. Ding, H., Gao, Z. Deng, and J. Tao, "Wheel Slip-sinkage and its Prediction Model of Lunar Rover," *J. Cent. South Univ. Technol.*, vol. 17, pp. 129-135, 2010.

[76] L. Ding, H. Gao, Z. Deng, K. Yoshida, and K. Nagatani, "Slip Ratio fot Lugged Wheel of Planetary Rover in Deformable Soil: Definition and Estimation," in *International Conference on Intelligent Robots and Systems*, St. Louis, 2009.

[77] B. Witney, "The Determination of Soil Particle Movement in Two-Dimensional Failure," *Journal of Terramechanics*, vol. 5, no. 1, pp. 39-52, 1968.

[78] E. Lee, S. Sullivan, J. Chandrasekar, S. Gnanamanickam, "Direct Measurment of Large-Strain Deformation Field in Machining," in *SEM Annual Conference and Exposition*, vol. 2, 2007, pp. 1080-1087.

8 Appendix

8.1 SIIA Optical Flow Algorithm Error Analysis

8.1.1 Controlled rotation test

To quantify the error of soil motion measurement output by SIIA, GRC-1 soil [47] was spread out flat covering a plate (Figure 78), which was then rotated by a very precise amount: 0.02944 rad ± 0.00003 rad.

Figure 78. GRC-1 spread flat on a plate, viewed from directly above. A sharpened pin at the center marks the point of rotation for ground-truth testing.

The ground truth of this prescribed motion was compared to soil motion measurement output by SIIA by processing pre- and post-motion photographs, as shown in Figure 79. The largest displacement, at the corners of the image, is 15.6 pixels, or 3.12 mm.

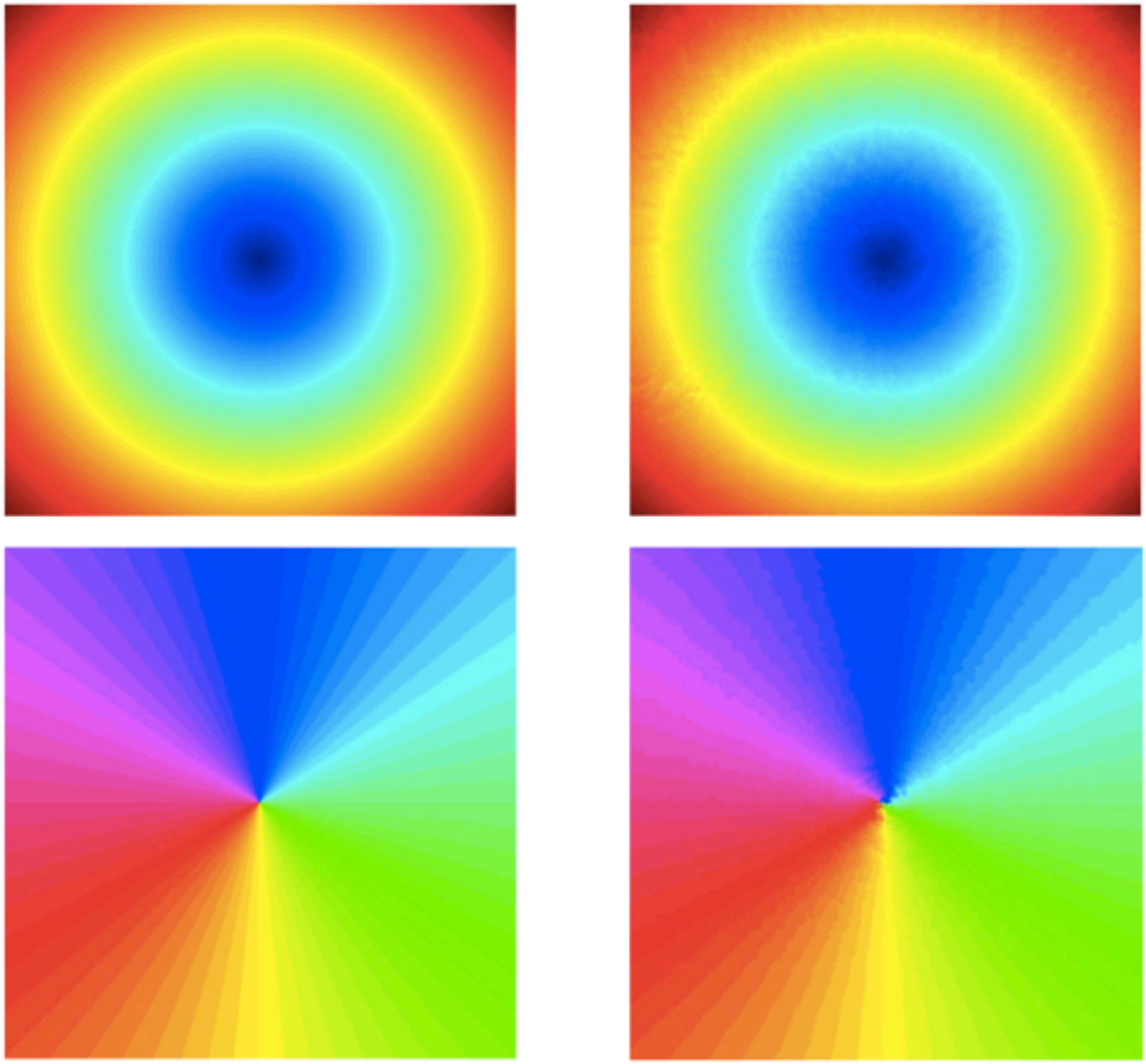

Figure 79. Ground truth (left) and measured (right) soil displacement magnitude (top) and direction (bottom), induced by a prescribed 0.02944 rad rotation.

Motion error at each pixel is measured by:

$$\sqrt{\left(u - u_{ref}\right)^2 + \left(v - v_{ref}\right)^2} \qquad \text{Equation 12}$$

This error is shown in Figure 80, according to its distribution in the image as well as its statistical distribution by magnitude. Errors are sub-pixel in magnitude throughout the image, with more of the higher magnitude errors observed near the edges where motion magnitude is also larger (as high as 15.6 pixels); regression shows a weak correlation of error magnitude with motion magnitude, with an R^2 of 0.25. The large displacements at the extremes of this test case are 2 to 3 times larger than the largest displacements observed during typical testing. Combined with the fact that error magnitudes are correlated with signal magnitudes, this suggests that the distribution shown in Figure 80 may be considered an upper bound on the error.

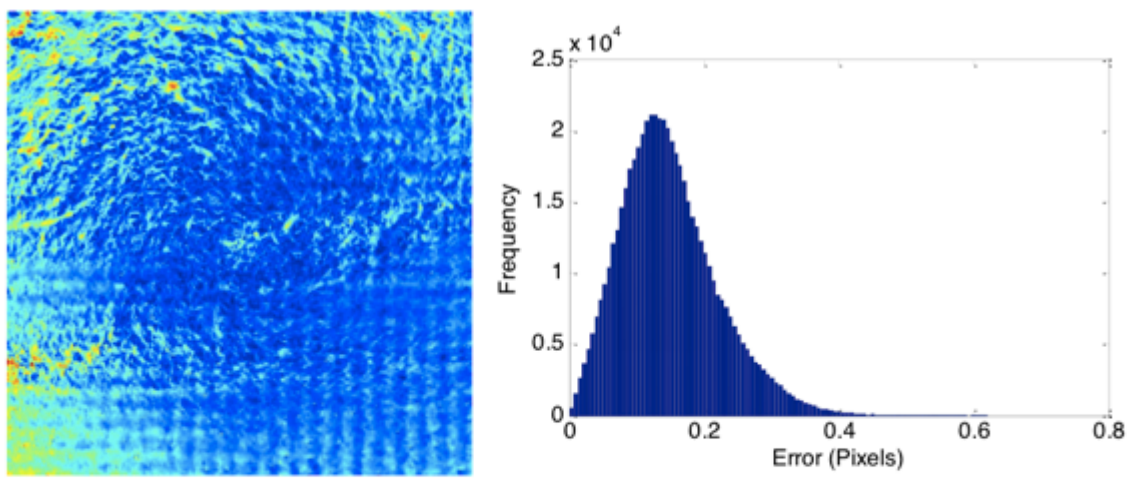

Figure 80. Motion error at each pixel of the image (left; warmer colors indicate higher error). Distribution of motion error by magnitude (right; median error = 0.14 pixels, 95th percentile = 0.28 pixels)

8.1.2 Constant horizontal speed tests

Typical SIIA tests involve moving the test implement and camera horizontally at a constant speed (and, in the case of wheel tests, coordinated rotation of the wheel for constant slip, as described in 8.1.1). The majority of the soil captured in the image is not influenced by the test implement, and remains static (see the large region of dark blue in Figure 7, for example). This static soil should thus move horizontally through the passing camera's field of view, at the speed that the carriage is commanded. The velocity of the static soil in the camera's reference frame may deviate slightly from this constant horizontal speed due to error in the processing technique, error in the control of the horizontal motion, vibrations in the structure between the test implement and camera, and/or inconsistencies in the camera's frame rate.

Figure 81 shows a sample of processed output from a 20% constant slip test. Results from a single frame pair are shown; the full test consists of 51 frames (and thus 50 frame pairs). The wheel is commanded at a tangential speed of 1 cm/s, and the carriage is advanced at 0.8 cm/s to maintain the desired 20% slip test condition. From the median horizontal soil flow of each of the 50 frame pairs of the test, the average horizontal speed was estimated to be 0.79 cm/s, and the 95% confidence interval for the horizontal speed was [0.75 cm/s, 0.83 cm/s]. This horizontal motion corresponds to average and 95% confidence values of 7.23 ± 0.34 pixels/frame. The error in horizontal motion detected is thus not much higher than the error introduced by the processing technique alone (± 0.28 pixels/frame, as shown in Figure 80), suggesting that the additional potential sources of error are not as significant as the error in the optical flow itself.

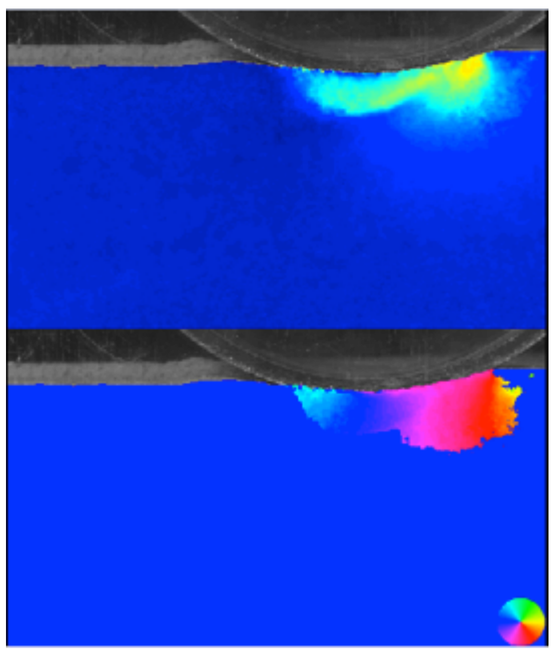

Figure 81. Sample output from a constant horizontal speed (constant slip) wheel test. The region colored dark blue in the velocity magnitude plot (top), covering the majority of the image, represents static soil unaffected by the test implement.

8.1.3 Cross-validation with feature tracking

Ground-truth measurements of soil displacement can be made for simple motions, such as the rotation and horizontal flow described in Section 8.1.1 and 8.1.2, but are not easy to obtain or enforce for more complex flows. Where validation against ground-truth is infeasible, it is useful to at least cross-validate against other techniques.

To gain insight into how the optical flow technique described here handles complex soil flows, its output is compared to corresponding output calculated via scale-invariant feature tracking (SIFT). SIFT searches for robustly distinguishable features in an image, and can then match that feature in a subsequent image. Soil displacement can thus be calculated at key points between an image pair.

Cross-validation tests for optical flow and SIFT were run using GRIP-1 soil. This is GRC-1 with 5% of its particles dyed black to increase the number of features discernible by SIFT. Sample output from both techniques for one of the GRIP-1 tests is shown in Figure 8. The top image shows motion of the tracked SIFT features between a pair of images, indicated by line segments. For each SIFT feature, the optical flow at the nearest pixel center is plotted on the bottom image. Where the error (Equation 13) between the computed optical flow (OF) and SIFT displacements is greater than 0.56 pixels (i.e. twice the 95% percentile error calculated from the ground-truth rotation test), the motion is displayed in red.

$$\sqrt{(u_{OF} - u_{SIFT})^2 + (v_{OF} - v_{SIFT})^2} \qquad \text{Equation 13}$$

Note that these instances are rare, but do tend to occur in regions of the soil affected by the test implement (where more complex flow occurs). Again, SIFT output is not ground-truth, so differences between optical flow and SIFT should not automatically be considered as errors on the optical flow side. However, these cross-validation tests do explicitly show that capturing soil motion for regions of complex flow is more challenging than for simple rotations and translations. Errors in these regions may thus be higher than those characterized in ground-truth testing.

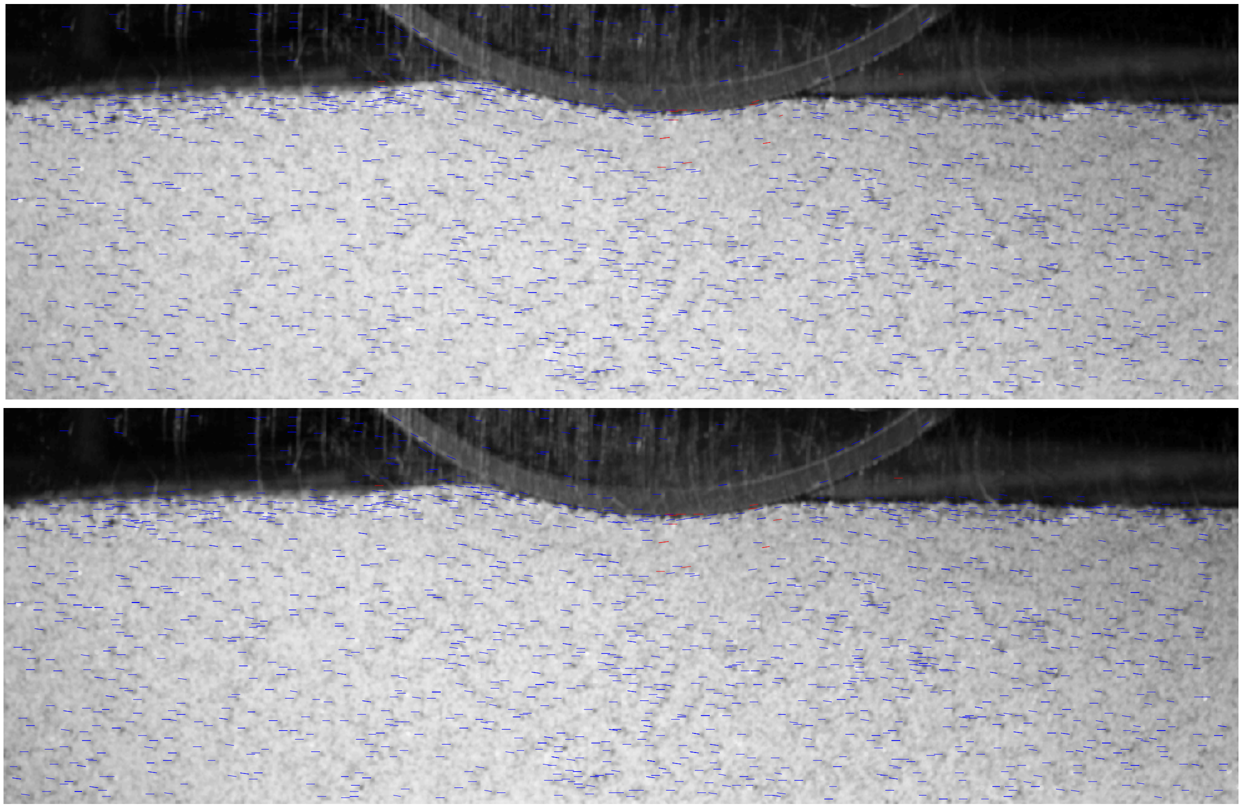

Figure 82. Soil flow captured using scale-invariant feature tracking (SIFT; top image), for cross-validation of soil flow computed by optical flow (bottom). Blue line segments show agreement between the two techniques within 0.56 pixels. Red lines indicate larger disparities, and occur where the wheel interacts with the soil causing complex flow.

For an extended explanation of the soil imaging software and error analysis see [72]. The information provided in this chapter is largely an excerpt from this publication.